Department of Chemical and Biological Engineering

BIOFILM DEFOULING USING MICROBUBBLES GENERATED BY FLUIDIC OSCILLATIONS

A Thesis Submitted to the University of Sheffield for the Degree of Doctor of Philosophy (PhD) in the Department of Chemical and Biological Engineering

By

Mohammad Hakim Che Harun

Supervisor:

Professor William Zimmerman

Dr Robert Edyvean

May 2019

DEDICATION

I dedicate this research to Almighty Creator for every knowledge researched, exploited, and understood upon His graciousness. "Glory to Thee, of knowledge We have none, save what Thou Hast taught us: In truth it is Thou Who art perfect in knowledge and wisdom."

ABSTRACT

The physical separation offered by membrane filters such as Reverse Osmosis (RO), Microfiltration (UF), Ultrafiltration (UF), and Nanofiltration (NF) has reduced the operating cost of such processes compared to distillation and chemical extraction. The advantages of the membrane such as high selectivity, high capacity, feasibility and cost effectiveness make them very good alternatives in separation industries especially cleaning technologies. Membranes, however, are easily fouled. Since the methods developed to defoul a membrane such as ultrasonic and chemical backflushing are always damaging to the membrane, this study is to explore the potential of microbubbles to restore the membrane to its operational condition. Microbubble clouds generated using fluidic oscillation produce non-coalescent bubbles, smaller and more uniform in size. Fluidic oscillation generated microbubbles are influenced by adjusting flow rate and oscillation frequency in conjunction with the diffuser pore size. The size of the microbubble produced is ranging from 30µm to 500µm at the lowest flow rate of air. The effect for cleaning purposes of microbubble injection with and without fluidic oscillation is explored by examination using Scanning Electron Microscopy (SEM), Total Suspended Solid (TSS) and system operational pressure drop (TMP). The smaller microbubble means higher surface contact area to remove the biofilm on the membrane filter. To further validate the effect of microbubbles on detaching and cleaning, FO generated microbubbles were sparged on biofilm (Chlamydomonas algae and HeLa cells) cultured on microscope slide surface. The detachment rates were compared by observing the density of algae and cells removed from the surface using lux meter and cell counting method. It is found that microbubbles generated using Higher Oscillation frequency of Fluidic Oscillator (HOFO) has a higher detachment and defouling rate. The highest defouling rate recorded for MF filter was 9.53mbar/min using HOFO, followed by 6.22mbar/min of microbubbles generated using Lower Oscillation frequency of Fluidic Oscillator (LOFO). Similar trends were observed in algae and cell detachment, the highest oscillation frequency of 335Hz has the highest detachment rate of 1.775lx/min and 1.7×10^4 cell/ml respectively. For MF systems, microbubbles generated using Higher Oscillation Frequency Oscillator (HOFO), increased the defouling rate by 64%. Similar observation recorded where HOFO increased detachment rate of Chlamydomonas algae and HeLa cells by 42% and 95% respectively.

ACKNOWLEDGEMENTS

TABLE OF CONTENTS

LIST OF FIGURES

LIST OF TABLES

LIST OF EQUATIONS

NOMENCLATURE

Symbol	Description	Unit
A	Area	m^2
ABFR	Air bubble flow rate	
BWRO	Brackish water reverse osmosis	
C_f	Feed water concentration	$mg.L^{-1}$
CF	Cartridge filter	
C_{fs}	Feed concentration	$mg.L^{-1}$
C_i	Concentration of all constituents in a solution	$mg.L^{-1}$
C_P	Permeate concentration	$mg.L^{-1}$
D	Diffusion coefficient	$m.s^{-1}$
D_b	Mean Bubble Diameter	um
DMEM	Dulbecco's Modified Eagle's Medium	
ε_G	Gas Holdup	
F	Frame rate	fps
FCP	Feed channel pressure drop	bar
FCS	Fetal Calf Serum	
FO	Fourier Fluidic Oscillator	
FTIR	Transformation Infrared Spectrophotometer	
HeLa	Henrietta-Lacks Cells	
HOFO	High Oscillation frequency of Fluidic Oscillator	Hz
ID	Inside diameter	mm
J	Membrane flux	$l.m^{-2}.h^{-1}$
K	Mass transfer coefficient	
KCl	Potassium Chloride	
L_c	distance between channel inlet and outlet	
L_s	length of the inlet section of the element	
LOFO	Low Oscillation frequency of Fluidic Oscillator	Hz
MBs	Microbubbles	
MF	Microfiltration	
NF	Nanofiltration	bar
NTU	Nephlometric Turbidity Unit	
OD	Outside diameter	
P_c	Concentrate pressure	
Pen Strep	Penicillin Streptomycin	
P_f	Feed pressure	bar
PSI	Pound per square inch	
Q_c	Concentrate flow rate	$m^3.h^{-1}$

Q_f	Feed flow rate	$m^3.h^{-1}$
Q_G	Gas flow rate	
R	Universal gas constant (8.314)	$kPa\ m^3.g^{-1}\ mol^{-1}$
RO	Reverse osmosis	
SDI	Silt Density index	
SEM	Scanning electron microscopy	
SP	Salt passage (%)	
SR	Salt rejection (%)	
SWRO	Seawater reverse osmosis	
t	Time of the test	min
T	Temperature	K or ºC
TDS	Total dissolved solids	$mg.L^{-1}$
TMP	Transmembrane Pressure	bar
TOC	Total organic carbon	$mg.L^{-1}$
TSS	Total suspended solids	$mg.L^{-1}$
UF	Ultrafiltartion	
UV	Ultraviolet absorbance	m^{-1}
V	Volume	m^3
V_G	Volume occupied by the gas phase	
V_L	Volume occupied by the liquid phase	

CHAPTER 1

INTRODUCTION

This chapter introduces the research study, starting with a general background to put the work into perspective before narrowing down to the problem the research aims to address and the already available solutions. A detailed description of the research hypothesis is presented followed by the research aims and objectives. Next, the scope of the investigation is highlighted, as is the limitation. In the final section, the significance of the study is explained before describing the work structure.

1.1 Background

Separation processes in chemical engineering are central to industrial process integration. They contribute to both purifying of the products and specifying the characteristics of the feedstocks in any industrial manufacturing sector. The separation techniques and materials are selected according to the operational conditions of the processes that involve chemical and physical separation process. In petrochemical industries, distillation is among the most popular separation techniques used in the recent decades. Since the distillation column is sometimes costly and poorly suited to the requirement, membrane technology has seen rapid developments to augment and replace the existing separation techniques in the production industries.

1.2 Problem Statement

It is important to defoul the membrane to avoid any disturbance to the process operations. Unfortunately, even effective already developed defouling methods, are unable to remove the biofilm non-destructively from the operating membrane assembly. Flemming, (1997) stated that there is no technology available to defoul membranes non-destructively. Due to their promise of gentleness, proposed cleaning mechanisms mediated by microbubbles through their momentum transfer properties and ability to generate free radicals, will be explored in this research. The following three hypotheses are proposed for experimental exploration:

- Since existing membrane defouling methods damage the membrane through the chemical reaction by direct contact, microbubbles will be explored for their

ability to scour porous surfaces without contact. *It is proposed that the cloud of microbubbles requires a population of bubbles that are near pore size to accomplish this defouling.* Backwashing or back flushing requires the process to be shutdown, interrupting production. In situ microbubble cleaning could be a continuous process, requiring little maintenance cycle or even no maintenance shutdown.

- Gentle microbubble defouling will cause substantially less damage. This will prolong membrane lifetime, thereby decreasing maintenance costs. *Bubble size distribution, flow strength, and orientation should influence the cleaning effectiveness. This hence permitting the selection of operating conditions that achieve the threshold of defouling effectiveness with a very slow rate of membrane damage.* This should be detectable through a microscopic morphology study.

- Positive effects of the microbubbles on cleaning are obvious to remove and detach biofilm form a surface. *In this research, the more effective cleaning action of microbubbles should be more effectively and efficiently detach biofilms that are especially resistant to defouling approaches.*

Thus, introducing cleaning mechanisms using different microbubble operation conditions has great potential to defoul the membrane at the lowest cost and the highest biofilm removal efficiency. Different conditions of microbubble flow regimes will be generated by manipulating the fluidic oscillator operation. These conditions can then be compared for their effectiveness, more shear stress with a higher contact area and time to defoul the membrane and biofilms. The four types of membrane selected will be used as trial filtration membranes due to their representativeness – common and widespread usage, while easily fouled in any application.

1.3 Membrane Filtration

The various membrane separation approaches that were selected have been progressively developed, based on the requirements of the applications such as high temperature, pressure and energy consumption. The table below shows different

membrane technologies and types commonly chosen as suitable for various application and their characteristics.

Table 1.1: Overview of Membrane Applications (Baker, 2004)

Membrane Types	Pore Size diameter (μm)	Common Application
Reverse Osmosis	0.45	Desalting water Concentration of foodstuff
Ultrafiltration	0.01-0.1	Water Treatment and Protein Concentration
Microfiltration	0.1-10	Water Treatment and Sterilization
Gas Separation	<0.1	Nitrogen Separations

These membranes are widely used in most processing industries mainly for separation and purification. Membrane technology is the major constituent for modernisation of process plant design through process integration, which has been shown in recent years to increase process efficiency substantially (Fazel et al., 2013). Unfortunately, they found that membranes were easily fouled by the formation of a gel layer which forms by concentration due to polarisation which reduces the permeate flux. Since fouling is commonly discovered in every membrane operation, defouling methods such backwashing, backflushing and usage of detergents or acidity have been developed and applied. For instance, defouling using ultrasonic irradiation allows an average of 215% permeate flux increase during 3 hours of filtration (Feng et al., 2006).

1.4 Microbubbles Cleaning

The potential of microbubble in cleaning has been exploited widely by Fazel et al., (2013), Agarwal et al., (2012), and Choung et al., (1993). The main principle for microbubble intensification of cleaning is its size. The smaller the size of microbubbles will provide higher surface area to allow the contact between the microbubble surface and impurities (Zimmerman et al., 2008; Burns et al., 1997). The higher the surface area of the microbubbles will results in better shear force to detach the biofilm and impurities from the surface (Lee et al., 2014; Li et al., 2010; Sharma

3

et al., 2005). The shear force can simply be further increased by decreasing the size of microbubbles that is generated by using fluidic oscillations. Zimmerman et al., (2008) explained the size of microbubble can be further influenced by using fluidic oscillations. This thesis will prove the technology of fluidic oscillator to generate microbubbles towards cleaning of filtration membrane and biofilm detachment from a surface.

1.4.1 Principle of bubble removal

In this thesis, microbubbles are used mainly to detach biofilm from a surface. **Figure 1.1** shows a velocity profile of flow with and without microbubbles. The biofilms adhere on the surface were exposed to such flow. The flow with the presence of microbubbles will result in higher flow velocity as the bubble has 1/1000 density of the liquid (Wibisono et al., 2015; Sharma et al., 2005). This explains the flow with microbubbles will have higher energy when V2>V1. Sharma et al., (2005) measured the surface tension detachment force provided by the bubbles. The force overcome the adherence force of the biofilm on the surface, hence detach the biofilm from the surface.
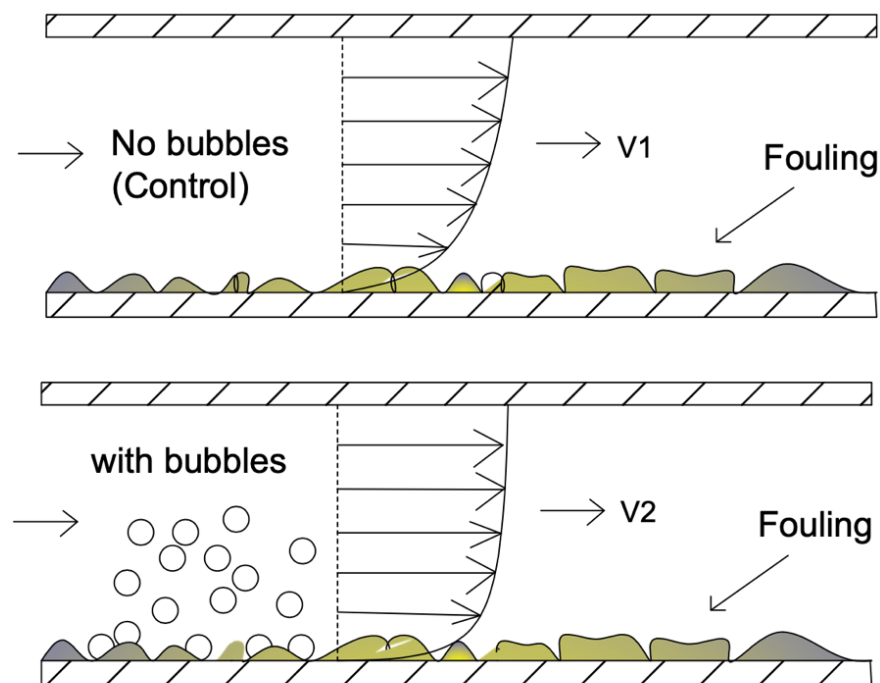
Figure 1.1 Hydrodynamic detachment force due to fluid flow and surface detachment force, due to the passing microbubbles (air-liquid interface)

1.5 Research Hypothesis and Aims

The primary goal of this research is to use the microbubble to remove biofilm from the filtration membranes used by wastewater treatment and manufacturing industries. Based on this aim, the following research objectives are proposed to use microbubble clouds in the cleaning mechanisms, to study the effectiveness and characteristics of bubble injection regimes and configuration towards cleaning. The following objectives map to the hypotheses proposed to direct the research:

1) To measure the envelop of the bubble size distributions produced from pulsatile flow directed through microporous diffusers.

2) To explore the relationship of microbubbles size generated using fluidic oscillation through microporous diffusers, on cleaning efficacy.

3) To compare the defouling effectiveness toward fouled filtration membranes by such flows.

4) To study and compare the efficiency of such microbubble clouds on biofilm detachment.

1.6 Study Scope and Limitations

This study will cover the flow configurations used to generate microbubbles using fluidic oscillation. High, low, and zero frequency to study the efficacy of microbubble clouds generated by fluidic oscillation towards filtration membrane defouling and biofilm detachment. A filtration system is also developed for probing the three oscillated microbubble conditions generated for efficacy towards cleaning. The limitations of this study only allow one kind of membrane configuration; tubular. The effects of the microbubble injection were then further investigated by testing the level of membrane detachment with HeLa cells and Chlamydomonas microalgae. The biofilms were cultured on a surface; the microbubble cloud is sparged impingent on the surface where the biofilm is to be removed.

1.7 Research Significance

There are many filtration challenges based on various types of membrane applications. The membrane will be easily fouled without the right mitigation step. This research

will demonstrate the application of the microbubble to defoul the membrane. It is important to defoul the membrane which contributes primarily to the pharmaceutical industry, water treatment, food, manufacturing, and every production industry.

<u>Microbubble</u>

1) The microbubble should be able to remove the biofilms in the membrane without damage the membrane.

2) Lower permeate flux which is a symptom of membrane degradation can be opposed using microbubbles.

3) Microbubbles can be injected into the existing process without the need of shutting down the plant, avoiding associated higher operating and capital costs.

<u>Membrane</u>

1) The usage of microbubbles in the membrane defouling processes should allow the expensive membrane material to be reused without altering its original properties.

2) The prolonged membrane life will reduce the operating and capital costs of the entire process

1.8 Contribution of Thesis

The contribution of this thesis mainly in exploring the potential of microbubbles to detach biofilms or cleaning applications. The following contributions are successfully demonstrated in Chapter 4, 5, 6, 7, and 8.

- Characterizations of fluidic oscillator (FO) generated microbubbles
- Design of FO microbubbles sparging unit
- Design of microfiltration (MF) system with microbubbles Cleaning in Place (CIP)
- Utilizing Arduino sensor and coding to record the data
- Design of biofilm detachment apparata using microbubbles

1.9 Structure of Thesis

Chapter 1 introduced the research work. In this chapter, background information concerning the problems of conventional cleaning methods are provided with details about those approaches in providing solutions. Introduction to the main idea of using fluidic oscillation to generate microbubble clouds for cleaning. Further, the research hypothesises are established, as are the aims and objectives that test and explore the hypotheses.

Chapter 2 critically review and demonstrates the novelty and originality of the hypotheses, and, in the context of literature, their significance. The applications of fluidic oscillation for microbubble generation, such as bio-fuel production, fermentation, and medical imaging are reviewed. In this chapter, microbubble applications however focus on cleaning applications such as membrane filtration defouling, biofilm detachment, and various other surface cleaning including dental plaque removal. This chapter reviews fluidic oscillation generation controls to produce better microbubbles for cleaning.

Chapter 3 describes and motivates the design of experimental apparata, instrumentation, and methodologies including chemical, morphological and data analysis. The membrane-defouling rig is designed to accommodate fluidic oscillation generated microbubble for cleaning and pressure recovery. Biofilms of algae and cell bases of Chlamydomonas and HeLa, respectively, are cultured along the designated detachment unit. Some of the analytical instruments are designed using Arduino microcontrollers for instrumenting pressures sensor, a flowmeter, and an accelerometer.

Chapter 4 shows the details of systems design to run the experiments. Microfiltration membrane housing and the system itself are designed to fit microbubbles sparging unit. This include designing a control box to regulate the air flowrate and pressure. The data obtained recorded using the designated microcontroller, Arduino. This device connects and records instruments such as pressure sensor, temperature, frequency and flowrate. The data logger and experimental design are combined to collect data for

microfiltration membrane defouling and biofilm detachment from a surface of microscope slide.

Chapter 5 presents the results from the characterisation process of microbubble sizing. The size variations of microbubbles within clouds results from the variation of fluidic oscillation configurations are measured using a high-speed camera and digital image analysis. The effects of flowrate, oscillation frequency, and microbubble size as control variables are characterised in this chapter. The research employs a range of oscillation frequencies for the study its cleaning efficacy and biofilm detachment.

In *Chapter 6,* the effect of microbubbles generated with and without oscillation to defoul filtration membrane system are compared. Filtration systems are designed to occupy the Microfiltration (MF) cartridge as a pre-treatment process. The filter are fouled by colloids and impurities from the sea water (collected from Kilnsea, Hull). The study also compares the cleaning efficacy of microbubbles generated by two conditions of fluidic oscillation control.

Chapter 7 establishes an understanding of the role of microbubble clouds to detach biofilm from a surface. In this chapter, Chlamydomonas algae are cultured on microscope slide as a source of biofilm. The biofilm has been sparged with microbubbles to expose a biofilm to microbubble contacting to scrape off the biofilm from its surface. The exposures of the biofilm to injected microbubble clouds are arranged in three different configurations and range of oscillation frequencies to study the detachment rate.

The methodology in *Chapter 8* is almost identical to chapter 7. This chapter further validates and aids understanding the properties of microbubble sparging induced shear forces to detach biofilms where HeLa cells are used. This detachment however has a different application approach. The properties of microbubbles which could detach HeLa cells from a surface has a potential to replace a harmful enzyme such as Trypsin in tissue culture activities.

Chapter 9 summarises all the results obtained in each chapter. The results are discussed and the learning from applications are assessed. The analysis of the results are discussed in light of the errors in estimation, intrinsic variations and limiting factors in inferences from the nature of the experimental systems. The challenges and limitations are addressed for future works.

Figure 1.2 outlines and summarises the progression of thesis. Literature on generation and applications of microbubbles and their characterisation are discussed in Chapters 2, 3 and 4. The outcome of the microbubble testing for particular applications of biofilm detachment are presented in Chapters 5, 6 and 7. Overall, in the final chapter, general conclusions are drawn from the results and analysis obtained.

```
┌──────────────┐     ┌──────────────────┐     ┌──────────────────┐
│              │     │ Literature Review:│     │                  │
│              │     │ Summary of        │     │ Methodology:     │
│ Introduction │ ──> │ microbubbles      │ ──> │ Fluidic oscillator,│
│ (Chapter 1)  │     │ cleaning mechanism│     │ membrane         │
│              │     │ and cleaning      │     │ defouling, and   │
│              │     │ applications      │     │ biofilm detachment│
│              │     │ (Chapter 2)       │     │ (Chapter 3)      │
└──────────────┘     └──────────────────┘     └──────────────────┘
```

Experimental design: Defouling rig, biofilm detachment unit, and Arduino **(Chapter 4)**

Characterizations of Microbubbles and Biofilms: HeLa cells and Chlamydomonas Algae **(Chapter 5)**

Filtration membrane defouling using fluidic oscillator **(Chapter 6)**

Application of microbubbles on biofilm detachment (Chlamydomonas algae) **(Chapter 7)**

Application of microbubbles on HeLa cells detachemnt for splitting **(Chapter 8)**

Conclusions and future works **(Chapter 9)**

10

Figure 1.2 Outline of the research presented in the thesis

CHAPTER 2

LITERATURE REVIEW

2.1 Introduction

This review of the academic literature demonstrates the main concept and the state of art behind the dynamics of microbubble clouds for membrane filtration and biofilm removal in cleaning processes. The microbubble generation techniques are reviewed as well as their various applications, especially for cleaning. The best generation of microbubbles in terms of energy efficiency, capital cost, and operating technology by using fluidic oscillation, are then studied based on the early information of biofilms such as colloids, Chlamydomonas algae, and Hela Cells. The properties of microbubbles, cells, algae, and filtration systems are assessed to test the hypothesis of biofilm cleaning using microbubble generated by fluidic oscillations.

Cleaning technology has been widely used in every industry to increase the process optimisation and efficiency (Cui et al., 2015; Mavredaki et al., 2007). This technology is important to eliminate or control the production of secondary compounds to maintain safe and clean environment (Sinnott, 2005). Membrane applications for wastewater purification have developed numerous methods to improve water quality. The use of microbubbles has been recognised as one of the most efficient routes for cleaning technology regarding energy efficiency, capital cost, and operating technology (Zimmerman, 2011a). Various industrial applications using microbubbles have shown promising results on process efficacy such as beneficial antibacterial activities for industrial biotechnology (Kamaroddin et al., 2016).

Small gas bubbles are used in many environmental and industrial processes for solid-liquid separations and also to facilitate heat and mass transfer between phases (Parmar & Majumder, 2013; Khuntia et al., 2012). Typically, smaller bubbles are preferred due to both their high surface area-to-volume ratio and their increased bubble density at a fixed flow rate (Chahine et al., 2015; Lee & Lee, 2002). The smaller size of the microbubbles increases the high surface area as the packing or phase density of microbubbles increase (Zimmerman, 2011a). In general, there are three ways of generating microbubbles. The most common class uses compression of the air stream

to dissolve air into the liquid, which subsequently is released through a specially designed nozzle system, to nucleate small bubbles as potential nanobubbles, based on the cavitation principle. Another class uses an air stream delivered under low offset pressure, and breaks off the bubbles due to an additional feature, such as mechanical action such as vibration, flow focusing, or fluidic oscillation (Parmar & Majumder, 2013).

2.2 Membrane Fouling

2.2.1 Introduction

Fouling is usually caused by the deposition of small colloidal particles on the inner walls of membrane pores. The blockages are built-up of particles in the form of a cake layer on the membrane surface and membrane pore openings. The effect of permeation flux reduction due to fouling is twofold. First, pore blocking and cake formation lead to the increase in flow resistance. After that, the presence of colloidal particles deposited on the membrane surface hampers liquid mixing. Thus, a relatively high concentration of solutes persists near the membrane surface which causes the reduction of the solvent flux crossing the membrane (Henry et al., 2012)

Fouling in a membrane is usually distinguished by either the non-adhesive or adhesive cake formation. Particle depositions from the effect of filtration-induced macro solutes are considered to be non-adhesive formation. Kroner et al., (1984) and Al-Malack & Anderson, (1997) suggest to use cross-flushing and backwashing, the application of low-frequency pressure and velocity pulsing leading to flow instability, and the addition of coagulants for the formation of layer particles, which are easily swept off the membrane surface respectively. Adhesive fouling which is irreversibly formed usually is caused by van der Waals attractions, hydrogen bonding, hydrophobic interaction, extracellular macromolecular interactions and other effects. (Baker, 2004) illustrates the formation of colloidal material deposited on the ultrafiltration membrane (UF) as a part of the filtration process.

Separation process technology has been widely developed to facilitate the industrial requirement to separate, clean or purify the products. The membrane is one of the preferable methods where there is no heating, or thermal separation involved in the processes. Since the process does not require any heating elements and purely physical

processes, hence membrane separations are considered as low energy separation processes. The most popular separation process in industries with the widest application, distillation, however, involve a lot of energy as thermal energy is consumed to separate the products.
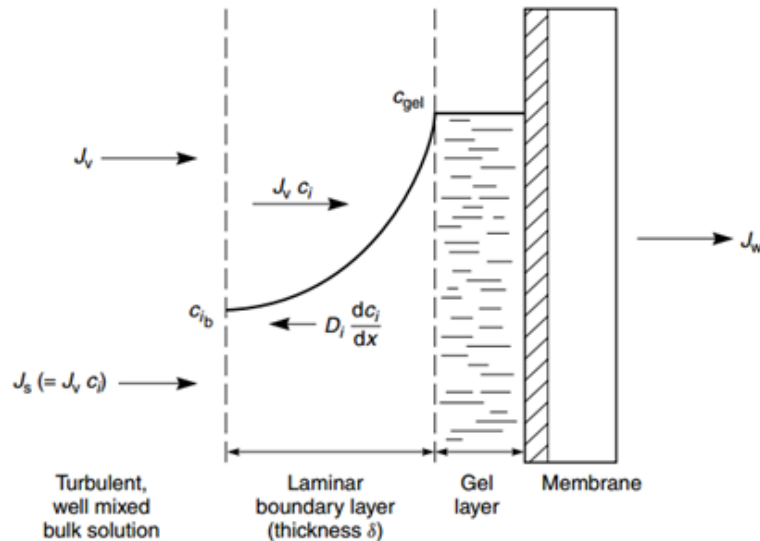
Figure 2.1 Gel layer of colloidal material deposited on the ultrafiltration membrane (Baker, 2004)

2.2.2 Applications

There are broad applications of membrane separations in the process industries. Membranes neither acts as primary separation mechanisms nor enhance by-products of the process. For example, selectively permeable membranes can be used to separate the constituents of azeotropic mixture for which thermal distillation cannot. Also, membranes are widely used in the production of drinking water and wastewater treatment. This technology also being implemented in the food technology, biotechnology and pharmaceutical industries. High demand of the membrane modules expects to have market growth around 8% annually to reach 25 billion USD in 2018 (Sutherland, 2004).

2.2.3 Defouling Mechanisms

The separation mechanisms of membranes are distinguished by four types of operational driving force. The driving force could be pressure driven, concentration driven, electric potential gradient driven, or temperature gradient driven. Pressure driven are always associated with the microfiltration, ultrafiltration, nanofiltration and

reverse osmosis. Concentration driven are associated with the dialysis, pervaporation, forward osmosis, and gas separation (Sutherland, 2004). Conventionally, smaller membrane pore size would block the macromolecules from the solutions and form filter cake on the membrane surface.

2.2.4 Factors Affecting Membrane Fouling

Zhao & Yu, (2014) summarise the general likelihood for membrane fouling. The fouling occurs due to the formation of a dynamic membrane wherein ultrafiltration fouling occurs predominantly on the membrane surface area. Also, depositions of proteins within the pores structure in microfiltration have reduced the effectiveness of membrane surface porosity. Fouling also occurs at the pore entrance to obstruct the pore entrance to preventing and reducing the separation efficiency. Zhao & Yu, (2014) and Balmann & Nobrega, (1989), listed the following factors which contribute membrane fouling:

- Concentrations pH and Ionic Strength
- Component Interactions
- Membrane Material
- Pore Size
- Porosity and Pore Size Distributions
- Physio-chemical properties
- Transmembrane Pressure
- Temperature
- Cross-flow velocity and turbulence promoters

2.3 Filtration Membrane: Defouling Methods

2.3.1 Hollow Fibre Membrane Oscillations

Gac & Gradoń, (2014) are the first to adopt a method to prevent colloidal fouling using membrane oscillation by bulging the membrane. Numerical methods simulated forcing the deposited particles into motion to decrease the formation of the agglomerate structure. The detachment of a particle can be seen as a result of a collision with the oscillating bulge. Gac and Gradoń concluded that placing an oscillating magnetic field and a hamper bulging would facilitate the detachment of the deposited particles better.

Later, they found that cross-section characteristics of the hollow membrane might lead to the oscillation of whole fibre membrane. It is observed that the application of membrane oscillations reduces the packing density of the filtration cake. The amplitude of the oscillations and the flow rate of water play the important role to influence the dynamics, packing density, and final equilibrium value. This mechanism, however, is considered nearly independent of the physicochemical parameters of the particle, membrane, solution and electrical potential itself.

The oscillations of the hollow fibre prevent the colloidal fouling due to their interaction with the oscillating of the external field and mechanical oscillations. The mechanical oscillations could be caused by the membrane module shaking by which have the same manner of defouling as the oscillating external field at a frequency above 100 Hz. The simulations also show that lower flow rate per fibre length results in lower final packing density. To achieve final packing density less than 0.2, frequency of less than 1000Hz is needed with 0.25 flowrate per fibre length while the flow rate of 0.75 cm^3/s/m needs the frequency of more than 20,000Hz.

2.3.2 Electrochemical Generations of Nanobubbles

Nanobubbles for the prevention of fouling

The development of this method to prevent the fouling of the membrane is the same as the other methods which to maintain the surfaces of membrane free of proteins or cakes formation. Instead of keeping the surface clear for maximum membrane operational conditions, Wu et al., (2008) believed the combination of electrochemical methods would prevent bacterial growth. This approach is also being compared with the ethanol-water exchange method for the production of nanobubbles. It is not preferred, however, as the nucleation of the supersaturated gas is hard to regulate.

The nanobubbles able to prevent the fouling on the surface of the membrane and at the same time ensure the removal of protein which already has been fouled within the membrane. The fouling prevention is achieved by covering a surface with nanobubbles. In the experiment tested by Wu et al., (2008) shows that sample of Bovine Serum Albumin (BSA) packing size is decreased as the formation of the physical barrier by the nanobubbles against the adsorption into the pores.

Electrochemically, high density of nanobubbles would be formed on the surface results in the protein adsorption prevention.

Defouling using nanobubbles

Figure 2.2 shows the mechanisms of the nanobubbles defouling by forming nanobubbles on the surface electrochemically using conductive properties of the substrate. Wu et al., (2008) divided the mechanisms into three main stages where; stage 1: Protein (BSA) Adsorption; stage 2: Electrical Treatment; and finally stage 3: Nanobubble Defouling. As shown in the **figure 2.2**, the protein is adsorbed to the solid-liquid interface from its bulk solution. Since the substrate is used as working electrode to produce nanobubbles, hence the bubble formed under the layer of protein.
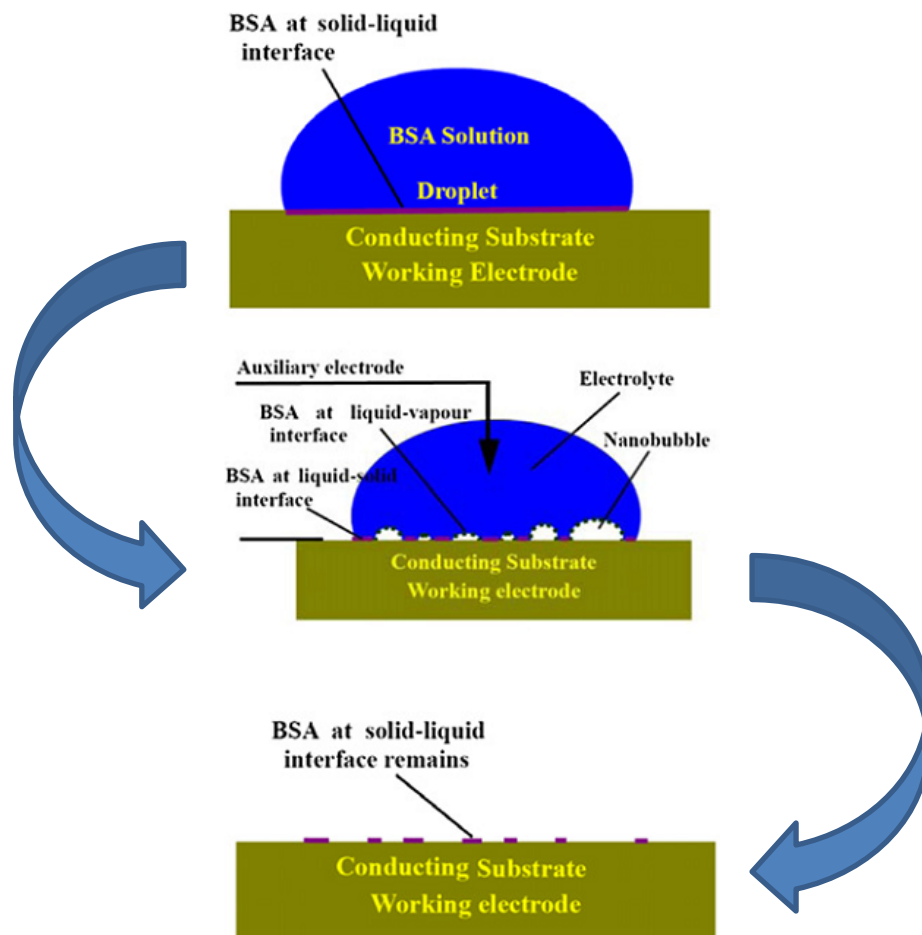
Figure 2.2 Defouling Mechanisms by Nanobubbles (Wu et al., 2008)

The bubble formations create liquid-solid interface and liquid-vapour interface between the nanobubble and proteins as well as between nanobubble and substrate. The nanobubble growth enforces the protein molecules to migrate from solid-liquid interface to the liquid-vapour. Once the protein is adsorbed into the liquid-vapour interface, nanobubbles containing the protein are forced to detach from the solid-liquid interface. The removal of the proteins are observed where the electrochemical desorption of adsorbed protein present is in the nanobubbles formation.

2.3.3 Ultrasonic Cleaning or Ultrasound

Commercially, polyamide based reverse osmosis membrane uses ultrasonic cleaning to remove the fouling during the cross-flow filtration of carbon sulphate. Feng, van Deventer, & Aldrich, (2006) investigate the effect of ultrasound to defoul the membrane specifically in terms of permeate flux, with no loss in rejections. The data compiled by them shows the permeate flux increase in the presence of sonication while filtering calcium sulphate and iron chloride. It is recorded that approximately 50.8% and 69.7% of permeate flux increment for 500mg/L and 1000 mg/L calcium sulphate solution respectively in the presence of ultrasound during three hours filtration time.

The ultrasonic effect also shows that the permeate flux increased by about 215% for a $FeCl_3$ solution with 20 mg/L Fe^{3+} during three h of filtration in the presence of ultrasound. The permeate flux increased by approximately 264% and 113%, respectively, for a 500 and 1000 mg/L CMC solution during three h of filtration in the presence of ultrasound. The figure below shows the difference of permeate flux over the filtration time of $CaSO_4$ and $FeCl_3$ solutions (Feng et al., 2006).
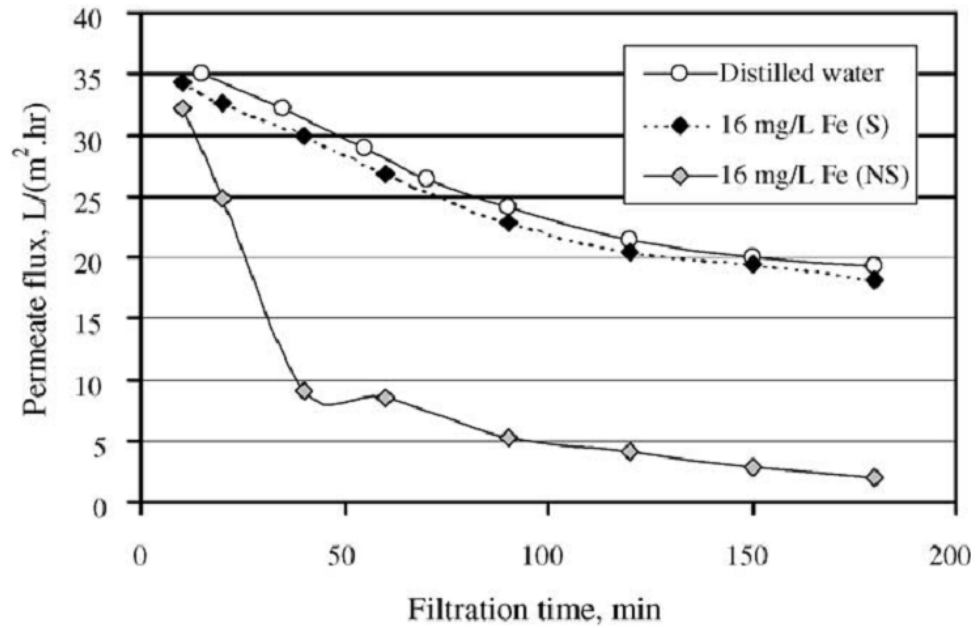
Figure 2.3 Effect of ultrasound on the permeate flux of membrane filtration for a FeCl3 solution. S and NS indicate sonication and sonication (Feng et al., 2006)

The **Figure 2.3** shows that the permeate flux for the membrane filtration of the FeCl$_3$ solutions is almost identical to the distilled water in the presence of sonication. According to Feng, van Deventer, & Aldrich, (2006) the average flux increased by about 215% during 3hours of filtration. The same concentration of the FeCl$_3$ solution which is 16mg/L is used to observe the effect of the sonication and the trends show a fluctuation of permeate flux at the minutes of 40 for the solutions without sonication. The presence of the ultrasound avoids Fe(OH)$_3$ flocs from being deposited on the membrane surface. Apart from losing some of the flocs, the membrane surface remained undamaged during the sonication process. The morphological analysis has been carried out to support the results of the experiments.
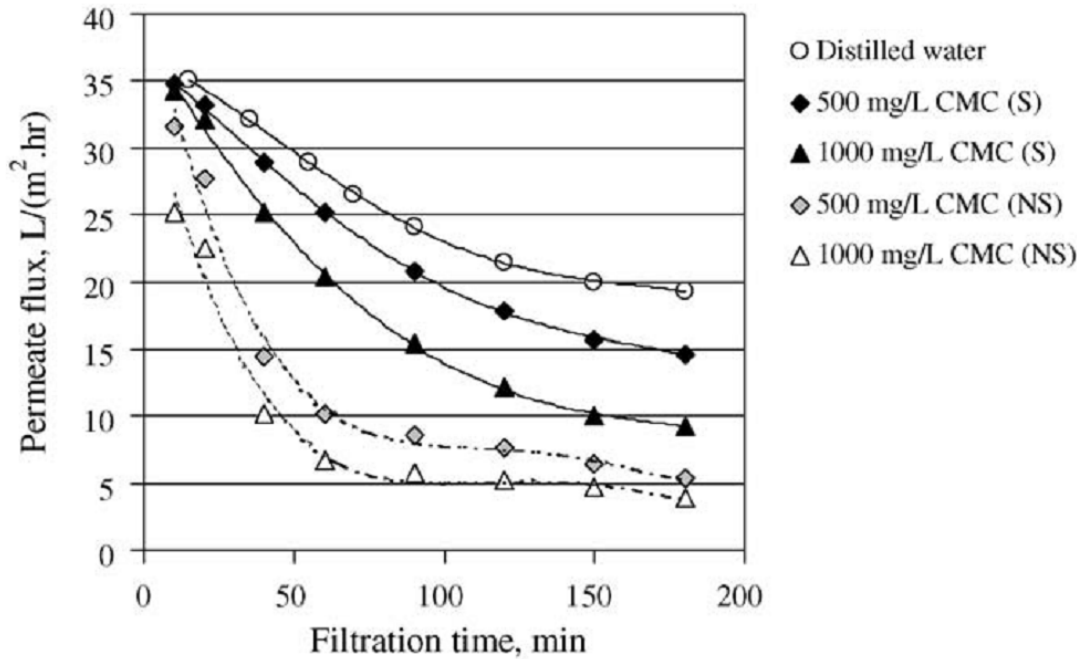
Figure 2.4 Effect of ultrasound treatment on the permeate flux of membrane filtration for CMC solutions. N and NS stand for Sonication and No Sonication (Feng et al., 2006)

Apart from the $FeCl_3$ solutions, the sample of carboxymethyl cellulose (CMC) also being prepared at two different concentrations to observe the effect of the ultrasonic irradiation on the permeate flux. Apparently, a higher concentration of the solution results in lower permeates flux. However, in the presence of the ultrasound, the permeate flux for both concentrations are lower in the presence of the ultrasonic. The permeate flux of the 1000mg/L CMC concentration even higher than 500 mg/L CMC concentration (no sonication) in the presence of ultrasonic.

2.3.4   Using Polymer Beads Containing Magnetic Micro Particles

The experimental carried out by McLachlan, (2010) used encapsulated SA hematite into Poly Acryl Nitrile (PAN) beads to see whether the magnetic bead system could be used to clean membranes in commercial plants. First, the PAN magnetic beads are prepared, and then magnetic fields are configured to magnetise the hematite pole. McLachlan using five types of magnetic field configurator which are; the E core field magnetic, black magnets, rotating magnet, and pump magnet. The motion of the pole beads appeared to be sufficient for cleaning purposes due to the wet flat surface of the PAN beads.

Three procedures have been carried out for the low-pressure fouling layer and to clean the filtration experiments. The procedures used for the experiments which to clean the fouling is by flowing beads and a finite Transmembrane Pressure (TMP) (yeast), at zero TMP, and Reverse Osmosis (RO) cleaning at zero TMP. At finite TMP, no significant cleaning has been overserved; likewise, at zero TMP beads, membrane fouling can be avoided. However, beads do not continuously keep membranes from fouling at zero TMP because magnetic beads could only partially clean the membranes. The materials or foulant in the pores which are firmly bonded to the surface have not been removed.

Table 2.1 The permeate conductivities of 500ppm salt solution with and without cleaning (McLachlan, 2010)

Conductivity Readings (μS)	Permeate	Feed	Rejections %
3 times fouling, 2 times cleaning, 500ppm salt at the end	274	1489	81.5
3 times fouling, 2 times cleaning, 500ppm salt at the end	269	1390	80.6
2 times fouling, 2 times cleaning, 500ppm salt at the end	203	1408	85.5
2 times fouling, 2 times cleaning, 500ppm salt at the end	199	1456	86.3
Control 1 (membrane conditioning and 500ppm NaCl addition)	198	1460	86.4
Control 2 (membrane conditioning and 500ppm NaCl addition)	181	1401	87.0

As the objective of the experiment carried out by McLachlan is to provide the chemical-free cleaning, the results from the data collected shows positive possibility but are not practical in the spiral wrap membrane. Also, to run the experiment at zero TMP, large AC magnetic is required which is concluded to be not cost effective. Unfortunately, no enhanced flux is observed for a lightly fouled RO membrane. Experiments also showed that an enhanced flux for a badly fouled RO membrane cleaned by rotating beads was obtainable but that the resulting flux has been similar to that obtained for a lightly fouled membrane. This plus the SEM images allow one to conclude that while the beads can remove thick, flaky layers, they are incapable of removing the well bonded initial scaling layers (McLachlan, 2010).

Table 2.2 Membrane defouling comparison by effectiveness, costing and time

Membrane Defouling Methods	Advantages	Disadvantages	Reference
Hollow Fibre Membrane	100% defouling at ten kHz but could be unrealistic	Approximately zero defouling at low frequency High packing density fluctuation	(Gac & Gradoń, 2014)
Electrochemical Generations of Nanobubbles	High defouling by careful control of voltage. Cheap Defoul 26-34% in the 20s	Difficult to determine the bubbles, which produced between the surface and protein film. The film concentration would increase in case of evaporation.	(Wu et al., 2008)
Ultrasonic	Increase 264% permeates flux*. Membrane surface remained undamaged.	Less efficient for solution with higher concentration and viscosity	(Feng et al., 2006)
Using Polymer Beads Containing Magnetic Micro Particles	Sufficient cleaning using pooled beads on dry or wet flat surface	Defouling is only conducted at zero TMP Only partially clean membranes leaving the material in the pores No cost effective studied	(McLachlan, 2010)

2.4 Cleaning (defouling) with microbubbles

2.4.1 Filtration Membrane

The classes of filtration membrane (MF, UF, NF, RO) defouling using microbubbles and two-phase flow are reviewed. **Table 2.3** shows gas sparging using various types bubble flow patterns for three types of membrane modules: flat sheet, tubular and hollow fibre. The flat sheet membrane type is the most commonly studied type for

research findings collected concerning defouling the membrane using bubbly flows. It is also has the highest maximum flux enhancement compare to tubular and hollow fibre membrane classes. There are many air sparging units installed to clean spiral-wound membranes, however, the flow pattern is not clearly stated apart from the research reported by Genesysro.com (2017). Therefore, this research focuses on defouling spiral-wound RO membranes by injections of microbubble clouds to remove the blocking foulants in the membrane pores.

Table 2.3 Overview of research using microbubble flow to enhance membrane processes adapted from Wibisono et al. (2015)

Membrane Material	Channel width or diameter	Module and flow orientation	Feed Suspension	Liquid Rate	Gas Rate	Max. enhancement	Refs.
Flat Sheet Membranes							
Polysulfone (PSf)	2 mm	Upward vertical	BSA-lysozyme mixture	0.5 L/min	0 - 0.1 L/min	450% (MTC)	(Mercier-Bonin et al., 2004)
Polypiperazineamide (PPA)	5 mm	Upward vertical	Stabilized & non- stabilized oil-in-water emulsion	0 - 0.4 m/s	0 - 1 m/s	240% (Flux)	(Ducom, Matamoros, et al., 2002)
Not stated	5 mm	Upward vertical	Clay Suspension	0.08 - 0.24 m/s	0 - 0.4 m/s	110% (Flux)	(Ducom, Puech, et al., 2002)
Polyamide in (PSf)	5 mm	Upward vertical	Electrolyte	0 - 0.24 m/s	0 - 0.4m/s	Not Stated	(Ducom et al., 2003)
Not stated	2 mm	Horizontal	Yeast Suspension	0.1 - 0.5 m/s	0.02 - 0.08 m/s	15% (Flux)	(Hwang & Hsu, 2009)
Not stated	1 mm	Horizontal	Polymethylmethacrylate (PMMA) suspension	0.1 - 0.5 m/s	0.049 m/s	30% (Flux)	(Hwang & Hsu, 2009)
Mixed cellulose ester	Not stated	Horizontal	Polymethylmethacrylate (PMMA) suspension	Not available	0- 0.054 L/min	400% (Flux)	(Hwang et al., 2010)
Not stated	Not stated	Horizontal	Yeast/BSA suspension	0.1 - 0.5 m/s	0 - 0.06 m/s	200% (Flux)	(Hwang & Chen, 2010)

Not stated	600 mm	Upward vertical	Activated Sludge	Not available	1.2 – 9.6 L/min	Not stated	(Yamanoi & Kageyama, 2010)

<div align="center">**Tubular Membranes**</div>

Polyvinilidenediflouride (PVDF)	12.7 mm	Upward vertical	HAS-dextran mixture	1 L/min	0.0067 – 0.5 L/min	HAS: 75% (Rejection) Dextran: 100% (Rejection)	(Li et al., 1997)
Carbon	6 mm	Upward vertical	Ferric hydroxide suspension, dextran solution, wastewater effluent	2 m/s	0 – 3 m/s	70% (Rejection)	(Vera, Delgado, et al., 2000)
ZrO₂	6 mm	Upward vertical	Ferric hydroxide suspension, wastewater effluent	3 m/s	0 – 3.7 m/s	150% (Flux)	(Vera, Villarroel, et al., 2000)
Al₂O₃	6 mm	Upward vertical	TiO₂ suspension	0.5 - 4 m/s	0.2 – 3 m/s	90% (Flux)	(Pospíšil et al., 2004)

<div align="center">**Hollow-fibre membrane**</div>

Polyvinilidene difluoride (PVDF)	40 mm	Upward vertical	Biologically treated wastewater	3.3 L/min	0 – 5.3 m/s	Not stated	(Yu et al., 2003)
Polypropylene (PP)	0.39 – 1.8 mm	Upward vertical	Yeast suspension	Not available	2 – 10m/s	Not available	(Wicaksana et al., 2006)
Polyvinilidene difluoride (PVDF)	0.3 mm	Upward vertical	Yeast suspension	Not stated	0.05 – 0.15 L/min	Not stated	(Lu et al., 2008)
Polyvinilidene difluoride (PVDF)	0.85 mm	Upward vertical	Raw water	Not available	16.67 – 125 L/min	Not stated	(Tian et al., 2010)

2.4.1.1 Microfiltration (MF)

Wastewater technology has developed many types of the filter elements for wastewater processing. MFs are among popular filter types used in this process because of its ability to eliminate particulates and colloidal matters. However, the

biggest problem of MF is that the fouling rate is considerably high and difficult to control. These challenges are always associated with secondary effluents which contain small particles or colloidal foulants such as Extracellular Polymeric Substance (EPS) and Soluble Microbial Products (SMP).

Lee et al., (2014) studied the influence of microbubbles in the physical cleaning of MF membranes compared to a standard aeration system. Plate and frame type of polytetrafluoroethylene membranes with 0.45 μm pore size are cleaned using the microbubble size ranging from 10-200μm. Two equally fouled membranes with a transmembrane pressure of 40kPa are cleaned using two different flow rates, which are 30L/min for typical bubble and 3L/min of microbubbles. The cleaning efficiency between two types of bubbles is calculated using the pressure values and flux using the equation below, where R_t, R_T, and R_m are total resistance, total resistance after cleaning, and inherent membrane resistance in the unit of (1/m).

$$\frac{R_t - R_T}{R_t - R_m} \times 100$$

Equation 2.1

The experimental results showed that efficiency of microbubbles in cleaning has been observed to be twice as high as that of aeration by examining the Total Organic Content (TOC) concentration of the membrane tank after the treatment. The membrane surfaces that are analysed by FTIR device shows membranes cleaned by microbubbles had the smoothest surface. This leads to losses in the gel layer structure. The cleaning performance of microbubbles have been observed after 60minutes of the cleaning cycle. The efficiency of the cleaning is ~25% and 40% for fine bubbles and microbubbles respectively at the end of the cleaning cycle which is 180 minutes.

2.4.1.2   Nanofiltration (NF)

Fouled NF is usually mitigated by installing the ultrafiltration (UF) pre-treatment. However, it is no longer efficient according to the market analysis as the UF are not able to remove many of the dissolved organic compounds. Wibisono et al., (2015) studied the shear force induced by generating microbubbles to remove biofilms and determine its influence on the gas/liquid ratio. Their research found that bubbles

formed at a gas/liquid ratio of 0.5 incorporate microbubbles that are easier to identify due to the level of elongation in the flow direction. As they further increased the gas/liquid ratio, elongation was avoided, therefore, the cleaning efficiency increased. The removal efficiency, however, increased with increasing of the rising bubble velocity which is responsible for higher shear forces on the surface of the membrane.

2.4.1.3   Reverse Osmosis (RO)

This membrane is commonly associated with desalination and fresh water applications, for example purification of drinking water using a semipermeable membrane. Many advantages of the RO membrane are limited due to the fouling rate of the process which is explained in the membrane subchapter. Chesters et al., (2013) started the research in cleaning RO membranes using 99 completely fouled and failed seawater RO membranes by using microbubbles. The study concluded that the most common problem causing the membrane failures are biofouling, oxidation, metal oxide, abrasion, clay and mineral scale. Further research by Peña et al., (2012) reviewing over 500 autopsied membrane elements established that once the scale starts on the membrane surface, the failure of the membranes is almost irreversible.

Using microbubbles to clean RO membranes is one of the many approaches to decreasing the higher fouling rate in the RO wastewater plant. In 2013, Maqsood Fazel presented at the International Desalination Association (IDA) in China, stating that membrane cleaning was further improved using effervescing compounds to remove foulants compared to conventional cleaning methods. Fazel & Chesters, (2015) agreed that the microbubbles which are circulated in cleaning solutions would increase the turbulence on the membrane surface. The shear forces created agitate and dislodge the foulant on the membrane surface giving greater removal and reducing the treatment period.

Figure 2.5 shows how the RO membranes are cleaned using four types of cleaning approaches where only one used microbubbles. 1-2% of powdered acid and alkali at a temperature of 20-25°C and 35-40°C respectively are used as conventional cleaning agent at the beginning of the experiment. Meanwhile, two types of new cleaning agents which are mild acid and alkali are introduced to compare the cleaning performance. The microbubbles are then added the conventional alkaline cleaning agents which

improved the cleaning efficiency. Fazel et al., (2013) demonstrated that this modified conventional cleaning agents produces a large number of microbubbles. Despite this increase, they found that the bubble size was inconsistent. Fazel and co-workers introduced two types of mild acid and alkali that led to a reduction in microbubble size hence, alleviating inconsistent bubble size.

Key
Valve V1 = Valve in CIP line
Valve V2 = Bypass valve for inlet to Microbubble Genairator
Valve V3 = Bypass valve for outlet from Microbubble Genairator
Valve V4 = Air control valve for Microbubble Genairator
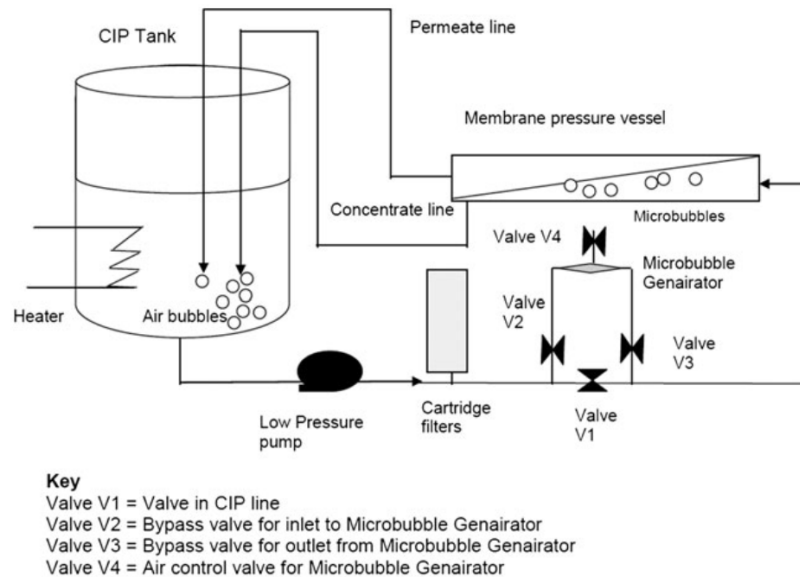
Figure 2.5 Schematic for the CIP microbubble generator for RO membrane cleaning (Fazel & Chesters, 2015)

The benchmark flux has been reduced from 544 gallons per minute (GPM) to 484GPM after one year of the process, then successfully increased to 531GPM using microbubbles. The results showed that microbubbles can significantly improve the membrane cleaning efficiency over the conventional cleaners (Fazel & Chesters, 2015). Using microbubbles to aid the cleaning agents to defoul the membrane is promising as the microbubbles would cause minimal or no damage to the membrane surface, have a higher cleaning rate, are easily applied to most kinds of membrane, and are cost effective to implement. In this study, microbubble generation using fluidic oscillation is expected to reduce production cost which results in higher cleaning efficiency from high-frequency generated microbubbles (Zimmerman, Tesar, et al., 2011).

2.4.2 Biofilm Detachment

Biofilms sometimes can be beneficial but mostly bring more harm than good in the certain industries, especially the water sector. The undesired deposition of a group of microorganisms (biofilm) on a solid surface such as a membrane always causes higher filtration pressure and low flux which increases the operational cost. Preventing the formation of biofilms has the potential to increase the overall process efficiency where chemicals such as chlorine and sodium hypochlorite are among the popular agents that have been used for decades. In recent years, chemical free biofouling mitigation like ultrasonic waves has been preferred and categorised as an eco-friendly technology.

Removing biofilms using chemical free methods such as ultrasonic and pressure waves are favourable as they are non-invasive approaches to remove the blockage caused by biofilm. Agarwal et al., (2012) applied the main features of dissolvable microbubbles which can shrink and subsequently collapse. The collapse generates pressure waves and radicals - a chemical free leaning technology for membrane cleaning. Mixed-species of microorganisms are cultivated on $0.2\mu m$ nylon pores membrane and are cleaned using microbubbles of diameter $5\text{-}10\mu m$. The self-collapsing microbubbles achieve 88% of biofilm detachment. The experimental results are compared to the detachment using Sodium hypochlorite, NaOCl, which 0.5% lower regarding fixed biomass, extracellular polysaccharides and protein removal.

Agarwal, Ng, & Liu, (2011) summarised two main potentials of a bubble in biofilm and algae detachment. It is found that continuous bubbling would be more effective than intermittent bubbling to scrub the membrane surface during filtration. It is observed that the smaller bubbles are more efficient to reduce fouling and formation of concentration polarisation. Not only in water industries, but biofilms also develop in human physiology which cause further health problems as they are inherently resistant to the most antibiotics (Costerton et al., 1999). Modjarrad & Ebnesajjad, (2014) explained that cavitation microbubbles are able to destroy biofilms nearby and allow small molecules such as vancomycin entrance for antibacterial activity.

2.4.2.1 Cell Culture

Conventional cell culture are explained by Penman (1966) & Eagle (1959). These authors stated that the serially propagated cell may be grown adherent to a glass

surface and overlaid with a fluid medium. The cell line culture is started by aspirating the old media out then followed by washing them out using a sterile salt solution such as Phosphate Buffer Solution (PBS). Preheated trypsin EDTA at ~37°C are then added to cover the cell for the purpose of detachment. The trypsinised cell are then incubated for few minutes in order for the enzyme to act and ensure all the HeLa cells have detached. This method which also outlined by Cantwell (2018). The method suspends detached cells by centrifugation then resuspends the cells from the trypsin for cell counting. The cell counting is very important to keep control the cell density at the beginning of the research as well as the control variables of the experiment.

2.4.2.2   HeLa cell: Morphology and Properties

On October 8, 1951 a patient name Herietta Lacks, a poor citizen from Baltimore died due to cervical cancer. HeLa is a derivative name of late Henrietta, as before she died, the cell line are derived from her and been exploited for a number of research. Nowadays, the immortal cell line has been one of the most famous cell line studied for vaccines, protein synthesis, intoxication, and biomechanics driven research (Liu et al., 2018; Borin et al., 2017; Tatalick et al., 2005; Basu et al., 1999) . **Figure 2.6** shows the general morphology of the HeLa cell line.
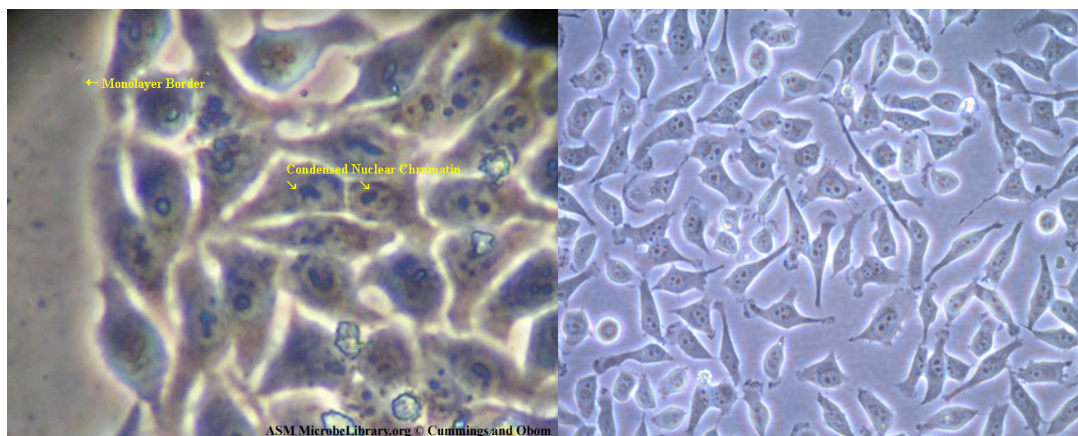
Figure 2.6 Morphology of HeLa Cell (Cummings & Obom, 2007; 'Expressing HeLa Cell Line')

Spotting the morphology of the HeLa cell could be challenging under microscope, **Figure 2.7** shows the cell cultured by Amini et al., (2016) for about 3 days. Under 24 hours of well-maintain cell culture at 35°C in the incubator as well as right density at the beginning, the healthy HeLa cell will be starting to be divided. The cell then will consume more media and within 48 hours, the culture flask will be more than 75%

confluent. At this stage, the gap between the cells started to be filled. Within 72 hours, the cell should be confluent and there is no gap found between the cells.
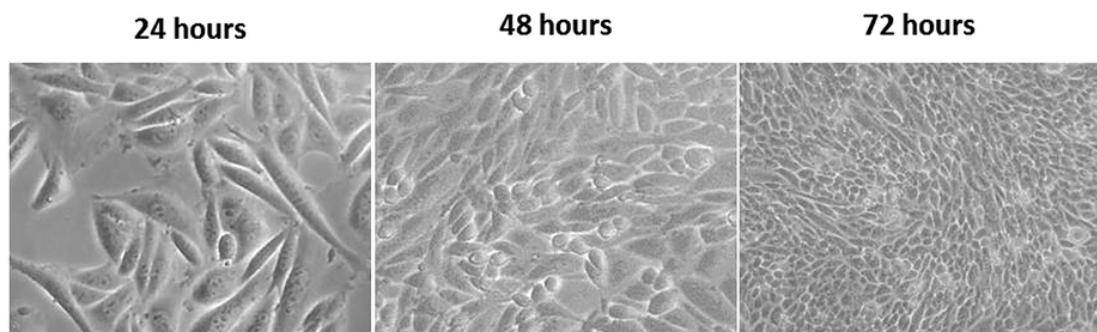
Figure 2.7 Control HeLa Cell Culture (Amini et al., 2016)

Celeromics through their website provided the details and general properties of the HeLa cell as shown in **Table 2.4**. The information tabulated provides an overview on the size, type and applications of the cell. The size of the cell, which is ~ 10-20microns in diameter, would help further the researcher to confirm the morphological shape of the cell. In this research, the type of the cell which is adherent, is the main reason why this cell is chosen in the first place. HeLa cell grew and adhered on the surface of the microscope slide will be used to study the cell detachment rate using non-destructive method by using the microbubble. The influence of microbubble flow enhanced the bacterial and cell line detachment, which benefits various industries including environmental and medical applications which is mainly inspired by (Agarwal et al., 2012; Sharma et al., 2005)

Table 2.4 HeLa Cell General Properties (Cantwell, 2018)

Size	10-20 microns diameter
Type	Immortal adherent cell
Applications	Transient transfection
	Cancer research
	Toxic research and radiation
	Gene mapping
	Photodynamic therapy
	Ribonucleic Acid (RNA) markers

Growth Media	High Glucose – Dulbecco's Modified Eagle's medium (DMEM) + 10% Fetal Calf Serum + 1% Antibiotics

2.4.2.3 Algae Culture: Morphology and Properties

2.4.2.3.1 Chlamydomonas Algae

Chlamydomonas exist in freshwater, seawater and even in snow. The green algae are circular in shape with green colour under microscope. **Figure 2.8** shows a cross-sectional diagram of the Chlamydomonas which showing main part of the cell such as flagella, head eye or stimulant, and pyrenoid. A single-cell usually size of 10μm in diameter where the cell wall made of hydeoxyproline-rich glycoproteins (Adair & Appel, 1989). This microalgae is phototrophically grown by consuming CO_2 and converts it to sugar and O_2 in the presence of light (Taghavi & Robinson, 2016).
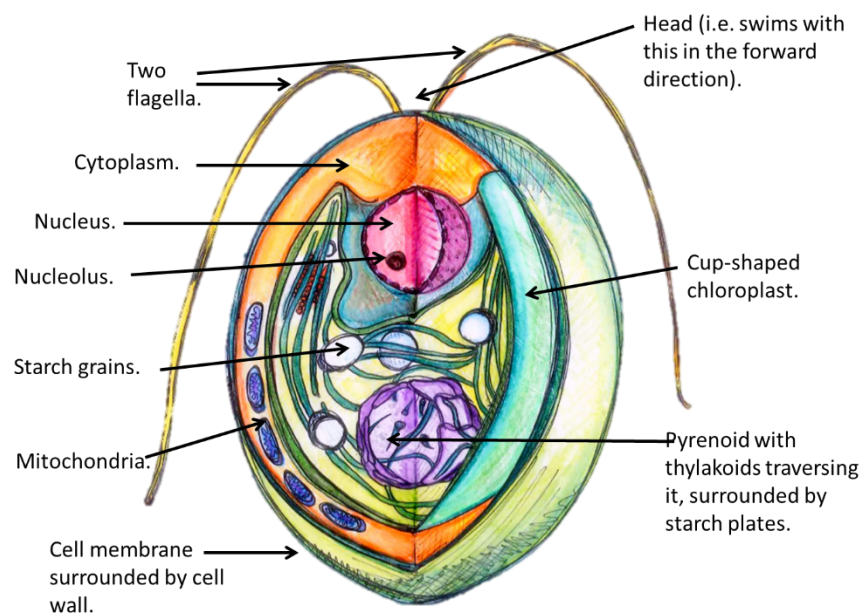
Figure 2.8 A 3D labelled cross-sectional diagram of Chlamydomonas cell (Griffith et al., 2013)

The application of Chlamydomonas has been exploited in many ways such as biosensing, water treatment, genome studies and even biofuel. **Table 2.5** summarised the applications of the Chlamydomonas in biosensing, water treatment, biofuel and so on. Using algae as biofuel nowadays is very popular, Oncel & Vardar-Sukan, (2011)

found that the potential of hydrogen production using algae would now be scale up as large scale of generation of electricity using microalgae.

Table 2.5 Applications of Chlamydomonas

Bio-sensing	(Gong et al., 2018)
Water treatment	(Khataee et al., 2009)
Biofuel and renewable energy	(Klassen et al., 2017; Taghavi & Robinson, 2016; Wirth et al., 2015; Oncel & Vardar-Sukan, 2011b; Mussgnug et al., 2010)
Photocatalyst	(Rao & Pennathur, 2017)
Protein production	(Shamriz & Ofoghi, 2017; Auger et al., 1988)

2.4.2.3.2 Disadvantages of Algae

Microalgae are very popular to cause the ecological problems towards environment. **Figure 2.10** shows the water contain algae that is harmful to humans and animals. Every environmental ministry around the globe has recognised the problem of algal bloom and eutrophication, and to be tackled seriously.
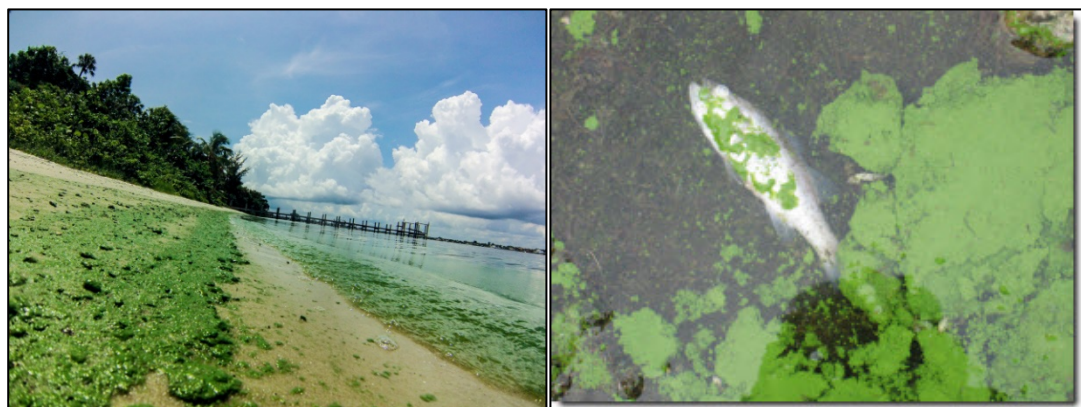
Figure 2.9 Major disaster caused by microalgae bloom ('The Effects: Environment', 2017; Sorentrue, 2016; Figurski & Shockley, 2009)

Without proper mitigation plan, microalgae bloom could cause all the impacts as shown in **Figure 2.10**. The thick layer of microalgae at the surface of water would

block the photosynthesis of aquatic trees and plants (Taft, 2015). According to Heisler et al., (2008) and Institutions & Ships, (1952) stated that the impacts of microalgae bloom has significant effect on reducing the efficiency of propulsion of ships as well as causing water contamination due to bacterial growth within the regime. In this research the potential of microbubble in cleaning have been studied upon the removal of Chlamydomonas algae from surface.
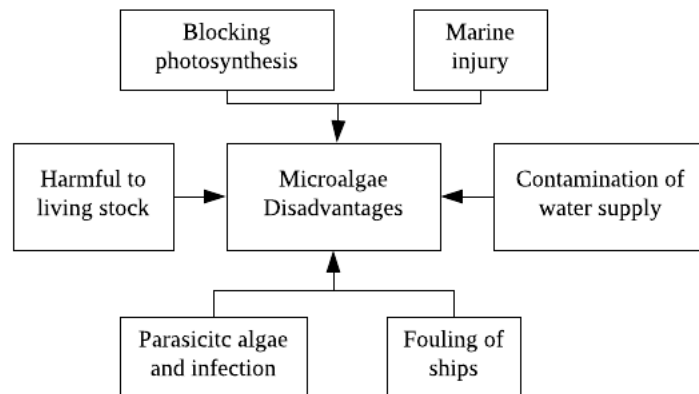
Figure 2.10 Various disadvantages of overgrown and uncontrolled growth of microalgae

2.4.3 Degreasing of Solid Surface

Grease, oil and fat are easily deposited on solid surfaces and bring a lot of impacts to domestic and industrial networks. Southern Water in the UK reported that the grease caused the blockage in wastewater pumping stations and sewers costing more than £15million annually for cleaning process. There are many methods for degreasing found to be environmentally friendly but less optimum regarding separation efficiency, uniformity, and throughput. A study of observing grease adsorption capability to bubble interface has been carried out using microbubbles generated by alcohol. The study used a microbubble size range of 100μm or less with the addition of specific additives at a temperature between 20-70°C found to be effective in bubble cleaning (Miyamoto et al., 2007).

Miyamoto et al., (2007) explained grease removal using three simple steps. The microbubble produced first is adsorbed onto the oil surface and stays for some duration and eventually the oil coats around its interface. The bubbles collide with each other, eventually coalescing to a size where buoyant forces detach them from the surrounding

of oil, rise while dragging the coated oil, and finally burst at the water-air surface, forming an oil layer above the water layer. The oil layer can be readily removed by flow over the weir. The greater flux of microbubbles will provide more surface area and higher removal efficiency as a small bubble is observed to adsorb and accumulate a greater portion of grease molecules. The **Figure 2.11** below shows striking grease removal efficiency using microbubbles by a factor of 60 by comparison to conventional grease removal. The grease residual has been decreased to 20.5μg/cm^2 after 2minutes.
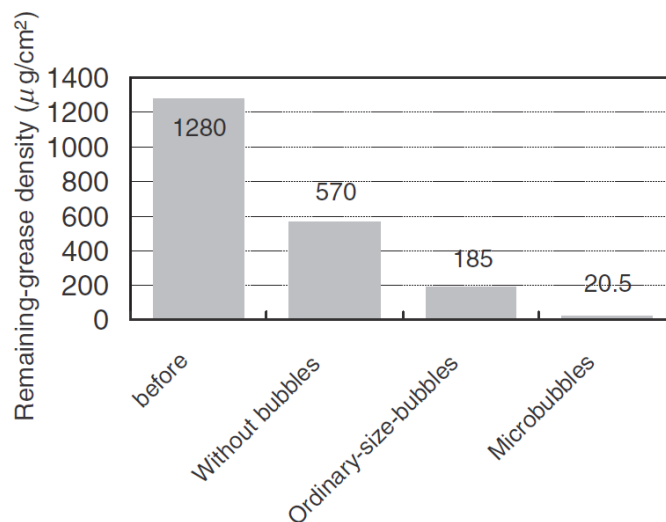
Figure 2.11 Hydrophobic Grease Removal Efficiency (Miyamoto et al., 2007)

2.4.4   Pipe Cleaning System

Piping is one of the most important features to transport and completing a process. Blockage in the pipeline is the main problem which would cause by the build-up grease, debris, or foreign objects contained in the transported fluid. It is important to keep the piping system cleared to ensure that the productivity and efficiency of the system remain high. Using microbubbles, Hiroyuki et al., (2010) studied pipe cleaning maintenance to remove lard oil, Jongseon et al., (2016) developed nuclear facilities piping cleaning system, Matsuura et al., (2015) clean polymer ink from the glass substrate. These applications have shown the potential of microbubbles to clean the membrane as it can clean and detach particles within piping systems.

The potential of microbubbles in pipeline cleaning systems is higher compared to normal water flows. Hiroyuki et al., (2010) found more lard oil removal using

microbubble flows. At time 300s of water flows, the difference between lard oil removal between non-microbubble and microbubble flow is recorded to be 80%. The lard oil removal which is registered by fluorescence intensity measurement showed that with higher Reynolds number, more removal is achieved, as shown in **Figure 2.12** below. The result shows that turbulent flow with microbubbles having the highest Reynolds number (Re=23000) number has the highest lard oil removal.
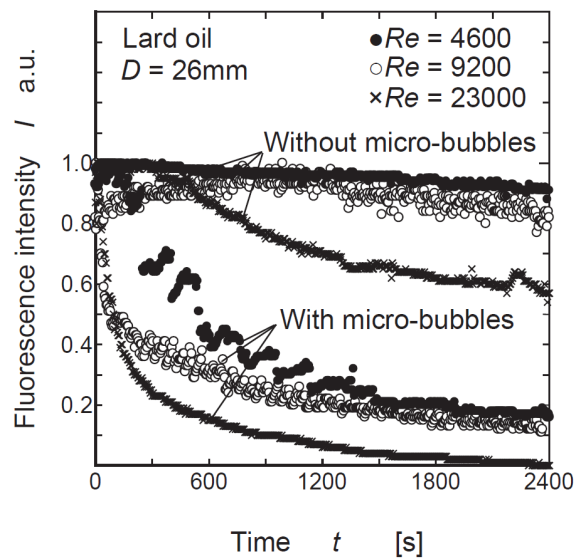
Figure 2.12 Change of fluorescence intensities on varying Reynold Numbers (Hiroyuki et al., 2010)

In piping facilities nuclear plants, radioactive sludge and corrosion products deposited on the inner wall of the pipe would increase the generation of secondary wastes. Jongseon et al., (2016) inject microbubbles along with the cleaners to decontaminate the spaces which are difficult to access as well as to prevent system damage. The average size of 20μm microbubble diameter has been used by adjusting the pH, temperature and concentration of different cleaning solutions. The experimental results confirmed that microbubble decontamination is higher than non-microbubble decontamination which is 2.4% and 1.7% respectively, so relatively ~40% improved.

2.4.5 Cleaning silicon wafer of a solar cell

Over time, deposition of layers of impurities on the silicon wafer surface of solar cells reduces the efficiency of the solar panel. Cleaning the wafer using microbubbles has advantages, as existing techniques such as cleaning using alkali and acid, ionised water, and mechanical cleaning create additional problems in waste disposal and

environmental impacts (Yoon & Lee, 2015). Cleaning the wafer surfaces in solar cells using microbubbles would reduce the water consumption and wastewater generated. The ozone microbubble cleaning system fabricated by Yoon & Lee, (2015) consists of loading, cleaning, rinsing, drying and unloading zones to investigate the cleaning rate using 3 levels of ozone concentration; 5ppm, 8ppm, and 10ppm. The usage of ozone and air microbubbles is compared as shown in **Figure 2.13** below. The experiments resulted in 99% percent removal efficiency using 10ppm ozone for 10 minutes.
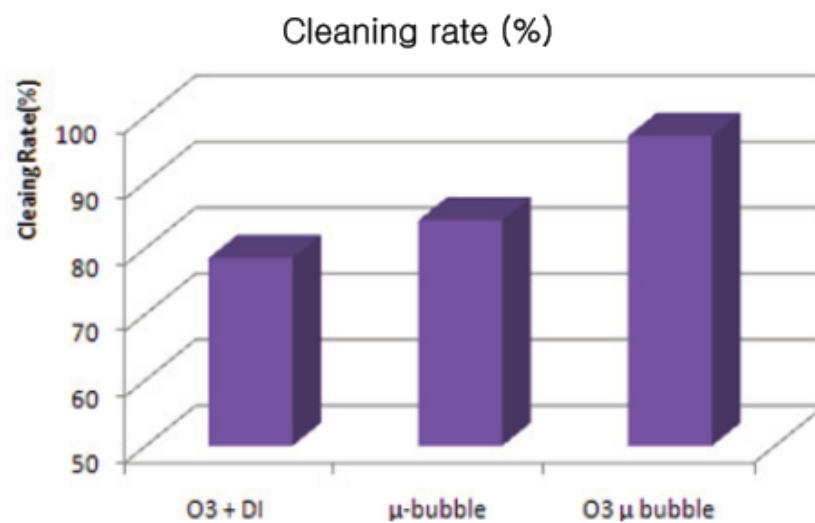
Figure 2.13 Comparison of the cleaning rate using distilled water formed microbubble, conventional microbubble and ozone microbubble (Yoon & Lee, 2015)

2.4.6 Dentistry (Cleaning Dental Plaque)

Commonly toothbrushes are used to maintain proper dental hygiene for a reasonably healthy person. However, this is impractical for sufferer's periodontal disease. The ordinary toothbrush encourages bacterial infection due to consequential bleeding of gums induced. It is important to remove dental plaque, which mainly consist of food residues to prevent the growth of bacteria. The principle of microbubbles as a cleaning agent with higher contact surface area between detergent and dirt is preferable as it is found to be a 'non-destructive' cleaning method. The keys performance of bubbles is always associated with smaller bubble produced which has larger surface area and longer retention time.

Lin et al., (2015) uses a cleaning device with five separate modified nozzles manipulating flow volume, velocity and diameter of the microbubbles. The dental plaques removal is used as a measure of the cleaning effect with microbubbles by comparing the colony counts of the control group. Results showed that more dental plaque was removed using a smaller nozzle diameter with smaller bubbles as compared to velocity. Approximately 60% overall plaque-removing efficacy has been achieved from this experiment, while 98% dental plaque removal is performed using smaller nozzle diameter.

2.5 Structure and Properties of Microbubbles

Many restrict the use of the term microbubbles to tiny spherical bubbles with diameter less than 50 microns, yet the term is appropriate to supra 1micron and submillimetre diameter ranges. Their physicochemical properties include low rising velocity in water, large curvature surfaces, high gas-liquid interfacial area, and an electrically charged gas-liquid interface. These electrically charged interfaces are typically associated with the microbubbles used for wastewater treatment processes (Khuntia et al., 2012). **Figure 2.14** shows the structure microbubbles, it consists of three layers from inside: inner gas core, aqueous film, and gas shell. The structure of the bubbles, however, can be modified by adding additional layers such as surfactants to decrease the rising velocity of the bubbles (Matsumoto, 2011). Many surfactants are being developed to stabilise the microbubbles (Dastgheyb & Eisenbrey, 2013; Wilson et al., 2013). Petroleum-based, biological surfactants, nanoparticles, pharmaceuticals and bioactive molecules have functionalised the microbubbles. It is proven that the smaller size of the bubble provides larger surface area and contributes to the high efficiency of the microbubbles in the industrial separation processes (Khuntia et al., 2012).
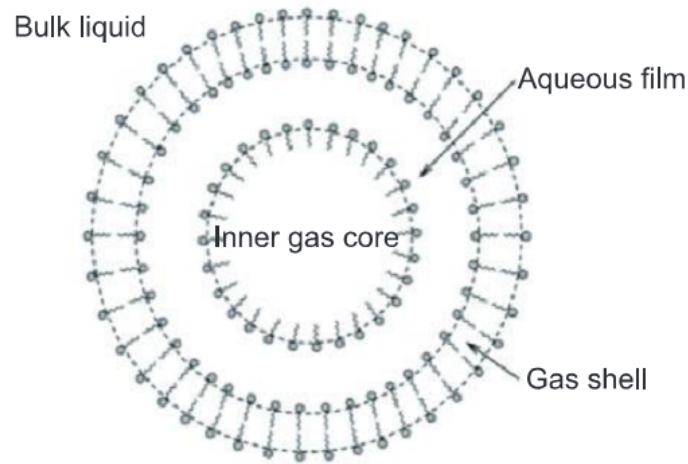
Figure 2.14 The Concentric-gas-sphere model of surfactant-stabilized microbubble (Khuntia et al., 2012)

2.5.1   Size and Shape

The microbubble, once generated has different behaviour in water in term of rising velocity, partial pressure, and flow direction, depending on how it is generated. It is important to keep the bubble size as small as possible specifically to have a higher cleaning efficiency. The smaller the bubble diameter, the more the increase in internal pressure of the microbubble. Eventually this increases the total surface area (**Figure 2.15)**. However, small bubbles released through a nozzle system subsequently grow into much larger bubbles due to rapid coalescence with conventional, steady flow of gas upstream of the injection nozzle. Zimmerman et al., (2008) stated that generating bubbles through the smallest aperture would be not sufficient. This is because of the random size and release intervals lead to rapid coalescence with neighbouring bubbles. When liquid does not wet the solid, porous material, the gas spreads along the surface, leading to much larger bubbles than the aperture size. The anchoring of the bubble surface formed, due to wetting solid, will restrain the bubble detachment and limit the transfer momentum to the bubble.
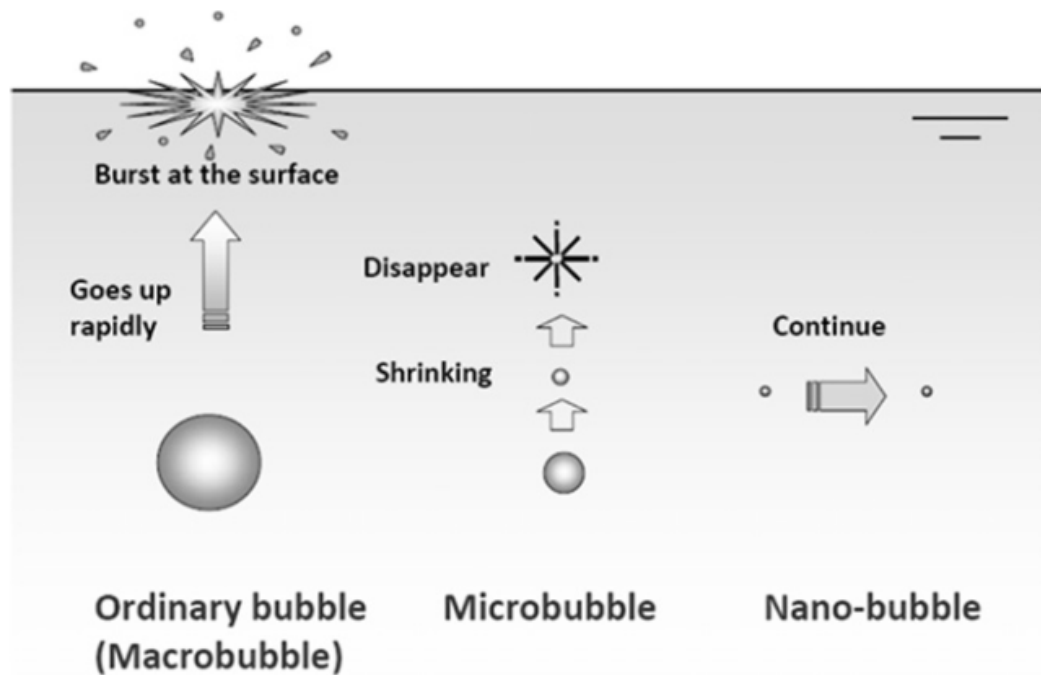
Figure 2.15 Schematic diagram of different size of bubbles dissolution (Agarwal et al., 2011)

Furthermore, a potential second layer 'anchors' the proto-bubble cloud as the gas spreads across the solid surface over a wider area than just the perimeter of the aperture, if the liquid does not wet the solid. Crucial to the formation process of microbubbles are the wetting properties of the liquid, gas, and solid – the attractive forces between each pair interaction (solid-gas, solid-liquid, and liquid-gas) which are in balance at the contact angle (Tesař, 2014b, 2014a; Zimmerman et al., 2011; Zimmerman et al., 2008). Contaminants such as chemicals, particularly surfactants, oil and particulate matter disturb this balance. For instance, if the solid is hydrophobic, water will not wet the surface so the bubble spreads out across the surface with a very high attractive 'anchor' force. On the other hand, larger bubbles produced from smaller apertures will diversify the bubble size with irregular spacing between the bubbles. This situation is leads to quick coalescence of the bubble cloud which then rapidly rises towards the water surface.

2.5.2   Surface Area and Rise Velocity

It is important to keep the rise velocity of the microbubble as small as possible to increase the bubble-biofilm contact time. The size of the microbubble is proportional to the terminal rise velocity of the air bubbles. Zimmerman et al., (2008) informs that the rise velocity of air bubbles follows the Stokes law of a rigid sphere using the

39

diameter of the bubble, but with a different constant of proportionality due to the deformable surface. Larger volume microbubbles with higher rise velocities would decrease the contact time of the interface with the liquid medium but also surfactants in the wastewater. Thus, the efficiency of the momentum transfer would be reduced. According to Tsuge, (2014) and Agarwal et al., (2011) surface area increases by the factor of 10^4 from 1mm to 10μm of bubbles diameter. The equation below shows the relationship between the bubble diameter and surface area for a single bubble which eventually contributes to higher gas dissolution fraction.

$$\frac{A}{V} = \frac{6}{d}$$

<div align="right">**Equation 2.2**</div>

2.5.3 Number of Bubbles

Ideally, the total amount of energy transferred should be larger by the smaller bubbles due to the finite height of the liquid layer to the ratio of smaller bubble size. It is proven that the bubbles three-fold smaller in size stay in the liquid tenfold longer, thus having a longer time to transfer the same momentum rate (Li et al., 2010). For a single bubble, the surface area and transfer rate scale as the square of the bubble size however bubble volume scales with its cube. Thus, it is important to produce smaller microbubble for higher transfer rate.

2.5.4 Interfacial Area and Gas Hold-up

The interfacial area is one of the most important characteristics possessed by a microbubble which provides benefits to many applications. Microbubble have a higher specific interfacial area which usually measured per unit volume of dispersion is expressed by the following equation (Tasaki et al., 2009; Kukizaki & Goto, 2006).

$$a = \frac{6\varepsilon_G}{D_b^{50}}$$

a is the surface area per unit volume (m^{-1})

<div align="right">**Equation 2.3**</div>

$$\varepsilon_G = \frac{V_G}{V_L + V_G}$$

ε_G: Gas Holdup
D_b : Mean Bubble Diameter
    corresponding to 50% vol.
V_G: Volume occupied by the gas phase
V_L: Volume occupied by the liquid phase

The above equation specifically expresses the interfacial area of spherical bubbles. Since microbubbles are dominated by surface tension forces, even though they are deformable, they are typically nearly spheres under steady flow conditions. There are various ways of estimating the mean bubble diameter but the most common is Sauter mean bubble diameter.

2.6 Microbubble Generation Methods

There are many ways of generating microbubbles, and the techniques may vary depending on their significance to the application. They are classified into five different classes of methods, (i) which are generation using flowing liquid, (ii) without accompanying liquid flow, (iii) chemical additives such as the polymers, (iv) high or low power consumption applied external fields and (v) other miscellaneous methods. The methods have been developed to satisfy the revolutionary approach to process intensification towards producing better products, safer process, cleaner, smaller size, and most importantly at lower operating cost. There are possibilities for these generation methods to be blended and combined/staged for improvement for some purposes among the five primary methods simplified as shown in **Figure 2.16**.
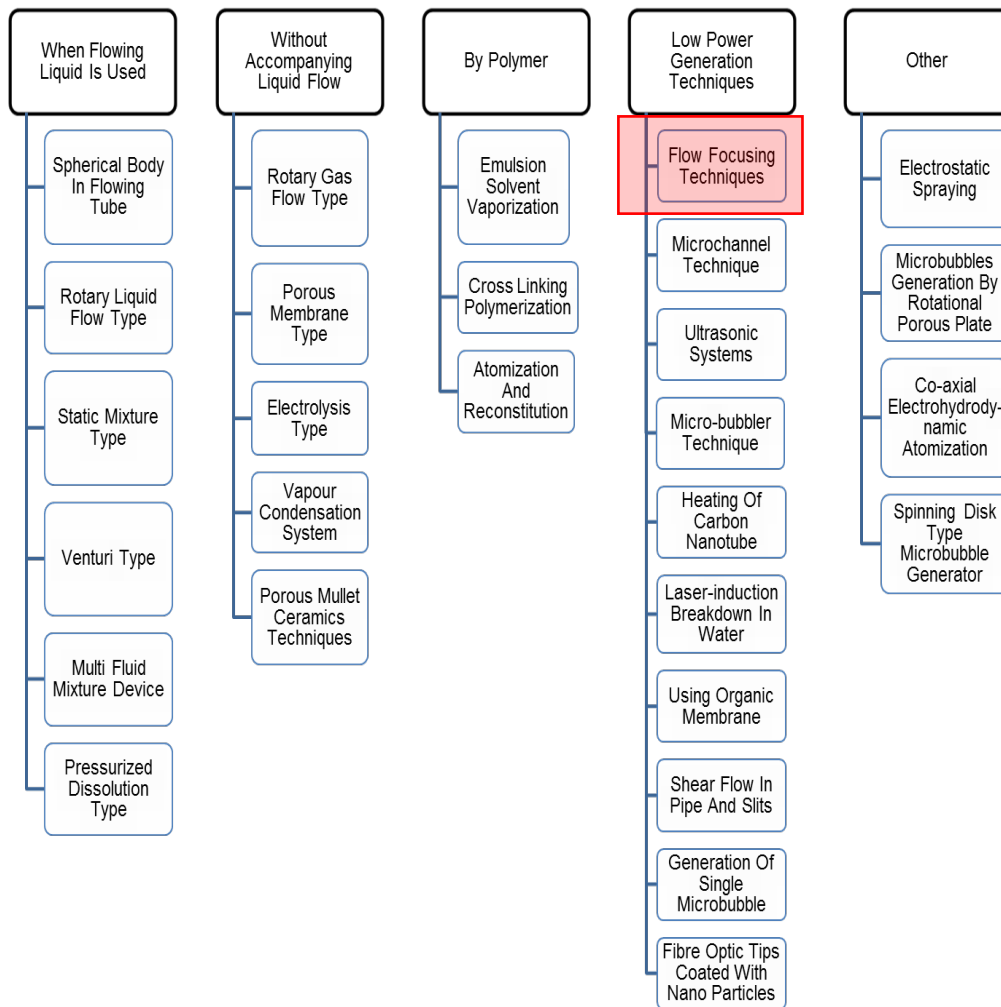
Figure 2.16 Microbubble Generation Techniques (Parmar & Majumder, 2013)

Figure 2.16 shows numerous ways of generating microbubbles based on different applications. According to Parmar & Majumder (2013), the size of microbubbles generated for every method is different and mostly in the range of 1.2µm to 200µm. Conventionally, ozonation of water and phenol require electrostatic spraying method, sludge stabilisation uses the ejector type, and water purification uses the venturi method (Pimentel-Domínguez et al., 2012; Chu et al., 2008; Shin et al., 1999). Microbubble sizes can vary within the same application depending on the process it is being used for. For example, rotary liquid flow processes use microbubbles at 50µm to remove metal oxides and 63µm to separate fine suspended carbon in water (Terasaka et al., 2008; Terasaka & Yasuyuki, 2007). Therefore, it is important to know the microbubble size as this will indicate which application this technology can be

used for. From the data collected by Parmar and Majumder, **Table 2.6** is tabulated, showing the different size of microbubble for various applications.

Table 2.6 Size of Microbubble on Different Application

Method of microbubble generation	Application	Size of microbubble (μm)
Rotary liquid flows type	Removal of fine metal oxide particle	50
	Separation of fine suspended carbon in water	63
	Oxidation of dimethyl sulfoxide	50
Spinning disc type	Synthesis gas fermentation	60
Electrostatic spraying	Ozonation of benzene, toluene, ethylbenzene and xylene	10-80
	Ozonation of water and phenol	50
Ejector type	Sludge solubilization	<58
	Treatment of textile wastewater	<58
Venturi Type	Water purification	70
Shirasu-porous-glass (SPG) membrane	Degradation of methyl orange	5.79
Pressurised dissolution type and Rotary gas flow type	Removal of residual pesticide in vegetables	10, 40
Hydrocyclone microbubble generator	Drag reduction	60
Air shearing type	Removal of chlorinated organic compound from waste water	10-30
Microfluidic device	Drug Delivery	160-200
Fluidic Oscillations	Airlift bioreactor	50-1000
		20-100
	Harvesting and dewatering of yeast	25-125
	Microalgae growth	20-100
	Oil Emulsion Separation	~100
	Ethanol-water separation	47-164
	Wastewater	~500

The generation of the microbubbles has been compared in term of its characteristics and operating properties. The size and shape, distribution, surface area, and gas hold-up as explained are among the control handles for the microbubbles production. Every investigation that has been reviewed was carried out to determine the optimum condition of these properties, however, the efficiency of the microbubble in term of power consumption, time-consuming, capital and operating cost or performance for standard application is not well assessed. Thus, this literature review will focus on the effectiveness of using low power consumption techniques, capital cost and maintenance free possible.

2.7 Comparison of the Methods of MB Generation

2.4.1 Surface Area vs. Time vs. Power

2.4.1.1 Electroflotation (EF) vs. Dissolve Air Flotation (DAF) vs. Electrostatic Spraying (ES)

Figure 2.17 shows the total surface area of microbubble produced using Electroflotation (EF), Dissolve Air Flotation (DAF), and Electrostatic Spraying (ES). The data collected by Parmar & Majumder, (2013) shows that DAF was the most efficient process of microbubble generations with value 0.054 surface areas produced per time as a function of power input (m^2/min/W). They explained that the power consumption does not have much significance in the surface area created, however, increases slightly as pressure increases. DAF has the highest efficiency to provide greater surface area; however, the generation has the narrowest distribution with largest average size. **Figure 2.17** summarised the bubble size distribution between the three methods. According to Zimmerman & Tesar, (2010) and Zimmerman et al., (2008), fluidic oscillator have no moving part and requires no electricity to generate a tenfold smaller size of microbubbles. This made FO generated microbubbles are better in all aspects compare to electrofloatation, DAF, and Electrostatic spraying.
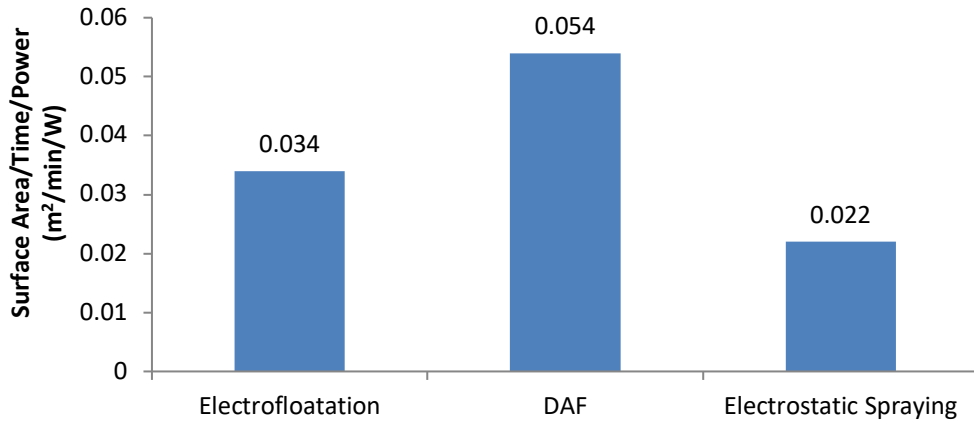
Figure 2.17 Comparison of Surface Area Produced/Time/Power for Three Methods of Bubble Generations (Parmar & Majumder, 2013)

Table 2.7 Distribution and Average size of Microbubble for Three Methods (Janssen & Hoogland, 1973)

	Bubble Size Distribution	Average Size	Surface Area	Average Bubble Diameter
Fluidic Oscillator	Narrowest	Smallest	Maximum	Small
Electroflotation	Intermediate	Smallest	Intermediate value	Smallest
Dissolve Air Flotation	Narrowest	Largest	Maximum	largest
Electrostatic Spraying	Widest	Intermediate	The Least	-

2.8 Fluidic Oscillator (FO)

(a)   (b)
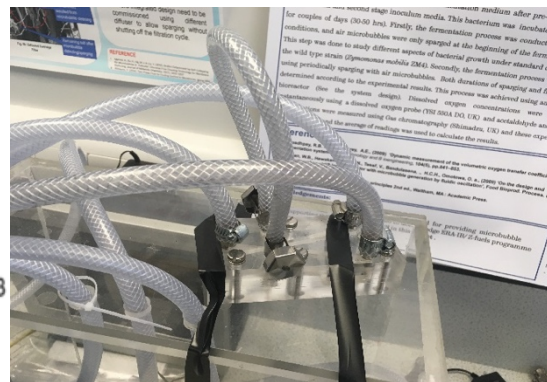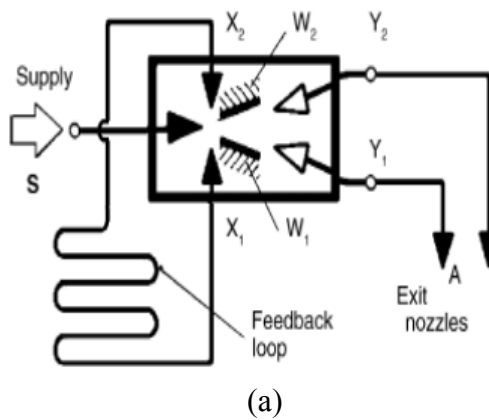
Figure 2.18 The Fluidic Oscillator (a) Schematic by Hanotu, (2013) **(b) Tesar-Zimmerman oscillator used in this project**

The fluidic Oscillator (FO) shown in **Figure 2.18** has been pioneered by Zimmerman et al., (2008) mainly in producing smaller microbubble by oscillation. There are many advantages using the FO in term of cost-effectiveness, robustness, reliability, immobile parts and no requirement of electricity (Zimmerman & Tesar, 2010). FO are categorised as a fluidic amplifier with a potential to pinch off hemispherical cap bubble by controlling the fluidic flows to improve the previous bubble generation. FO mainly consist of 3 parts; one inlet for air supply, two mid ports for the feedback loop, and two exit ports as the oscillation channel outlet. A remarkable feature of this system is that the frequency of the oscillation is adjustable by manipulating the air flow rate and the length of the feedback loop (Tesař, 2014a). **Figure 2.19** shows the effect of microbubble size generated with **Figure 2.19**(a) and without fluidic oscillator **Figure 2.19** (b).
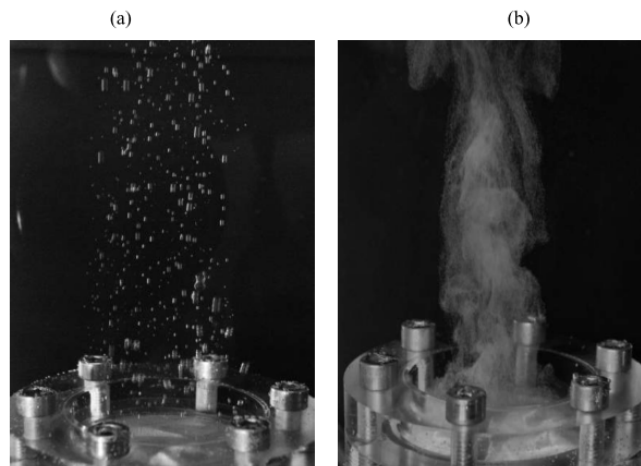
Figure 2.19 Fluidic oscillator schematic with images of bubbles (a) coalescent and non-uniform bubble without fluidic oscillator (b) Uniform size and non-coalescent bubbles with fluidic oscillator (Hanotu, 2013)

2.9 Other Applications of FO Generated Microbubbles

Microbubbles are used in many applications such as cleaning, soil washing, and removal of oil from the soil and water, fermentation, marine fish farming, horticulture, food technology, absorption of acid gas by alkali. Medically, microbubbles have evolved rapidly in diagnostic imaging, gene and drug delivery, oxygen transfer and therapy for ocular diseases (Kanchan Maske et al., 2012; Xu et al., 2008). In the recent times, microbubbles have enhanced the algae-derived biofuel operations. CO_2 rich fossil fuel has been introduced with the exhaust gases inject to the bioreactor in the form of microbubbles. The microbubble size which is 50 times smaller than the

conventional bubbles provide 50 times greater mass transfer because of the higher surface area to provide higher yield in algal biofuel production (Zimmerman, 2011a). The characteristics and size distribution of microbubble clouds provide a unique set of opportunities for exploitation to this research by understanding the mechanisms and optimising the behaviour of the microbubbles for cleaning purposes.

2.9.1.1 Column Flotation

Column flotation was developed in the early 20th century to purify coal in the mining industry. The same principle of selectively separating the hydrophobic material from hydrophilic particles has been applied using microbubbles. The **Figure 2.20** below illustrates the selective attachment of microbubble to only hydrophobic particulate matter. The resulting floc eventually lifts the hydrophobic particles upward to the water surface via buoyancy force. The column is designed with two zones - cleaning and recovery area - to allow the separation between these two types of particles. The process offers many advantages including enabling the achievement of high product purification with less energy consumption, and capital cost reduction (Lee & Lee, 2002).
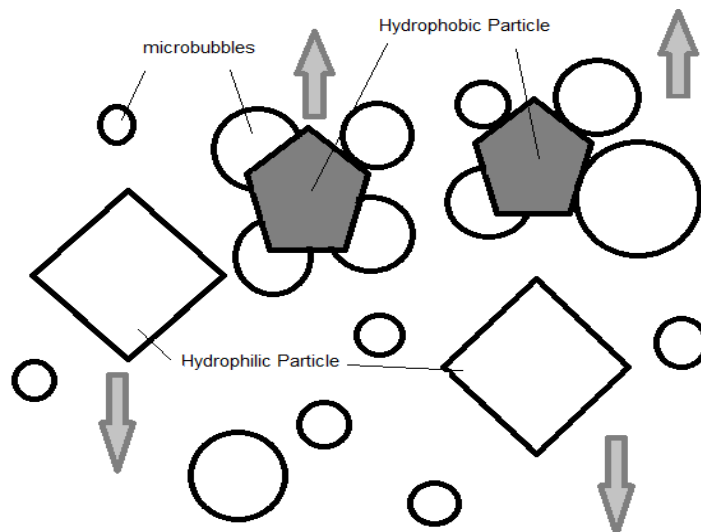
Figure 2.20 Attachment of hydrophobic particle to bubble Hydrophilic particles (diamonds) are repellent to microbubbles, so sink due to their greater density than water. Hydrophobic particles (pentagons) attract microbubbles, eventually forming flocs that rise due to greater buoyancy of the collective floc (Wang et al., 2017; Hanotu et al., 2012)

The role of bubbles in the column flotation to separate particles is further improved using microbubbles. The study by Choung et al., (1993) summarised that the bubble-

particle attachment in recovery and cleaning zone of the column would predict the total recovery of the production in the column. Cao et al., (2009) introduced cyclonic-static microbubbles in a flotation column to separate copper-nickel sulphide. They found that better separation was achieved compared to standard a flotation cell by using a cyclonic-static microbubble. The gas holdup of microbubbles in cyclonic-static in flotation column has been measured and simulated using differential pressure method with a single-phase turbulent flow model (Yan et al., 2012; Xia et al., 2011).

2.9.2 Bio-Fuel Production

The shortage of the fossil fuels spurs the transition to and research and development (R&D) for alternative green energy. A specific area is the algae biomass for biofuel production and co-combustion. Zimmerman (2011) grew a microalga using CO_2 rich microbubbles generated by fluidic oscillation. The microbubble of size less than 50μm has higher surface area to allow the gas dissolution for the CO_2 uptake by the algae. Microbubbles also have higher retention time which encourages the growth of the microalgae D Salina in this instance. The process is furthered explained by Zimmerman et al. (2011) concerning high dissolved oxygen content, which is not conducive for algal biomass growth. It needs to be strip out using microbubbles, thus removing the inhibition and allowing faster growth rate. This process shows the role of microbubbles in delivering CO_2 rich and stripping out O_2 from the algal medium. It is important to maintain rapid growth rate as a key for the efficient biofuel production. A recent publication by Kamaroddin et al., (2016) using in-situ disinfection in the medium has increased the efficiency of production of microalgae biomass.

2.9.3 Fermentation

Yeast is the most traditional fermentation medium and widely used in food production, pharmaceuticals, and wastewater treatment. Yeast utilisation requires the yeast to be harvested and dewatered from its culture medium which can be challenging mostly due to its small particle size. Hanotu et al., (2014) and (2016) recovered 99% of the yeast cell using microbubbles and bioflocculant-chitosan, providing an alternative more efficient yeast cell recovery. The results showed that the recovery depends on the bubble size, alkalinity and flocculant concentrations. Small microbubble size is relatively efficient in the removal of small particles while larger bubble size is

effective in the removal of larger particles. Also, the alkaline conditions are less favourable due to slow floc formation rates, compared to acidic and neutral conditions.

2.9.4 Various Application of FO

The research group lead by Professor William Zimmerman used FO for a different application. The operation of the FO is usually different for every application in term of air flowrate, feedback loop length and size. The manipulation of the air flowrate and feedback loop results in different behaviour of microbubble and oscillation frequency as required by the system. **Table 2.8** summarises the application of fluidic oscillation to generate microbubbles. The microbubbles generated using fluidic oscillator generally are smaller in size, with narrower distributions and high frequency. Using the same principle, this research will be further extended for the membrane defouling.

Table 2.8 Fluidic Oscillator on different application

Application	Average Microbubble Size Range (µm)	References
Airlift bioreactor	50-1000	(AL-Mashhadani et al., 2015)
	20-100	(Zimmerman, Zandi, et al., 2011; Li et al., 2010)
Harvesting and dewatering of yeast	25-125	(Hanotu et al., 2014)
Microalgae growth	20-100	(Kamaroddin et al., 2016; Hanotu, 2013; Zimmerman, Zandi, et al., 2011)
Oil Emulsion Separation	~100	(Hanotu et al., 2013)
Ethanol-water separation	47-164	(Al-yaqoobi et al., 2016)

| Wastewater | ~500 | (Zimmerman, Zandi, et al., 2011) |

2.10 Biofilm Detachment Using Microbubbles

In this research, microbubble properties have been exploited for cleaning potential. Biofilms such as HeLa and Chlamydomonas have been cultured and grown for investigating the detachment potential caused by microbubble from a flat surface. Agarwal et al., (2012) proved that microbubbles are a chemical-free and eco-friendly technology for biofilm detachment. Sharma et al., (2005) concluded that flows containing microbubbles have been very effective in stimulating bacterial detachment due to the flow potentially being higher in shear force. From this, the research of detaching biofilm from a flat surface are further studied and improved using microbubbles that are generated by fluidic oscillation.

2.11 Defouling and Cleaning Using FO Generated Microbubbles
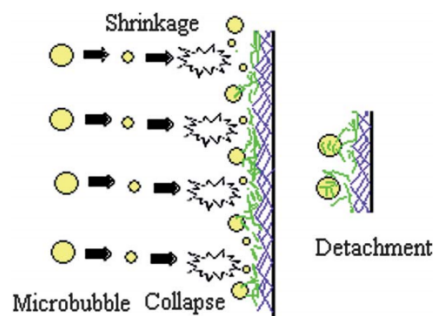
Figure 2.21 Schematic illustration of biofilm detachment by collapsing MBs (Agarwal et al., 2012)

The potential of microbubbles in removing the biofilm depends on the internal pressure of the bubble. As governed by the Young-Laplace equation, the internal pressure of the bubble depends on the diameter of the bubble. The smaller the diameter of the bubble lead to the higher internal pressure and subsequently bubble collapse resulted in higher energy. High energy generated allows more detachment of the biofilm and the cleaning efficiency. Illustration above shows the pressure waves are distributed over the domain of the self-collapsing bubbles eventually dispel the fixed biomass from the membrane surface. This concept contradicts to the finding of this

research, where MBs do not simply collapse as MBs are generated by using compressed air. Air contains mostly inert gas N2 and it is insoluble in water.

$$P = PI + \frac{4\sigma}{d_b}$$

P: Gas Pressure (kPa)
PI: Liquid Pressure
σ: Surface Tension of the Liquid
d_b: Bubble Diameter

Smaller Microbubble Generated (High internal pressure)	Microbubble burst on the surface of the membrane (Bursting other bubble similar to chain reaction)	High Pressure spot generated (continous biofilm matrix disruption)	Biofilm Detachment
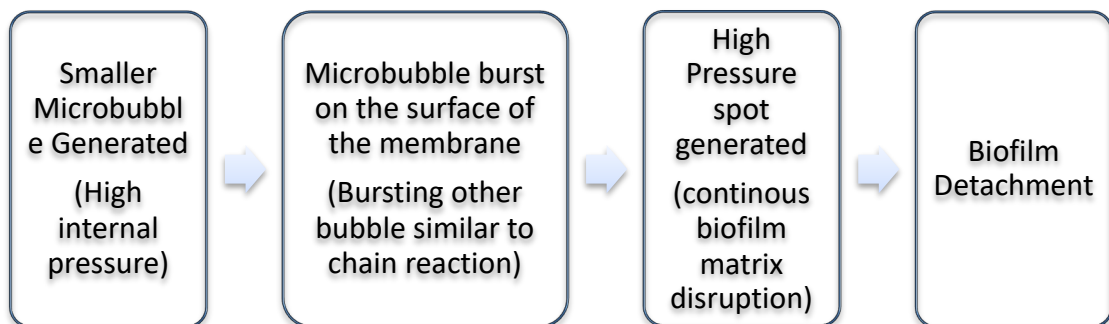
Figure 2.22 General Biofilm detachment process using microbubble

CHAPTER 3

METHODOLOGY

3.1 Introduction

The potential for microbubbles in cleaning has been widely investigated in various applications such as column flotation, degreasing solid surfaces, pipe cleaning system, and biofilm detachment (Agarwal et al., 2012; Xia et al., 2011; Hiroyuki et al., 2010; Miyamoto et al., 2007). Alongside with this opportunity, Zimmerman et al., (2008) also investigated the benefits of fluidic oscillation to produce a better functionality with microbubbles due to generation maintaining their laminar flow environment. This project is mainly to connect these two features: (1) the potential for microbubbles in cleaning, and (2) application of fluidic oscillation to improve bubble properties for cleaning. As reported in the literature, microbubbles have significant potential advantages in comparison to conventional methods, which create much waste with low cleaning efficiency. The experiments are designed to discover the potential of microbubbles generated by fluidic oscillation in three cleaning applications: cleaning filtration membranes, biofilm detachment and cell detachment. This chapter describes the details of the methodologies for investigation of membrane fouling, biofilm culture, and cell culture experiments characterising membrane defouling, biofilm and cell detachment respectively.

The following methodologies are outlined and described in this chapter.

- Handling procedure of control box to control the flow and oscillation frequency of fluidic oscillator.
- The design and assembly of Microfiltration (MF) filtration system to foul and defoul the membrane using microbubble.
- HeLa cells and Chlamydomonas algae culture procedures on microscope slide. The experimental set up for microbubble sparging also described in this chapter.
- Every equipment involved such as Scanning Electron Microscopy (SEM), mass spectroscopy, and Arduino Uno sensor for pressure transducers, accelerometer, and flowmeter are described.

3.2 Microbubble Generation

Microbubbles are generated by injecting a source of air, for example in this case, compressed air, into the microporous diffuser. The flowrate and pressure of the compressed air injected through, are controlled according to the conditions and suitability of the microbubble sizing. The control box is designed specifically to generate an oscillatory flow, appropriate for effective microbubble generation for cleaning. The understanding of flow and pressure control using the control box is essential for a very good cleaning efficacy in pressurised and in open systems.

3.2.1 Fluidic Oscillator
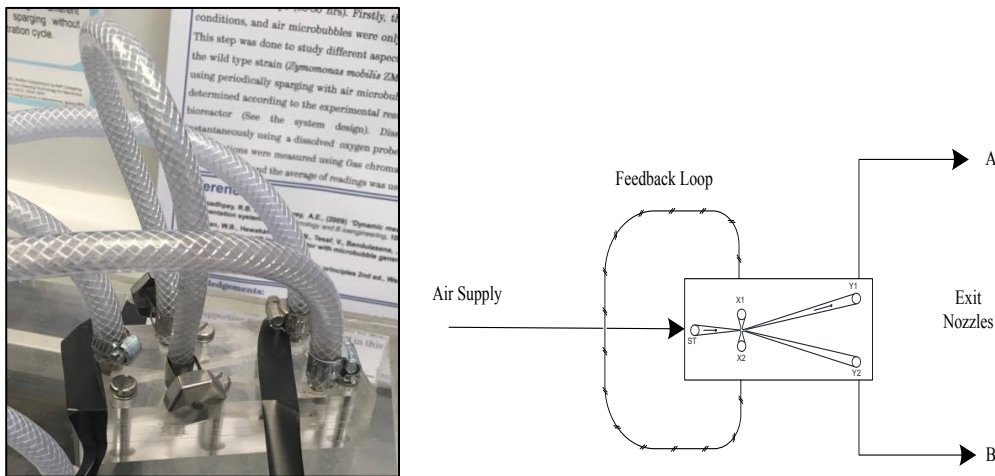
Figure 3.1 Fluidic Oscillator

For microbubble generation, the fluidic oscillator is connected to the air sources as shown in **Figure 3.1**. There are many advantages in using the fluidic oscillator in term of cost-effectiveness, robustness, reliability, immobile parts and no electricity usage (Zimmerman, Tesar, et al., 2011). The generation of bubbles by fluidic oscillation consumes little power – not much more than the thermodynamic ideal for displacing the liquid and creating gas-liquid interface. Low power consumption distinguishes the method from other methods such as ultrasonic and rotary disk with a significant supply energy consumption (Abdulrazzaq et al., 2015). Zimmerman et al., (2008) explained this device acted as a fluidic amplifier with a potential to pinch off bubbles not much larger than a hemispherical cap above the aperture. This early break off for bubble formation at the diffuser aperture offers the smallest possible bubble size. **Figure 2.21** and **Equation 2.5** illustrates the relationship of the smaller microbubble to have higher

surface area to volume ratio which leads to high momentum transfer rates, especially for scrubbing the surface of membrane (Abdulrazzaq et al., 2015; Agarwal et al., 2012). A fluidic oscillator mainly consists of three parts: one inlet for air supply, two mid ports for the feedback loop, and two exit ports as the oscillation channel outlet. The arrangement as shown in **Figure 3.1** oscillates the gas flow between two paths under constant pressure of gas (Zimmerman & Tesar, 2010). A remarkable feature of this system is that the frequency of the oscillation is adjustable by manipulating the air flow rate and the length of the feedback loop (Tesař, 2014c). **Figure 2.19** shows the effect of microbubble size generated with (a) and without fluidic oscillator (b).

3.3 Microfiltration (MF) membrane

(a)   (b)
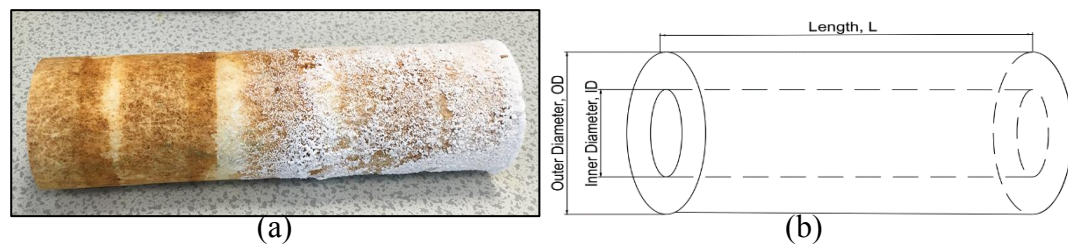
Figure 3.2 Configuration of the membrane cartridge fit in with the membrane housing

Figure 3.3 shows both ends of the MF cartridge surface resulted from the filtration process. The tubular MF membrane cartridge with inner diameter of 30mm and outer diameter of 65mm with 254mm (10") in length is used in this experiment. The micron rating or the porosity of the MF cartridge ranges from one to 100 micron. The membrane can be set-up both in either the dead-end or cross flow configurations and is operated under room temperature between 22.7 and 25.1°C. **Figure 3.3** shows a dried filtration membrane cartridge with the deposition of salt and colloids.

<div align="center">(a)   (b)</div>
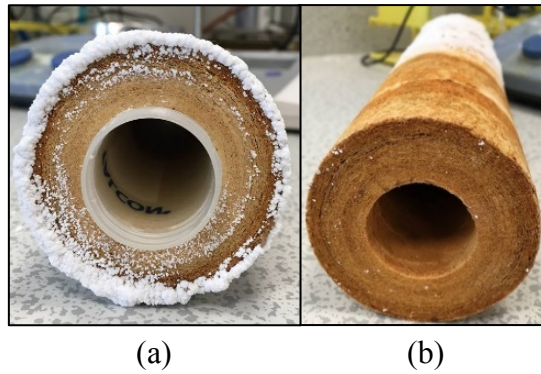
Figure 3.3 Both ends of MF (a) salt deposition resulted from filtration process (b) Cleaned MF using microbubble

3.4   Membrane Defouling

Exploring the potential of microbubble generated by fluidic oscillations towards filtration membrane consist mainly; sparging unit and filtration system.

3.4.1   Sparging Unit Design

The sparging unit schematically represented in **Figure 4.12**. The sparging unit comprises a pressure regulator, a pressure gauge, and a flow meter to instrument fluidic circuitry. The equipment is mainly to control and manipulate the pressure and flowrate of the air supplied to the fluidic oscillator and the microporous diffuser. Compressed air is supplied to the pressure gauge P1 according to the **Figure 3.4** to regulate the air pressure through the system. The pressure regulator P2 plays a key role to the pressure control of the air supplied to the fluid oscillator. With the feedback loop of length 50mm attached to the fluidic oscillator, the oscillation of the airflow through fluidic oscillator can be controlled using the flowrate of air, F3. Valve V4 is issued to create flow resistance to the vent from the unused outlet of the fluidic oscillator. If the resistance down this leg is higher than the diffuser outlet, then there is no oscillation - steady flow proceeds to the diffusers. If the resistance through the unused vent is lower than the diffuser outlet pathway, there is no flow at all to generate bubbles in the test chamber. By balancing the resistances (level of openness of V4), oscillation occurs. The vent with flow resistance balancing avoids duplicating the test chamber in order to create symmetric outlet resistances. Typically valve V4 is tuned by "feel" as the oscillation is strong enough to be felt when the resistance matches, either through touching the ducting or by hand in front of the silencer.

Figure 3.4 Sparging Unit process flow diagram

Figure 3.5 shows the lab scale for experimental set-up of the membrane filtration system. The seawater is circulated using the pump at 4.5-5lpm depending on the transmembrane pressure developed from the filtrate deposited on the surface of the filtration membrane. Before the system is fed with the seawater, the system is submerged and circulated with tap water for 24 hours to clean and allow pressure normalisation within the system. The system is then fed with the seawater collected and sampled from the Hull Coastal area. The impurities, salt, and colloids will then start to be deposited on the surface of the filtration membrane causing change in the transmembrane pressure. The transmembrane pressure profile is monitored and recorded using pressure transducer logger unit. The pressure transducer, P1 and P2 are placed at the feed and filtrate stream respectively. The difference between the recorded pressure of P1 and P2 is known as transmembrane pressure. In this case, the pressure difference at the beginning would be almost to zero. Once the colloids and impurities start to be deposited, filling the membrane pores, then P1 will start to increase while P2 is initially unchanged.
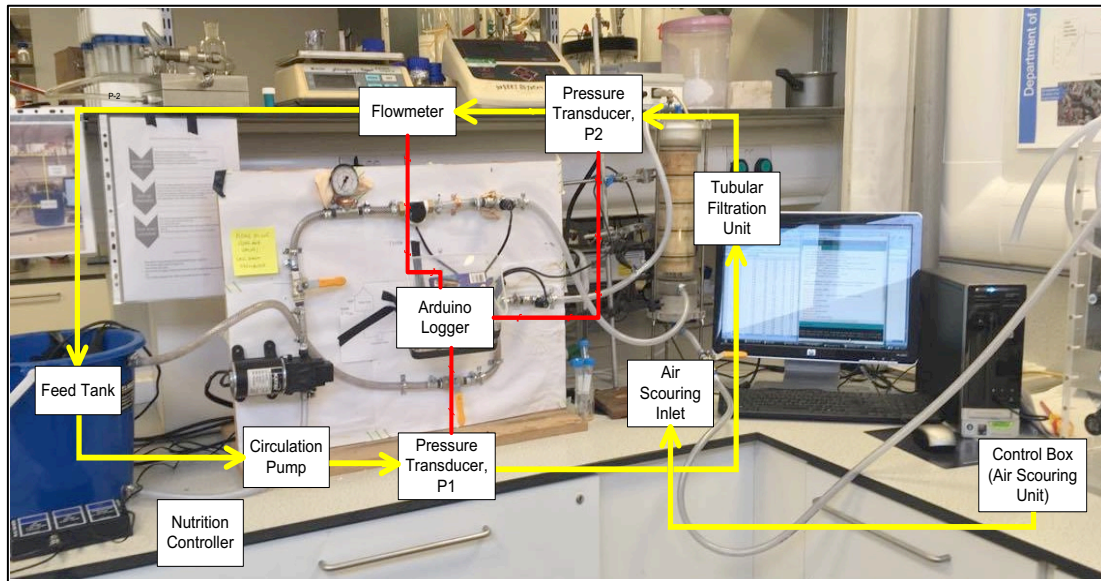
Figure 3.5 Experimental Set-Up

3.4.2 Membrane Unit
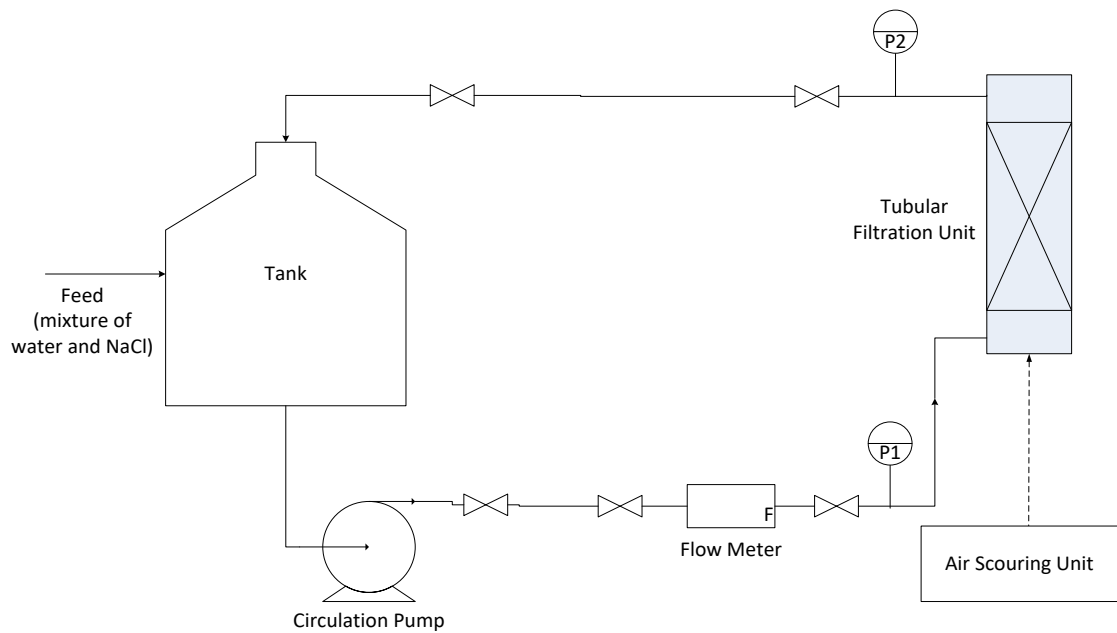
Figure 3.6 Membrane filtration system

3.5 HeLa Culture

The adherent properties of the immortal HeLa cell is the main reason this cell is chosen in the first place. In addition, the cell growth feasibility and simple culture media provide advantages for cleaning studies concerning cell detachment. The following method of cell culture in collaboration with Professor Craig Murdoch in Tissue Culture lab in Charles Clifford Dental School also supported by standard tissue culture

Cummings & Obom, (2007) and the famous Eagle (1959). Properties, application, and morphology of the cell discussed in the literature (see section 2.4.2.2).

3.5.1 Media Preparation

As mentioned by Lucey et al., (2009) and Cantwell (2018) HeLa cells are categorized as mammalian cells. Dulbecco's Modified Eagle's Medium (DMEM) with high concentrations of amino acids, vitamins, and other supplement is culture media well suited to HeLa cell metabolism. **Figure 3.7** shows the media prepared with addition of 1% of Penicillin Streptomycin (Pen Strep), 1% Glutamine, and 10% of Fetal Calf Serum (FCS). For this project, the 500ml of culture media are prepared which consist of 440ml of High Glucose-DMEM, 50ml FCS, 5ml PenStrep, and 5ml Glutamine.
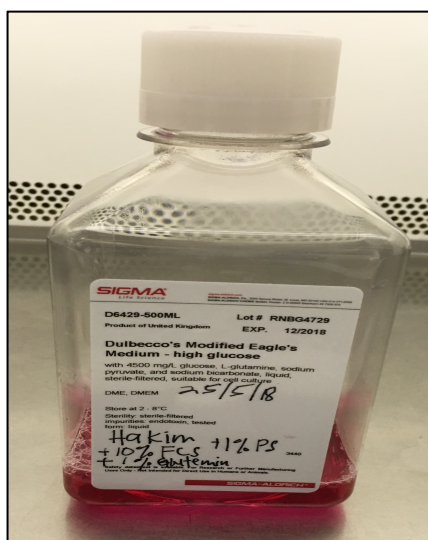
Figure 3.7 500ml media with DMEM-high glucose + 1% Pen Strep +1% Glutamine + 10% Fetal Calf Serum

3.5.2 Cell Culture

Using the media prepared, HeLa cells are detached from the culture flask by adding about ~3-5ml of Trypsin into T25 culture flask. The trypsinized culture flask are then placed in the incubator for 5-7minutes. The flasks are then placed under microscope to examine the entrained cell from the surface of the culture flask. The cells then are transferred into a 20ml falcon tube for centrifuge as shown in **Figure 3.8** (a). The centrifugal effect will remove Trypsin and inhibits the enzymatic effect of the Trypsin towards the cell. The settled cell at the bottom of the tube will be washed and dislodged using media for which it is ready for the cell 'splitting'. Finally, 10% of the HeLa cell are then transferred into petri dish with a very sterile microscope slide inside it as shown in **Figure 3.8** (b).

<div align="center">(a)   (b)</div>
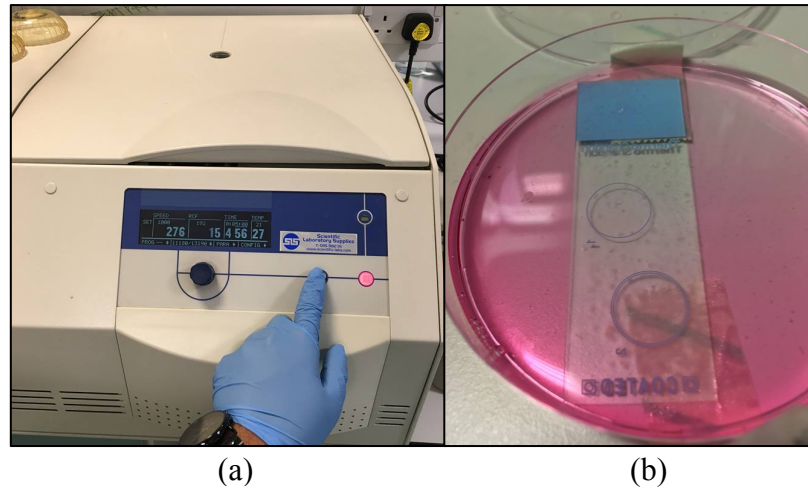
Figure 3.8 HeLa cell (a) centrifuge under 1000rpm for 5minutes (b) split and cultured in the petri dish with surface covered media

The following steps are taken for the confluent cultured cell to investigate the potential of microbubble for cleaning.

Figure 3.9 shows how HeLa cells are grown and cultured in the petri dish, on microscope slide.
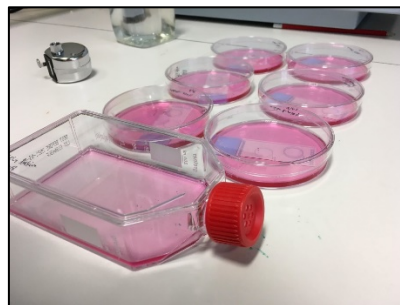
Figure 3.9 HeLa cell culture on microscope slide

3.5.3   Cell Cleaning/detachment

Figure 3.10 shows the confluent HeLa on the microscope slide that is mounted on the microscope slide holder and placed in the cleaning in place (CIP) tank with microbubble sparging inside a Phosphate Buffer Solution (PBS). The microbubbles are sparged at time intervals of 10s, 20s, 30s, 40s, 50s, and 1minute.
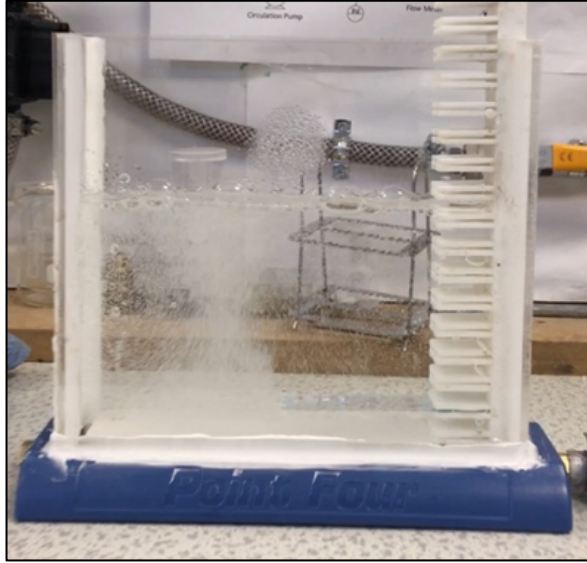
Figure 3.10 Microbubble sparging for HeLa cell cleaning

Figure 3.11 shows the microscope slide is then removed gently and placed in a sterile petri dish. To detach the remaining HeLa cell, ~5-10ml of Trypsin are added and soaked for ~5minutes. The cells are not recommended to be left submerged more than 10mins as they stick together, making the cell counting difficult.
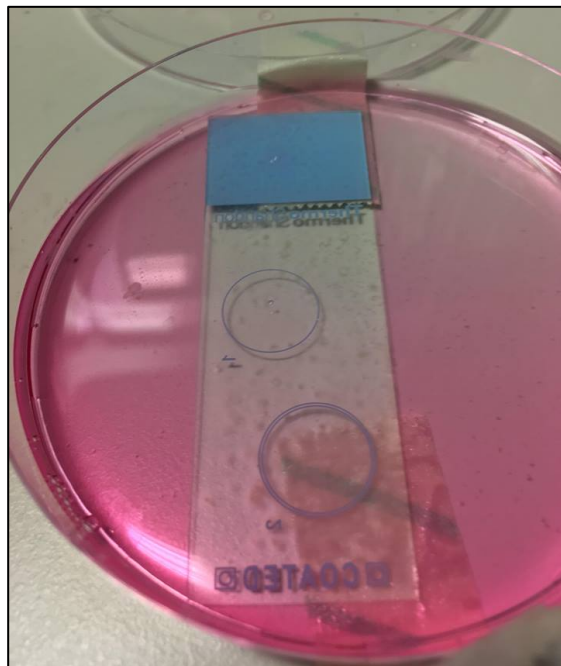
Figure 3.11 Confluent HeLa cell with filled with 10ml Trypsin

As a part of assessing cell counting and viability, 10µl of Trypan Blue is placed on the parafilm. 10µl of cells in Trypsin solution is taken and diluted with Trypan blue solution.

<div align="center">(a)   (b)</div>
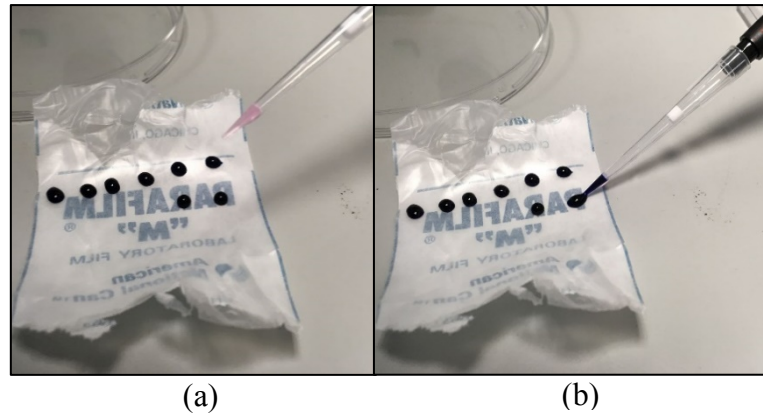
Figure 3.12 10µl of HeLa cell diluted with 10µl of Trypan blue that makes dilution factor=2

Figure 3.13 shows the diluted cells with Trypan Blue solutions are then placed on the haemocytometer for cell count and cell viability measurements. The cell count, detached by the Trypsin, can be used to infer the remaining cells that are undetached by microbubbles according to the time interval set.
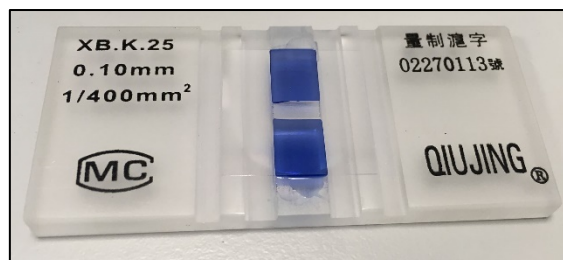
Figure 3.13 Diluted HeLa cell with Trypan Blue solutions for cell density and viability calculations

3.6 Chlamydomonas Algae Culture

Microalgae is one of the most important primary sources of biomass existing on earth. As mentioned in the literature review, an excessive growth of Chlamydomonas algae also would cause many problems such as water contamination (Heisler et al., 2008), reduction of ships speed (Institutions & Ships, 1952), and marine aquatic life disturbance (Anderson et al., 2002). In this research, Chlamydomonas algae have been prepared to explore the potential of microbubbles for biofilm detachment. **Figure 3.14** shows the steps taken to prepare the media for the Chlamydomonas algae to be cultured on the surface of microscope slides. For every 1 litre of water, 10ml of micronutrients and 1ml of trace elements are added into the beaker and well-mixed using a magnetic stirrer.

Micronutrients   Trace elements

(a)   (b)   (c)
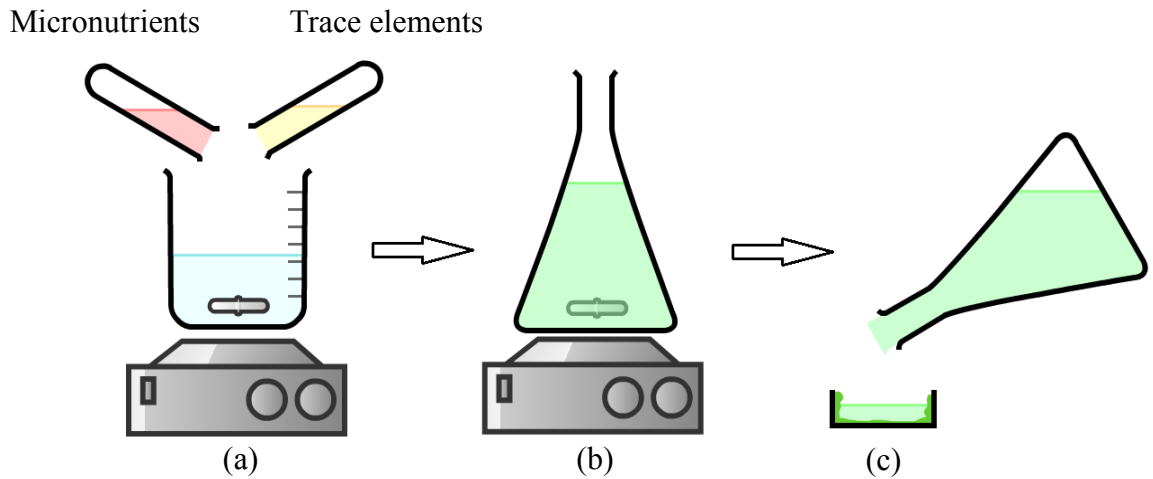
Figure 3.14 Preparation of Chlamydomonas algae (a) media preparation (b) Chlamydomonas algae stock (c) Chlamydomonas algae transferred onto microscope slide surface

Chlamydomonas algae have been cultured using the materials mentioned above under the source of light for 3-4 days and good mixing is ensured by using magnetic stirrer. The algae are sub-cultured every 21 days as suggested by *Chlamydomonas reinhardtii (ATCC® 30476TM)*. The algae are transferred onto a microscope slide within a petri dish for cultivation of the microalgae on the surface of the microscope slide. Within 24-36 hours of algae exposure, the surface of the microscope is dried to ensure a firm adhesion of Chlamydomonas on the surface of microscope slide surface as shown in **Figure 3.15**.
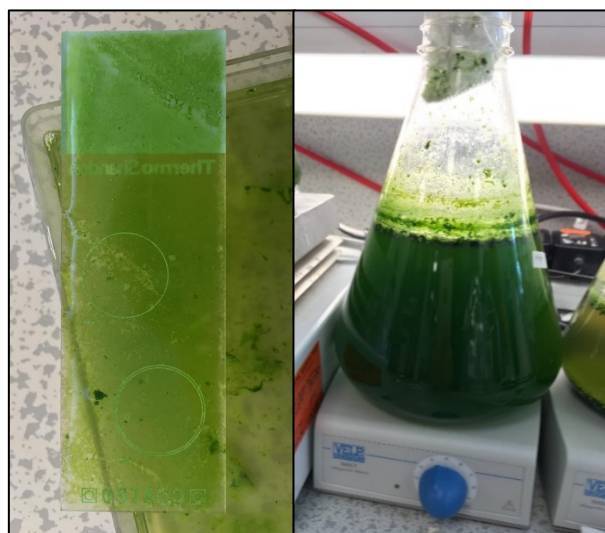
Figure 3.15 The transferred and grown Chlamydomonas algae on microscope slide from algae stock

3.7   Bubble Size Distribution: Imaging

The bubble size distribution has been measured using the most widely employed method, which is an optical method. There are two other methods available, which are an acoustic bubble spectroscopy, and laser diffraction (Spraytec, Malvern Panalytical, UK), but the optical method is used instead for simplicity. The bubble size distribution has measured on both of the spiral membrane defouler and biofilm detachment rig. 10cm x 5cm x 5cm of the fluidic oscillator has been used and connected to the diffuser through the air supply for the microbubble generation.

Figure 3.16 Bubble size distribution imaging using optical method

For the bubble imaging, a set up used by Hanotu (2013) was used with a high-speed camera system (Phantom V210) which is a different high-speed camera. The illumination has been provided by using halogen lamps positioned on the side of the camera for proper imaging and avoiding the reflection which causing poor bubble contour highlight. A ruler is used as a scale to determine the pixel value for calibration. The image of the bubbles is captured first at ten frames/s to calibrate the camera and then images at 2000 frames/sec are captured. A simple Image J algorithm is used to infer the bubble size distribution, using the pixel calibration.

3.7.1 Bubble Size Distribution: Measurement

The images captured at 2000fps are analysed and measured using Image J. It is important to choose the right image with less noise as representative of the overall set of images. The error could be reduced by using 'image threshold' function in the software to minimise the image noise. **Figure 3.17** shows a numbered red area which outlined all the circular part of the black area. The software read the area based on the corresponding scale set using scale bar. The number of bubbles are then listed corresponding to its area as can be seen on the right side of the figure.
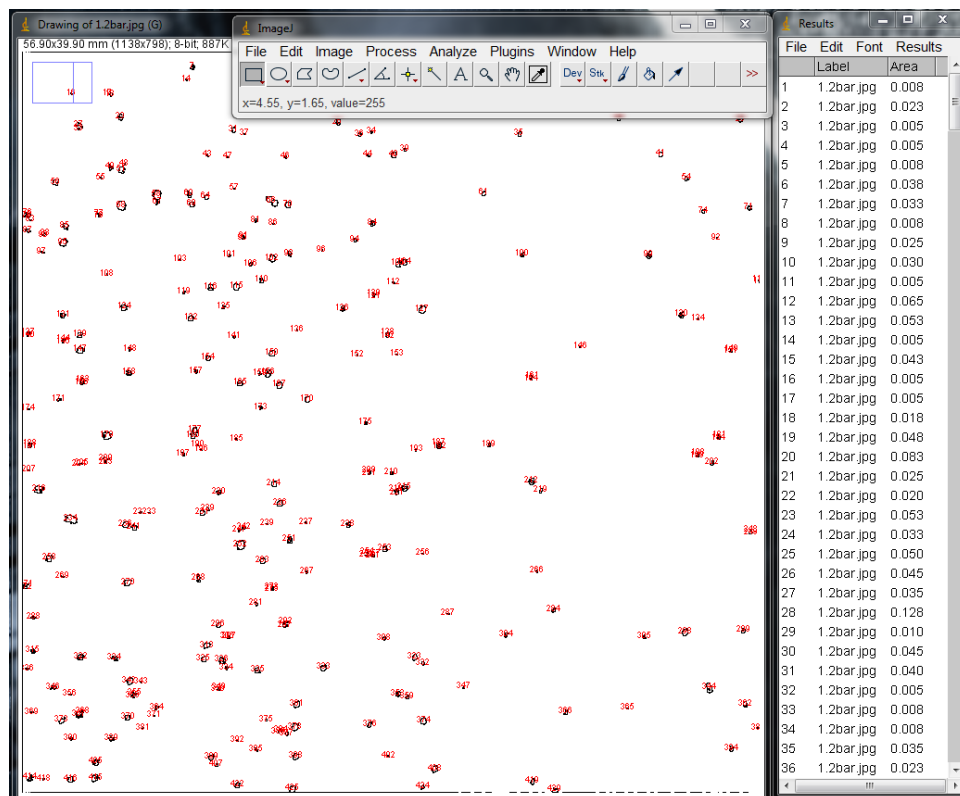
Figure 3.17 Microbubble size distribution measurement using Image J

The areas calculated by the software are converted into diameters using **Equation 3.1**. Microbubble size distributions are obtained by using frequency distribution commands in the Microsoft Excel and GraphPad Prism or using **Equation 3.2**.

$$D = 2 \times \sqrt{\frac{A}{\pi}}$$

$$Frequency\ size\ distribution = \frac{\sum(M \times F)}{n}$$

3.8 Analytical

3.8.1 Scanning Electron Microscopy (SEM)

3.8.1.1 Imaging Using the Microscope

Figure 3.18 Adjusting the Magnification, Contrast, and Stigma for Membrane Imaging

Creating an image using the SEM microscope begins by selecting the sample type as inorganic and coated sample. The coated sample has been placed carefully in the microscope chamber lower than the image detector to avoid crashing the detector. The microscope is closed, turned on and the location of the sample is adjusted using plane x and y. The z plane usually kept low to about 40mm. As the condition of the sample is set, START button is clicked using the software for the chamber to be pumped for about 5 minutes. The green filament feature on the software is turned ON, and a practical image appeared adjusted by using ACB (auto contrast and brightness) feature.

Once the sample is virtually clearly shown in the software, then the image is furthered analysed using auto focus, auto contrast and auto stigma features. It is preferable to start the image analysis from low magnification and then gradually to increase the magnification slowly. The cleared picture is then stored using STORE feature on the software to be downloaded and printed. The height, autofocus, magnification and scale size data is recorded so the clear imaged produced can be repeated and improved using the same imaging settings. The magnified image is reduced to the magnification of below 100x as part of the sample removal procedure as well as the filament is switched off. Finally, VENT is pressed followed by 'set specimen' and the chamber is ventilated for the sample to be readily removed.

3.8.1.2   Sample Coating (without thickness monitor)
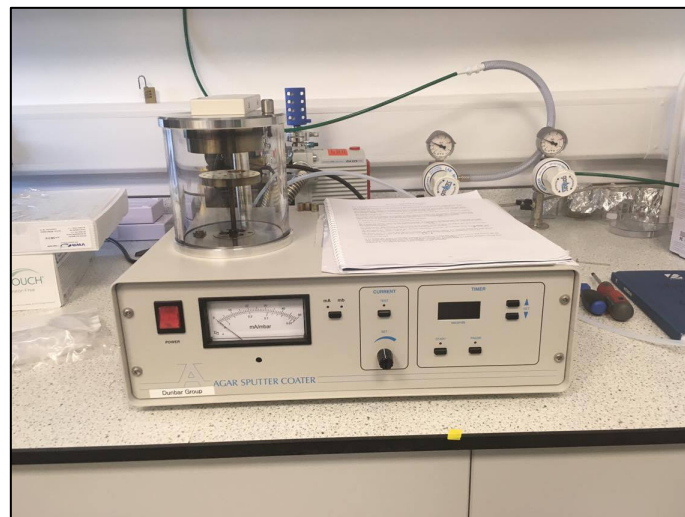
Figure 3.19: Gold coating

The coating activity started by allowing the sample to be dried thoroughly and free from any solvent-based adhesive. The suitable shape to allow a conducting path through the sample is mounted on a stub suitably using carbon tape. Before placing the sample on the sample table, the valve supply of the argon gas is checked to be fully opened, and the regulator gauge is set at 0.3bar. The sample table height in the coater is adjusted to ~25mm target-to-sample distance or at the relevance, distance depends on the sample coating difficulties. Once the sample and coating cylinder is ready, the sample is placed on the table, and top-plate is closed.

To operate the coating chamber, the chamber is pumped using a pressure lower than 0.05mb and the timer on the digital display is set to 5 seconds. The gas control valve is then adjusted using (SET) button to allow the filled argon gas chamber to be more than 0.4mb and is flushed for at least 10 seconds. The tests required to be operating under the desired pressure by adjusting the valve to 0.04mb as well as TEST button is pressed to check the sputter current which is set at 40mA. Finally, the START button is pressed, and the coating is ready once the timer is reset. Once the coating is complete, the control valve is closed, and the unit is switched off subsequently top plate is lifted to remove the sample.

3.8.2 Nutrition controller: pH Value, Temperature, and Electrical Conductivity (EC)

The properties of the fluid are recorded using a trimeter nutrition monitor device as shown in **Figure 3.20**. The meter displays the value of pH, electrical conductivity (EC), and temperature of the fluid. The two types of meter that are used almost identical but with different ranges of the EC value, range of 0-10 and 0-20 mS/cm^{-1} respectively. Temperature would be the least concern as the experiments are carried out under room temperature, however, monitoring is important to reduce the error. The pH and EC value are calibrated using two-point calibration pH buffers and saline solutions Potassium Chloride (KCl).

Figure 3.20 Nutrition controller (Trimeter) used to collect the pH value, Electro Conductivity (EC), and temperature of the effluent

3.8.3   Absorbance

The concentration and salinity of the fluid are measured using ultraviolet-visible (UV-Vis) spectroscopy machine. **Figure 3.21** shows the UV-Vis machine (Jenway 6705) used to analyse the absorbance value of seawater collected before and after filtration. This quantitative measurement utilises the concept of wavelength absorption to determine most of the water-soluble compounds, especially organic solvents. Each solvent has, according to The Beer-Lamber law, the absorbance value (cm^{-1}) that relates the concentration of absorbing species in solution (Mehta, 2012). The higher the value of absorbance, the higher the concentration of the salt in the tested fluid. In this research, the wavelength of 254nm are used as the lambda reference, indicating similarity to drinking water in practice.
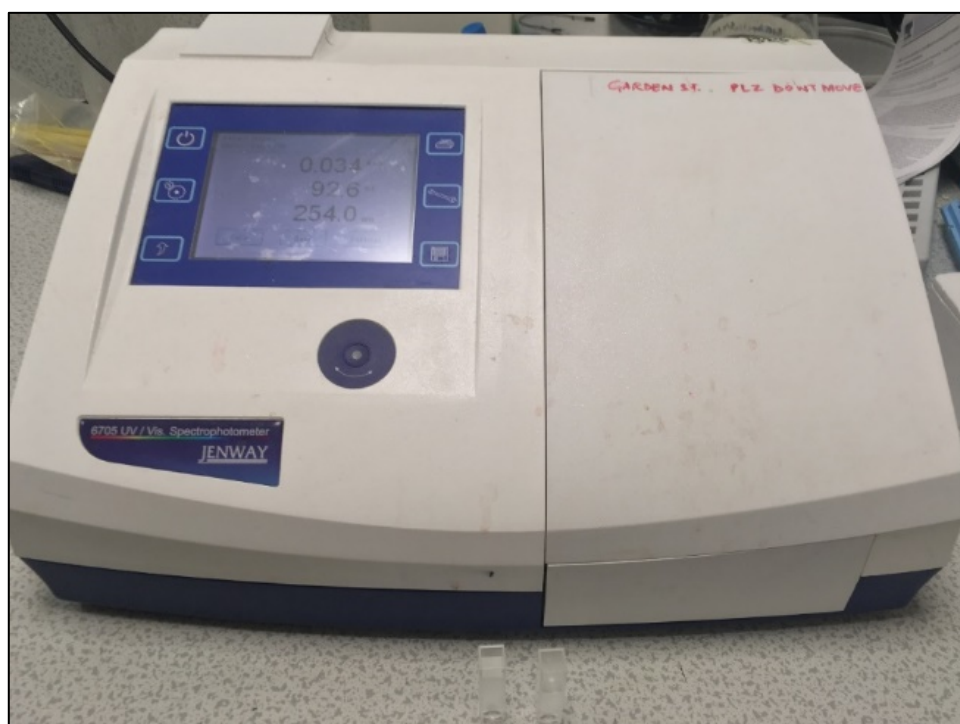
Figure 3.21 Spectrophotometer 67 series used to analyse the properties of seawater from membrane filtration

CHAPTER 4

EXPERIMENTAL DESIGN: DEFOULING RIG, BIOFILM DETACHMENT AND ARDUINO SENSOR

4.1 Introduction

Utilizing microbubbles as cleaning agent has many advantages to chemical engineering industry especially wastewater treatment. Microbubbles produce zero waste which could be harmful to the environment compare to other cleaning agents such as chemicals. According to Tesař, (2014a) and Zimmerman et al., (2008) microbubbles generated by using fluidic oscillator has the highest efficiency. Fluidic oscillator able to generate microbubbles at tenfold smaller size without using any electricity, moving part device, or even chemicals. This research focuses on testing the efficacy of microbubbles on cleaning the biofilm in filtration membrane and from a surface. Cleaning filtration membrane and biofilm from a surface using microbubbles has been widely done by many researchers. However, microbubbles generated by fluidic oscillation for cleaning application was never been done before. **Figure 4.1** shows outline of the experimental design to utilize fluidic oscillator to generate microbubbles. This includes designing a microfiltration system that able to inject microbubbles simultaneously. Most of the data obtained are recorded automatically using Arduino which also custumal designed for this purpose.
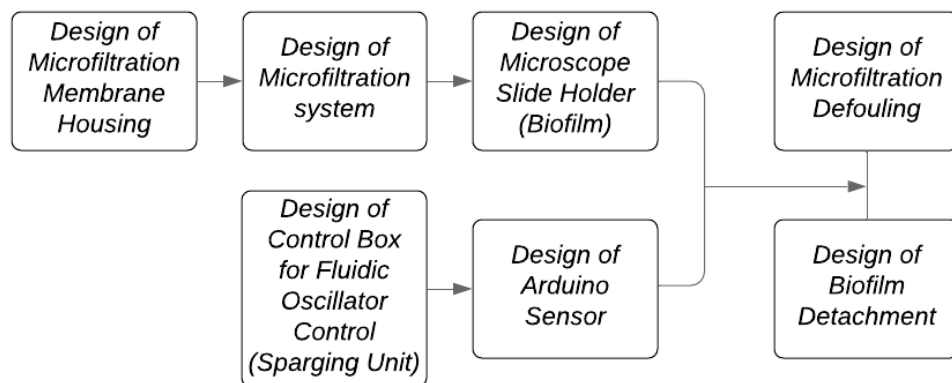
Figure 4.1 Experimental design to utilize microbubbles for cleaning

4.2 Microfiltration (MF) membrane housing

4.2.1 Housing unit: components

The membrane filtration housing is designed according to the specification of the tubular membrane cartridge configuration. The housing unit accommodates the tubular cartridge MF supplied by Aqua Industrial Group of size D×L: 63.5mm×250mm. **Figure 4.2** shows three parts of the housing unit to be assembled consisting of the threaded top lid, the body and the threaded bottom lid with microporous diffuser for microbubble generation.

(a)   (b)   (c)
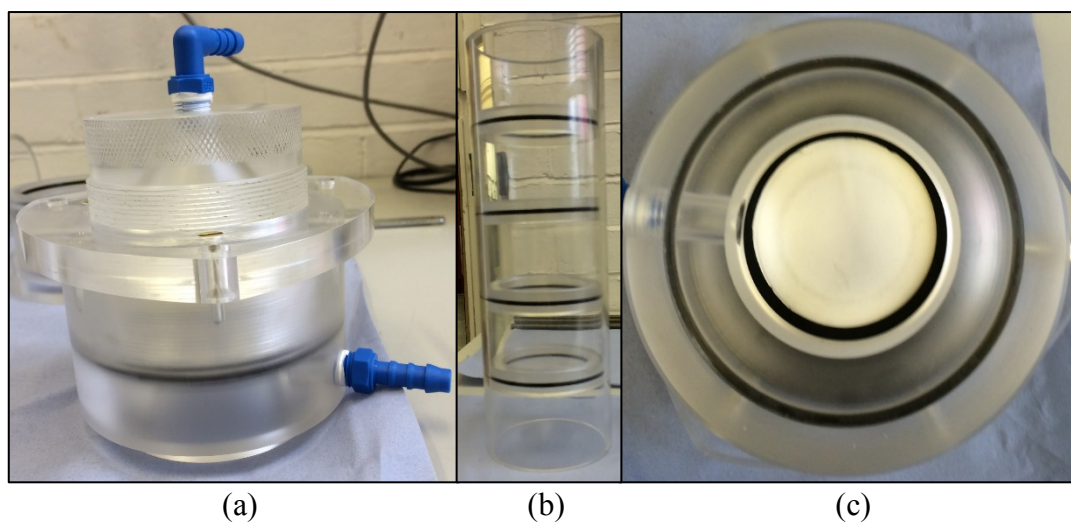
Figure 4.2 The membrane filtration housing unit consists of three main parts (a) Threaded top plug hole for housing lid (b) Body with holder equipped with O-ring (c) Threaded bottom lid plug hole with microporous diffuser

4.2.2 Housing unit: Assembled

In order to accommodate the microbubble cleaning feature into the filtration system, microporous diffuser is attached to the membrane filtration housing. This method and design has been widely used by Wilson et al., (2013), Peña et al., (2012), and Chesters, (2009) as part of Cleaning in Place (CIP) techniques with microbubble cleaning for filtration membrane systems. **Figure 4.3** shows the assembly of the filtration membrane housing unit with microporous diffuser (Point Four ceramic material, Sterner Aquatech, UK) attached to the bottom of the housing. Three steel brackets are used to affix the housing unit using suitable fastenings to avoid leakage.
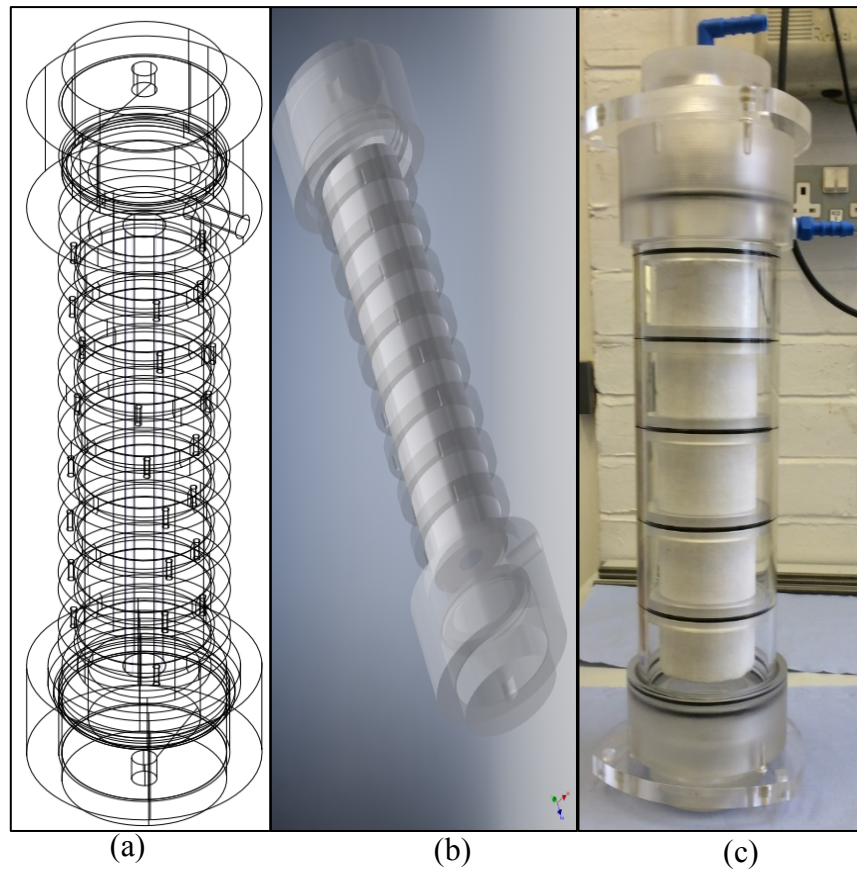
Figure 4.3 Photograph of the assembled tubular filtration membrane housing. (a) Detailed drawing produced using AutoCAD of the cross-sectional view of the membrane housing (b) Artistic representation produced by AutoDesk Inventory (c) Leakage tested and assembled housing filtration unit

4.3 Microfiltration (MF) membrane
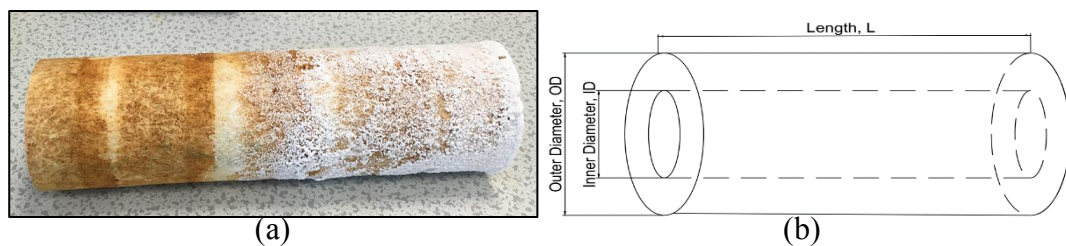
Figure 4.4 Configuration of the membrane cartridge fit in with the membrane housing

Figure 4.4 shows both ends of the MF cartridge surface resulted from the filtration process. The tubular MF membrane cartridge with inner diameter of 30mm and outer diameter of 65mm with 10" in length is used in this experiment. The micron rating or the porosity of the MF cartridge ranges from one to 100 micron. The membrane can be set-up both in either the dead-end or cross flow configurations and is operated under

room temperature between 22.7 and 25.1°C. **Figure 4.5** shows a dried filtration membrane cartridge with the deposition of salt and colloids.

(a)   (b)
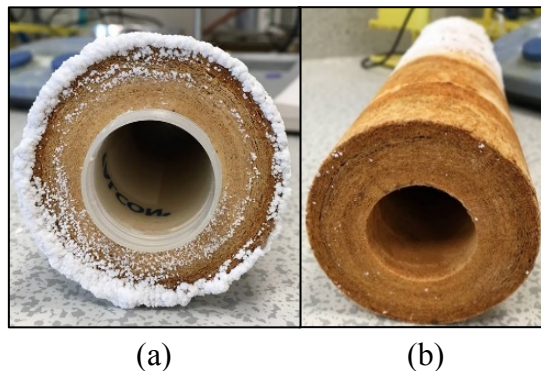
Figure 4.5 Both ends of MF (a) salt deposition resulted from filtration process (b) Cleaned MF using microbubble

4.4   Membrane Defouling

Exploring the potential of microbubble generated by fluidic oscillations towards filtration membrane consist mainly; sparging unit and filtration system.

4.4.1   Sparging Unit Design

The sparging unit schematically represented in **Figure 4.6**. The sparging unit comprises a pressure regulator, a pressure gauge, and a flow meter to instrument fluidic circuitry. The equipment is mainly to control and manipulate the pressure and flowrate of the air supplied to the fluidic oscillator and the microporous diffuser. Compressed air is supplied to the pressure gauge P1 accordingly as shown in the **Figure 4.6** to regulate the air pressure through the system. The pressure regulator P2 plays a key role to the pressure control of the air supplied to the fluid oscillator. With the feedback loop of length 50mm attached to the fluidic oscillator, the oscillation of the airflow through fluidic oscillator can be controlled using the flowrate of air, F3. Valve V4 is issued to create flow resistance to the vent from the unused outlet of the fluidic oscillator. If the resistance down this leg is higher than the diffuser outlet, then there is no oscillation - steady flow proceeds to the diffusers. If the resistance through the unused vent is lower than the diffuser outlet pathway, there is no flow at all to generate bubbles in the test chamber. By balancing the resistances (level of openness of V4), oscillation occurs. The vent with flow resistance balancing avoids duplicating the test chamber in order to create symmetric outlet resistances. Typically valve V4

is tuned by "feel" as the oscillation is strong enough to be felt when the resistance matches, either through touching the ducting or by hand in front of the silencer.

Figure 4.6 Sparging Unit process flow diagram

Figure 4.7 and **Figure 4.8** shows the lab scale for experimental set-up of the membrane filtration system. The seawater is circulated using the pump at 4.5-5lpm depending on the transmembrane pressure developed from the filtrate deposited on the surface of the filtration membrane. Before the system is fed with the seawater, the system is submerged and circulated with tap water for 24 hours to clean and allow pressure normalisation within the system. The system is then fed with the seawater collected and sampled from the Hull Coastal area. The impurities, salt, and colloids will then start to be deposited on the surface of the filtration membrane causing change in the transmembrane pressure. The transmembrane pressure profile is monitored and recorded using pressure transducer logger unit. The pressure transducer, P1 and P2 are placed at the feed and filtrate stream respectively. The difference between the recorded pressure of P1 and P2 is known as transmembrane pressure. In this case, the pressure difference at the beginning would be almost close to zero. Once the colloids and

impurities start to be deposited, filling the membrane pores, then P1 will start to increase while P2 is initially unchanged.
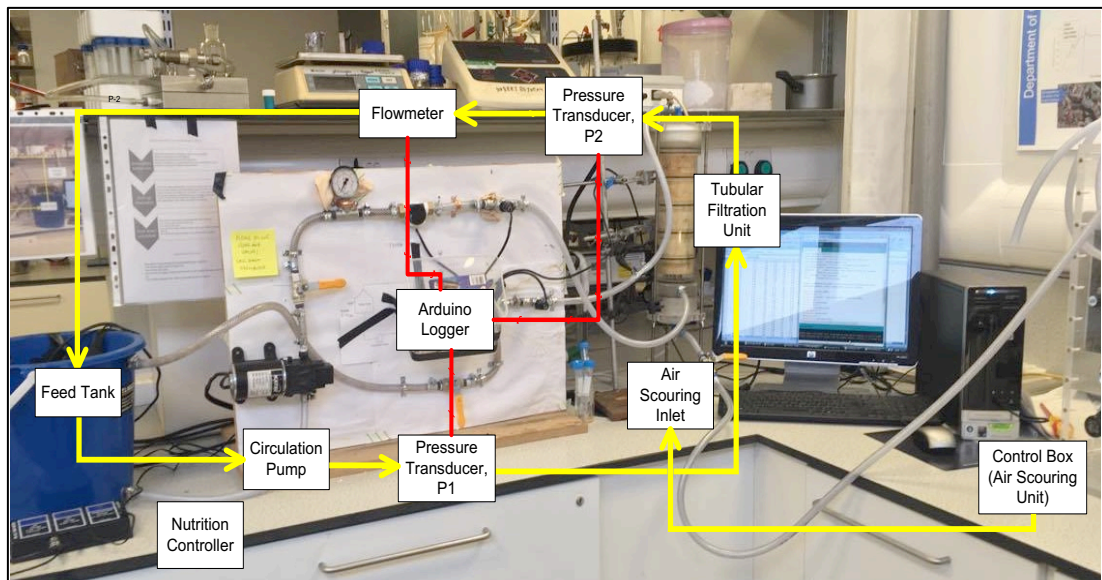
Figure 4.7 Experimental Set-Up
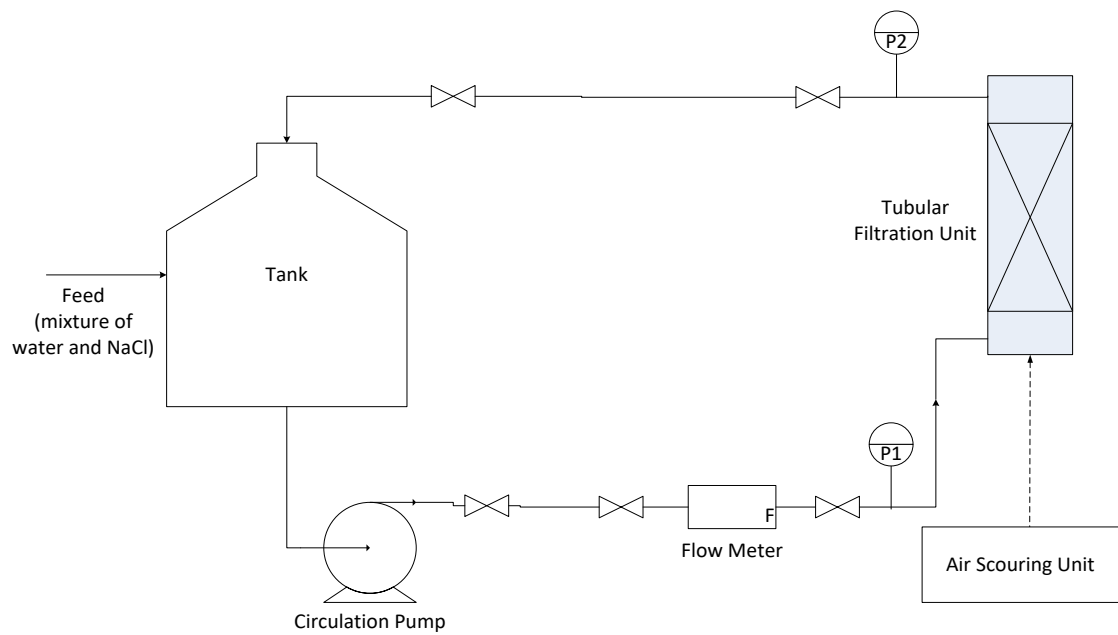
Figure 4.8 Membrane filtration system

4.5 Microscope Holder Design

The microscope slide holder is designed and fabricated using the laser cutter VLS series by Denford. **Figure 4.9** shows an AutoCAD drawing of the microscope slide used as input for the laser cutter machine. The length of the holder (30mm) is selected to accommodate the opaque part of microscope slide.
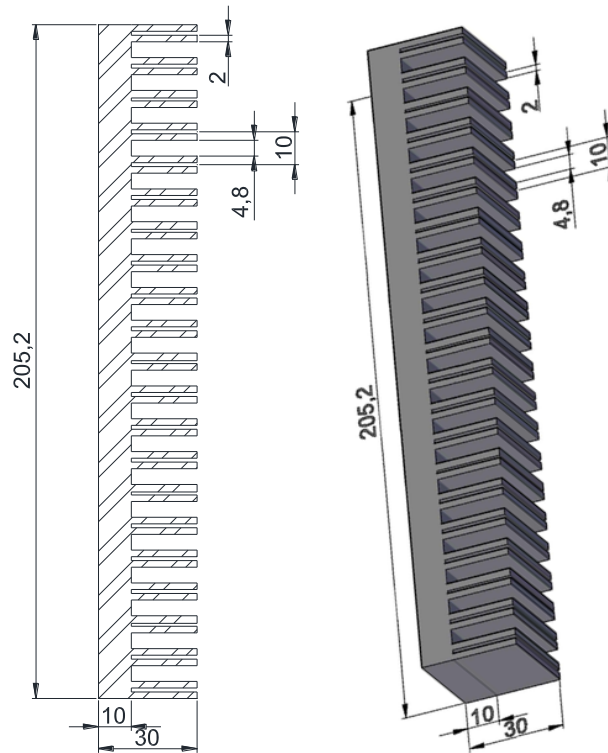
Figure 4.9 Microscope holder design for MB detachment experiment

4.5.1 Lux meter reading

Figure 4.10 shows the arrangement of the lux meter, with readings prior to and after the microbubble cleaning process. The experiment is carried out at the night and in a totally dark room to avoid measurement error. The light source of distance 20cm and 25cm from the light delimiter and photo detector, respectively are kept constant throughout the experiments. The measurements are made by selecting the desired range (x1 lux/fc, x10 lux/fc or x100lux/fc) and the photo detector are horizontally positioned to the light source. The measurements are recorded from the LCD. Specifications and measurement limit of the light meter are available in **Table 9.1**.
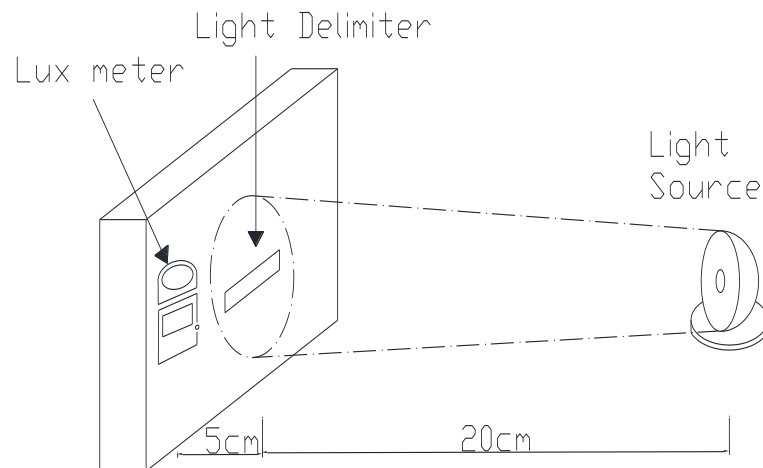
Figure 4.10 Lux meter (N76CC by Maplin) reading by projecting incident light through light delimiter

4.6 Control Box

The oscillation induced by fluidic oscillation is controlled by manipulating the flowrate of the air. Simple instruments such as a flowmeter and a pressure regulator are combined within the control box as shown in **Figure 4.11**. This box is also a part of the sparging unit with schematic diagram shown in **Figure 3.4**, only without the microporous diffuser for microbubble generations. Similar schematics and instruments for the arrangement to control the oscillation of the fluidic oscillations can be seen in the researched conducted by Kamaroddin et al., (2016), Abdulrazzaq et al., (2015; Brittle et al., (2015), Hanotu et al., (2014); and Zimmerman et al., (2011).
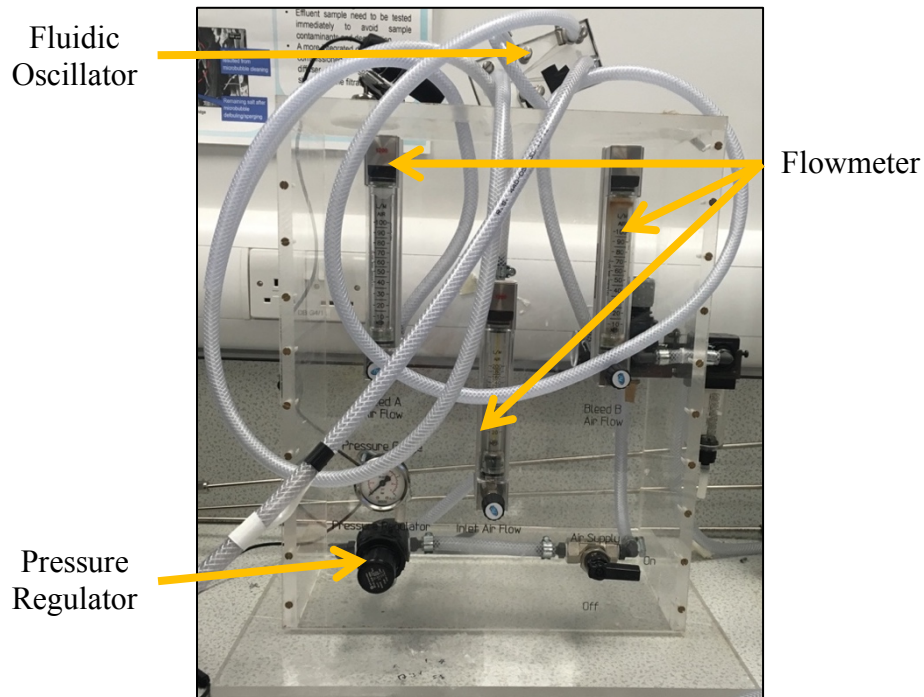
Figure 4.11 Fabricated control box with pressure regulator, safety valve, and flowmeter to control oscillation

The control box mainly consists of the flowmeter, fluidic oscillator, bleeding flow meter/valve, pressure regulator and ball valve. The control box operates starting by checking all the equipment is complete as shown in the general process schematic diagram. Tightened connections between all instruments are checked, and detergents are sprayed to check for any gas leakage. The length of the feedback loop is a selectable geometric variable, easily changed by replacing the Tygon tubing with the required length and connected to the accelerometer.
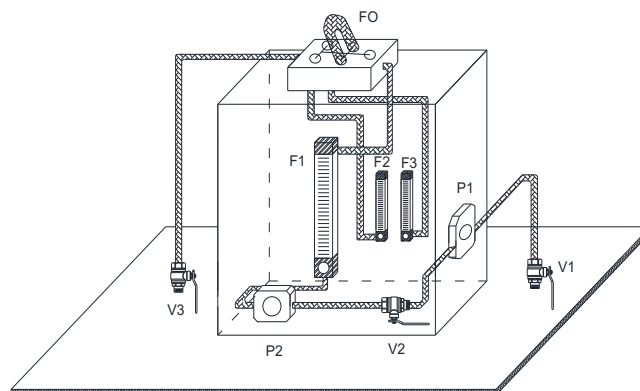
Figure 4.12 Designated control box unit of producing oscillatory flow for fabrication with instruments labelled

The main air supply valve which is connected to the compressed air source has been turned on and let the reading for the flowmeter F1 be 20L/m. The bubble cloud

generated in the water-filled rig is observed, captured, and measured for the bubble size distribution. The control box sets the rig operation conditions. Once the sampling is completed as well as the defouling cycle is completed, the control box is then prepared for the shutdown. All measurements and experimental results are stopped, and the air supply valve V1 is fully closed. No bubble formation at the diffuser is checked, and the air supply from the compressed air tap is then closed.

F1 and F2 have been controlled to manipulate the oscillation frequency as explained in the section 3.2.1. **Figure 4.13** shows how the control box are connected to the filtration system. The microbubbles produced in each system are varied in size and characteristics, depending on the pressure and system requirements which are presented by **Equation 2.3**. For example, the F1 and F2 value for filtration membrane system will not be the same as F1 and F2 required for biofilm detachment unit discussed in CHAPTER 7.
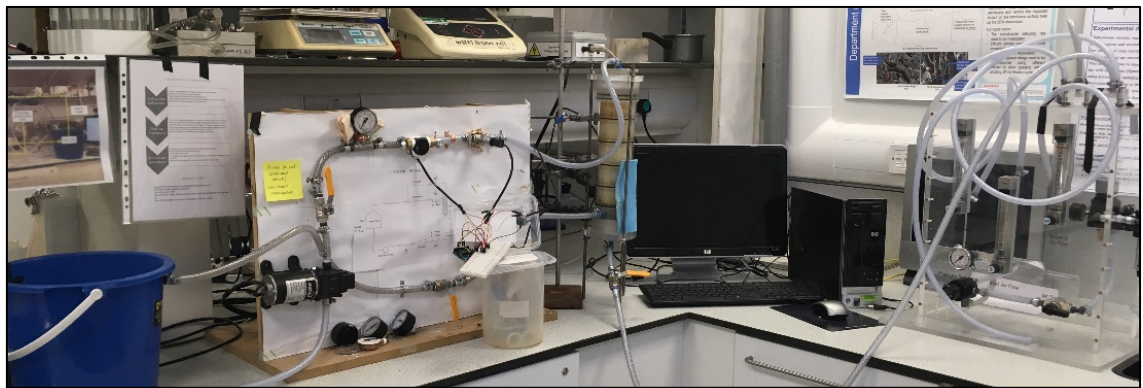
Figure 4.13 Overview of the control box connected to the filtration system

4.7 Arduino

Arduino both the name of a company in Italy and its major product, a microcontroller that interacts with various sensors that is readily programmable for inference and control action (Kushner, 2011). Arduino is one of cheaper options and alternatives for accurate data collection (Barber et al., 2013). This device also has been widely used in research and development program for monitoring environmental quality and for pedagogy (Karami et al., 2018; Sobota et al., 2013). **Figure 4.14** shows the programmable microcontroller supplied by Arduino that are used to connect to various sensors such as the flowmeter, pressure transducers, temperature sensors, and accelerometers at the same time. Arduino Uno boards are connected to the computer

using a Universal Serial Bus (USB) cable and read by the open-source Arduino Software (IDE) as shown in **Figure 4.16**. All of the coding is available in Appendices.
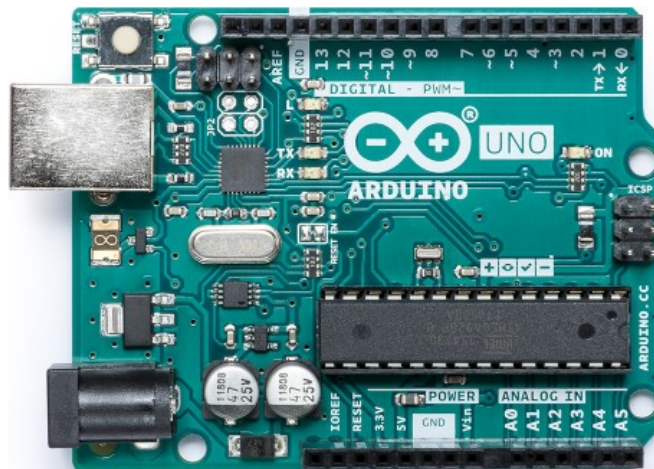
Figure 4.14 Arduino Uno board with input/output (I/O)

4.7.1 Pressure Recorder

Table 4.1 shows the 5V, 0-1.2 MPa pressure transducer sensor for oil, diesel, water and gas. The devices are waterproof sealed and mainly made of carbon alloy steel. It is easy to mount and connected through Arduino board with wiring of red as positive, black as negative, and yellow as output terminal as shown in **Figure 4.15**. The interval of the pressure recorded would be vary according to the needs of the experiment by changing its coding. The pressure transducers able to record up to 120bar at maximum temperature of 85°C, which is very suitable for the filtration system, that run only at maximum pressure of 2bar at room temperature.

Table 4.1 Specifications of the pressure transducers sensor use to measure pressure difference in filtration membrane system

Description	Specifications
Working Voltage	DC 5.0V
Output Voltage	DC 0.5-4.5 V
Sensor material	Carbon steel alloy
Working Current	≤10 mA
Working Pressure Range	0-1.2 MPa
The Biggest Pressure	2.4 MPa
Cable length	19cm
Destroy Pressure	3.0 MPa
Working Temperature Range	0-85°C
Storage Temperature Range	0-100°C
Measuring Error	±1.5 %FSO
Temperature Range Error	±3.5 %FSO

Response Time	≤2.0 ms
Cycle Life	500,000 pcs
Application	non-corrosive gas liquid measurement

As mentioned, the pressure transducer came with three main wiring terminals; positive, negative and, output terminal. **Figure 4.15** shows a photo of pressure transducer that described in **Table 4.1**. This device has been used to record P1 and P2 in the membrane filtration system. Various sizes are available, but ¼" of male threaded is chosen to fit with the tubing and piping system of the filtration system. **Figure 4.15** shows a detail dimension of the size and connection for the pressure transducer used in this experiment to record the transmembrane pressure.
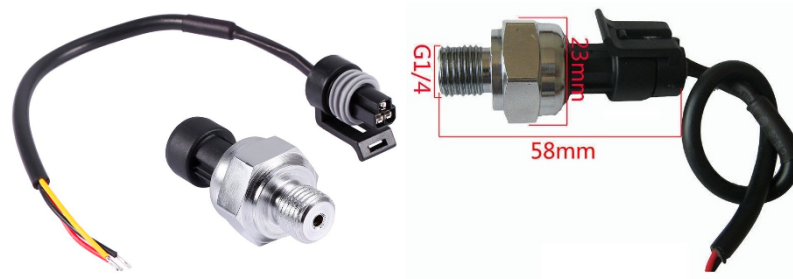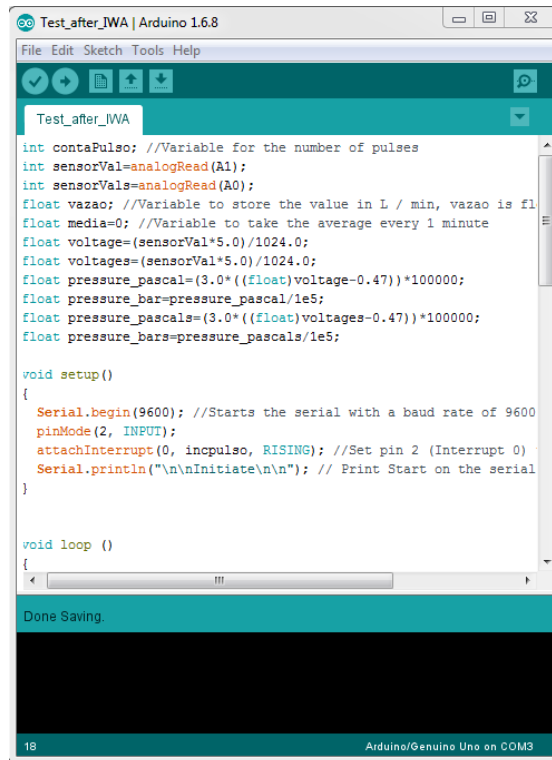
Figure 4.15 Pressure transducer

For the experiment to run between 48-72 hours requires continuous data monitoring and recording. The fluctuations and pressure shock in the transmembrane pressure could happen anytime and unexpectedly. The real challenges are to collect the data automatically without need for operator observation. For this, automated data monitoring is installed using the Arduino microcontroller. Details of the Arduino board, Arduino coding, and Arduino circuit connection are discussed in section 4.7 Arduino. A sample of Arduino coding is shown in **Figure 4.16** where analogRead(A1) and analogRead(A0) represents the terminal connected to the board from the instruments such as pressure transducers, flowmeter, and thermocouple.

Figure 4.16 Sample of Arduino coding for flowmeter and pressure transducer

An Arduino is used in this project, since it is very cost effective, flexible, and highly precise. **Figure 4.17**(a) shows the connection of two pressure transducer to record the pressure P1 and P2 for transmembrane pressure calculations and monitoring. This value is very important to monitor both fouling and defouling of the filtration membrane. The pressure transducers are connected to the Arduino Uno board and the signal is processed and read by the computer based on the coding entered as shown in Appendices and **Figure 4.16**. Digital and analogue pressure gauges in **Figure 4.17(**b) are used for calibration of the pressure transducer P1 and P2.

<p align="center">(a)   (b)</p>
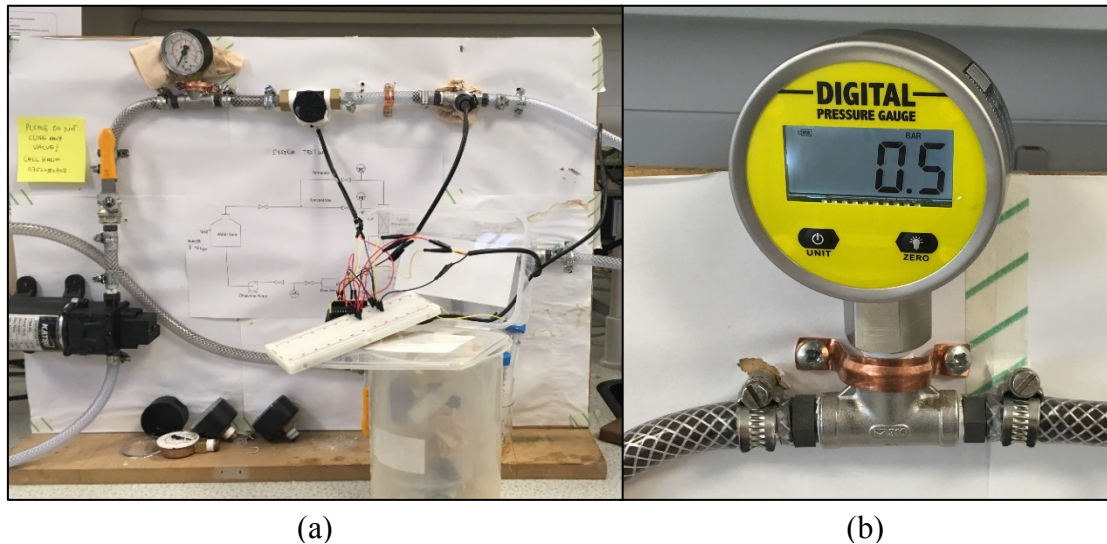
Figure 4.17 (a) Pressure transducer connected to Arduino for pressure recording (b) Digital pressure regulator used for calibrating the pressure recorded

4.7.2 Accelerometer: ADXL345 and GY-61

The accelerometer is used to measure the frequency of the oscillation induced by fluidic oscillator. The results obtained from 3-axis (X-Y-Z) of acceleration unit (m/s^2) have been converted into frequency value using SciDavis software by identifying the highest peak. **Table 4.2** listed the specifications of the sensor supplied by Analog Devices, the data sheets attached in the Appendices. The frequency of the fluidic oscillation measured by Hanotu, (2013) in his thesis were used as preliminary data. This data are then able to produce microbubble characterisation sizing and are discussed in 0. Frequency is one of the main experimentally manipulable variables causing influencing the size of microbubbles generated for effective cleaning, membrane defouling and biofilm detachment.

Table 4.2 Specification of accelerometer used to measure transmembrane pressure (P1 and P2) (Analog Devices)

Description	Specifications
Measurement	X-Y-Z axis
Measurement Range	±2, ±4, ±8, ±16 g
Output Data Rate (ODR)	0.1-3200 Hz
Noise	0.75 LSB rms
Sensitivity Deviation from Ideal	±1.0 %
Operating Voltage Range (V$_S$)	2.0-3.6V
Supply Current	140 μA
Operating Temperature Range	-40 to +85 ºC
Weight	30 mg

Figure 4.18 shows the connection of the sensor with the input/output (I/O) terminal of the Arduino Uno board. The connected sensors are then attached to the tubing ducting the flowing air. The sensor measured the frequency of the flow caused by the oscillation of air by the fluidic oscillator upstream of the inlet to the microporous diffuser. This device is very sensitive to the maximum pressure through the solid surface (Hjort & Holmberg, 2015). Since the switch of the jet (see section 5.3.1) creates a maximum (acoustic wave), there are two maxima per cycle. A downstream pressure sensor as shown in **Figure 4.18** goes through a maximum and a minimum in one cycle (minimum is the switch to other leg, which is the second maximum of the accelerometer). Coding and full connection of accelerometer available in Appendices.
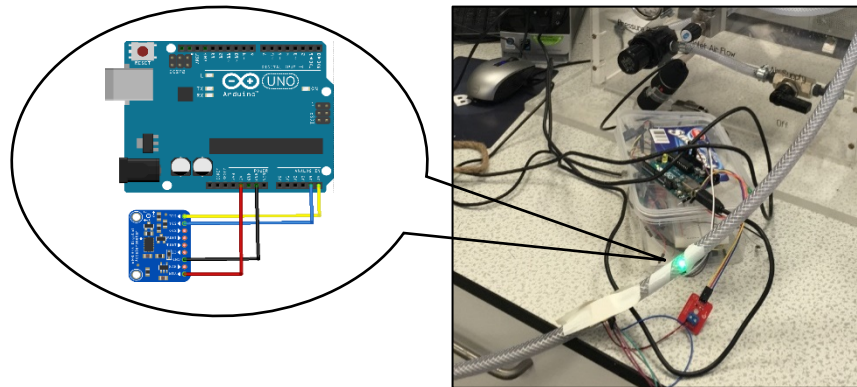
Figure 4.18 ADXL345 accelerometer to measure the frequency of fluidic oscillator

Various oscillation frequencies are induced resulting in different microbubble sizes for studying the effect on biofilm detachment and membrane cleaning. Accelerometery is commonly used by various researcher measured the acceleration in three dimension (x,y,z) which is then converted into frequency (Hz) using Fast Fourier Transform (FFT) and its associated power spectrum as shown in **Figure 4.19**. The oscillation frequency ranging from 220 to 335Hz is used to study the effect on the size of microbubbles generated as discussed in CHAPTER 5. All data of this frequency measurement are available in Appendices and CHAPTER 5.
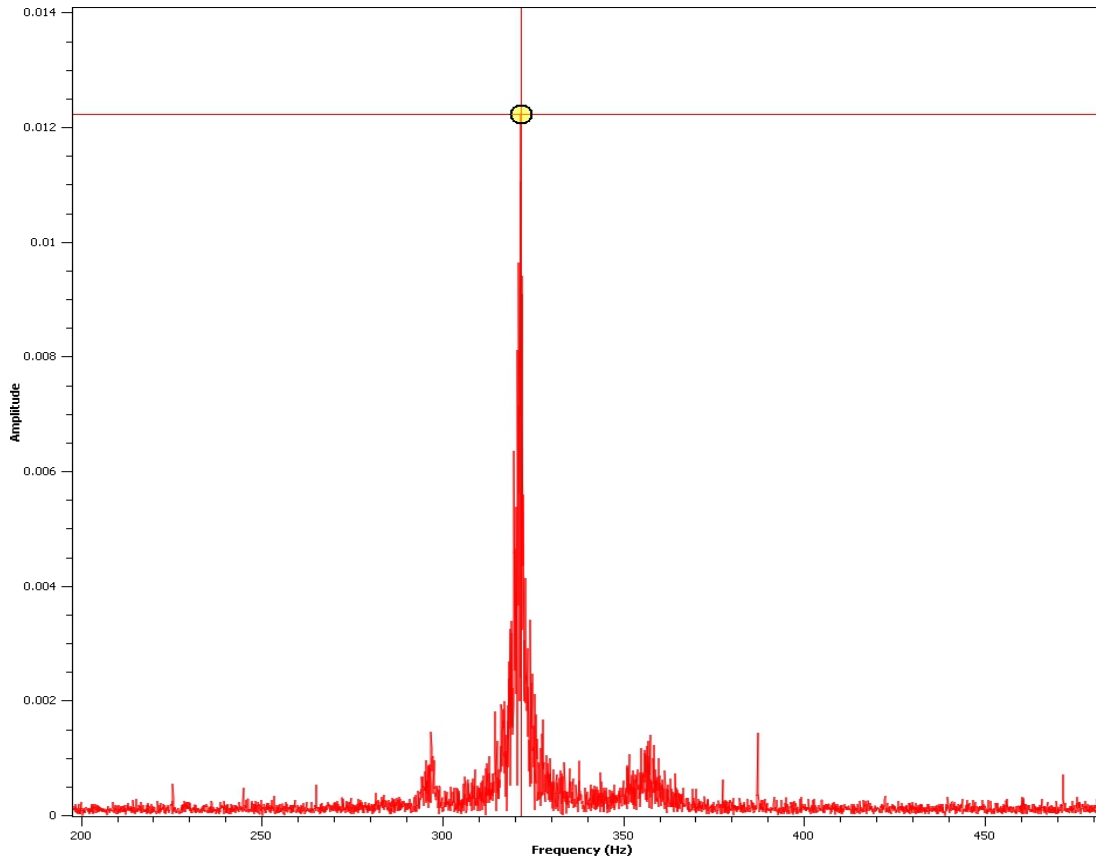
Figure 4.19 Fourier Power Spectrum with maximum power in the mode 321Hz

4.7.3 Flowmeter

The flowmeter is needed to monitor the flowrate of the membrane fouling system. It is constructed using flow meter as specified in **Table 4.3**. A flowrate of 4-5L/min is used which is far from rated maximum and minimum of the instruments. The flowmeter under Arduino coding available in Appendices, measured and collected the flowrate of every 1minute. The flowmeter has been calibrated by using water displacement method.

Table 4.3 Specification details of flowmeter

Description	Specifications
Flow Range	1-60L/min
Output Voltage	DC 0.5-5.0 V
Working Current	≤15 mA
Working Pressure Range	0-1.75 MPa
Working Temperature Range	0-85℃
Storage Temperature Range	0-100℃
Work humidity range	35%~90%RH
Application	Liquid (water)

84

Figure 4.20 shows the general connection of the flowmeter to the Arduino Uno. The connections however have been modified to accommodate the simultaneous data collection of flowmeter and Pressure (P1 and P2) for transmembrane pressure.

Figure 4.20 Flow meter connected to Arduino Uno microprocessor

CHAPTER 5

CHARACTERISATION OF MICROBUBBLES

5.1 Introduction

In this chapter, the sizing of microbubbles has been quantified based on the fluidic oscillator configuration and settings. Microbubbles generated with and without fluidic oscillation are used for an efficacy study for biofilm detachment of filtration membrane, Chlamydomonas algae, and HeLa cells. The methodology of this work has been described in CHAPTER 3 as the bespoke diffuser within a flow system for filtration defouling. The various oscillation frequencies used in this experimental programme resulted in different microbubble size distributions that have different impact on cleaning applications. Except otherwise stated, the results of microbubbles characterisation are presented as measured by high speed camera (Phantom V210) and Arduino (ADXL345) where the feedback loop length of 0.5m is fitted to the fluidic oscillator.

5.2 Bubble generations

Microbubbles have been one of the important alternative approaches to detach biofilms for filtration cleaning in industry (Lee et al., 2014; Agarwal et al., 2011). Size and number of microbubbles or so call microbubble size distributions, are essential operating and control variables for effective bubble-surface contact and cleaning efficiency (Fazel & Chesters, 2015; Wibisono et al., 2015). Thus, characterisations of bubbles using the right pressure and air flowrate are the first things undertaken prior to separation of biofilm from a surface in these bespoke cleaning configurations. In this research, microbubble sizes of 35 to 400µm are produced by using flowrate of 60-85L/min with the bespoke microporous diffuser incorporating alumina ceramics (point four, Sterner Aquatech, UK). Similar microbubble flow conditions have been used previously to defoul a filtration membrane, however the microbubbles were generated under higher pressure, theoretically producing higher microbubble generation rates and smaller in size distribution (Bae et al., 2019; Aslan et al., 2006). However, the low power consumption approach of fluidic oscillation driven microbubbles also results in a high shear rate against fixed surfaces - a consequence

of the laminar flow regime. Detailed and manuals of the bubble generation techniques have been listed and reported in   CHAPTER 3.

5.3   Microbubble size distributions

5.3.1   Effect of fluidic oscillator

Fluidic oscillators have been widely applied in aerospace with propulsion devices such as jet engines and rocket. As a device, it consists of a pair of bi-stable jets inside a flow switching configuration that consists of two potential exit routes for the inlet jet. Under different air flow control regimes, this flow actuator can have either a steady flow or an oscillating of mass flow over a range of frequencies to affect air-controlled flow (Raghu, 2013). This research utilizes such fluid actuation in generating microbubbles. Zimmerman et al., (2008) describes the methods and each functioning part of the fluidic oscillator device so that it can be operated to reduce the size of the bubbles generated, so that the size can be comparable to the micropore from which it emerges. The effect of fluidic oscillation on bubble size distribution has been adapted by Hanotu (2013) for the flotation applications. Various applications of the fluidic oscillation generated microbubbles such as ethanol-water separation, biofuel production and plasma injected flow chemistries are listed in **Table 2.8**. Tesař, (2017) described the advantages of fluidic oscillation to produce smaller microbubbles including high reliability, no maintenance cost, simple handling, and no electrical connections.

The device facilitates the microbubble generation by oscillating a stream of gas from a continuous upstream supply. **Figure 5.1** illustrates the position of microbubbles and water column during the oscillation cycle and microbubble formation. The study conducted by Tesař, (2015) found that the absence of conjunction which keeps the microbubble size smaller (or at the size of pores), is because of the temporary reverse flow direction of air. **Figure 5.1(d)** indicates a second microbubble formation when air is pushed towards the water without touching the first microbubbles that formed earlier. The distance or pulsation amplitude observed are large enough between (b) and (c) to prevent any conjunction between formations of two consecutives microbubbles. The air suction in (a) and (b) move the microbubble back into air passage before it is released to the water by inertia as shown in (c) and (d). Due to the

oscillations, the forward pulse on the upstroke and the minor flow reversal on the downstroke, result in the cut-off bubbles at the development stage as shown in (d).
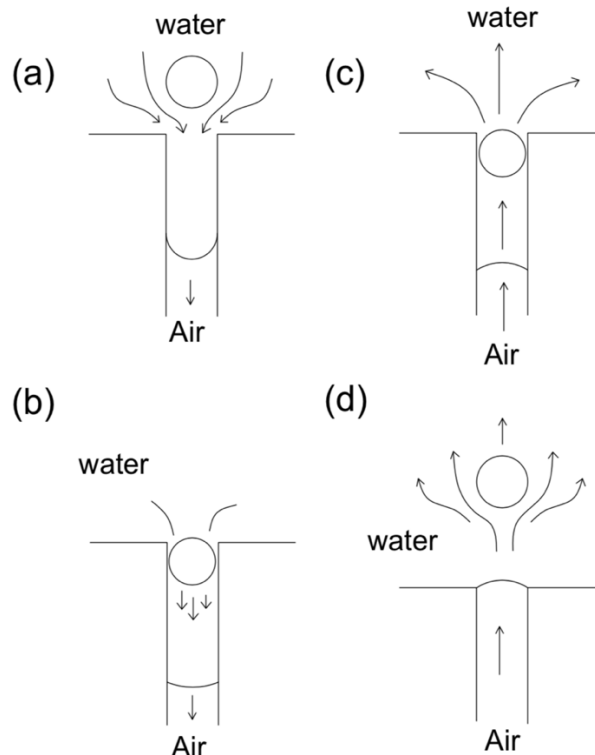
Figure 5.1 Bubble formation (knock-off) facilitates by fluidic oscillations

5.3.2 Effect of gas flowrate

The experiment is usually carried out by investigating the appropriate length of the feedback loop length fitted to the fluidic oscillator to identify the most effective, emergent bubble size. This research however adapted from the previous research of Kamaroddin et al. (2016) and Hanotu (2013) by using the optimised length of 500mm. The flowrate of the bleed valve (see **Figure 3.1**) is manipulated to influence the backpressure of flow towards the diffuser. **Table 5.1** shows the conditions that are used in this experimental programme. The size of microbubbles has been reduced and manipulated by controlling the vent valve flowrate and pressure. The vent valve flowrate is measured by using water displacement instead of an inline ball flowmeter that could dissipate the oscillation pulse. The input flowrate is almost identical to the bleed valve flowrate where over 99.9% is vented, since lab bench experiments would be overwhelmed by the flowrate through the oscillator necessary for the onset of oscillations. For larger scale operations, the fluidic circuit can be tuned to use all the flowrate, but through a much greater surface area of diffusers. According to Brittle et

al., (2015), the actual air flow entering the tank could be range from 0.2 ml/min and 0.5 ml/min depending on the oscillation frequency.

Table 5.1 Oscillation pulse and average bubble size generated at the respected flow of the bleed valve and pressure

Condition	Vent valve flowrate (L/min)	Air flow pressure (bar)	Oscillation frequency (Hz)	Average number of bubble size (um)
I	60	2.0	335	35
II	65	1.8	321	50
III	70	1.6	307	90
IV	75	1.4	285	125
V	80	1.3	256	150
VI	85	1.2	226	<300

Figure 5.2 presents the relationship between gas flowrate and average bubble size generated. The data obtained shows that the higher the gas flowrate of the vent valve, the lower the oscillation frequencies that have been measured by accelerometer ADXL345 (see section Accelerometer: ADXL345 and GY-61). This data are supported by Tesař, (2014b) & Zimmerman et al., (2008), where higher oscillation frequency results in smaller and uniform size of microbubble. **Figure 5.2(b)** shows that the average bubbles size are reduced from 200μm to 35μm with oscillation frequency of 256Hz and 335Hz respectively. Positive correlation also has been observed in **Table 5.1** where pressure increased with the gas flowrate which also supported by Hanotu (2013).
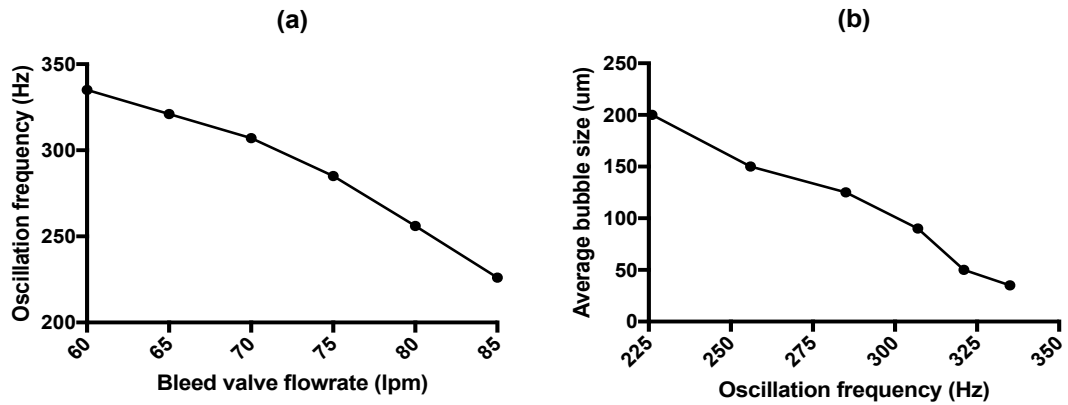
Figure 5.2 Plot the effect of gas flow rate on average bubble size generated (a) relationship between bleed valve and oscillation frequency (b) relationship between oscillation frequency and average bubble size (Desai et al., 2018)

The main objective for these microbubble characterizations is to vary microbubble size to investigate its efficacy on cleaning applications (see Chapter 5, 6, and 7). The size of microbubbles has been manipulated by the operation of the fluidic oscillator. **Figure 5.3** shows that smaller microbubbles size has been generated by increasing the oscillation frequency. The reduction in size of the bubble with increasing of gas flow rate can be explained by the growth mechanisms of the bubbles from their exit orifices and oscillation frequency. Desai et al., (2018) shows conclusively that there is a "sweetspot" in frequency for a fixed flow rate whereby the average bubble size is a minimum. Above this critical frequency, the average bubble size increases. Those authors show that the range of frequencies around the "sweetspot" frequency that achieve dramatically smaller microbubbles is rather narrow, indicating how unlikely microbubble generation by fluidic oscillation was to be discovered without an easy means to sweep a wide range of frequency. With the tygon tubing used for the feedback loop, such a frequency sweep can be achieved with scissors. The patented information by Zimmerman & Tesar, (2010) (Patent No: US 2010/0002534 A1) and several other authors (Bugg & Rowe, 1993; Antoniadis et al., 1992; Akagi et al., 1987) have reported about the microbubble generations through porous materials. This graph concluded that the higher the gas flowrate, the higher oscillation frequency resulted in smaller average microbubble size recorded. In theory, this relationship would aid the biofilm detachment better as the bubble size reduced which has higher contact area (Jang et al., 2017; Zimmerman et al., 2008).
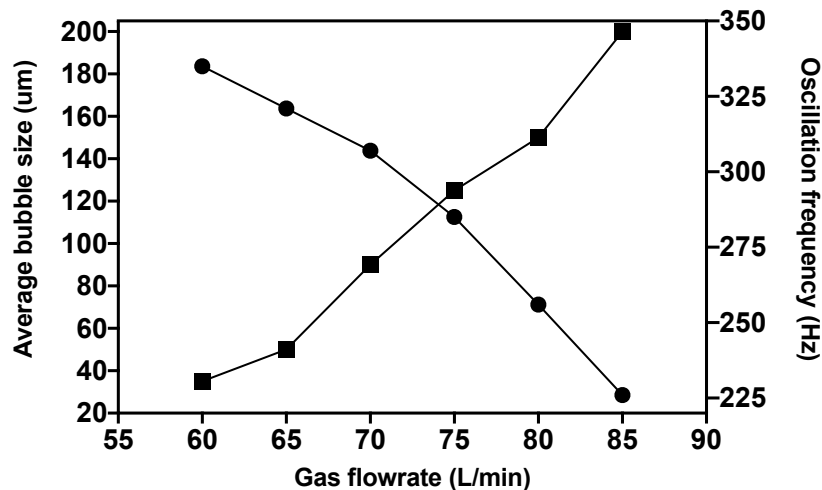
Figure 5.3 Plot of bubble size distribution and Oscillation frequency against flowrate. Average cumulative size distributions calculated for each flowrate bubble generation with a Point Four diffuser

Through a single orifice or multiple submerged orifices, a conventional, steady flow bubble forms due to its own buoyancy force by overcoming the binding wetting force (Simmons et al., 2015). Typically, a bubble tends to grow substantially larger than the diffuser pore size before the detachment. With fluidic oscillation, the inertial force of the pulse breaks this conventional force imbalance with smaller buoyancy force of smaller bubbles, and the detachment is strongly influenced by backflow (Tesař, 2015; Zimmerman et al., 2008). The growth of the bubble primarily caused by the gas supply (Hanotu, 2013). Apart from that, bubble size also increases when it coalesces with the neighbouring or preceding bubbles at their development stage. In this research, gas supply has been oscillated using fluidic oscillator to produce uniformly spaced and smaller non-coalescent bubbles compared to steady state bubble formation (Zimmerman, 2014; Tesař, 2014b). Using the same type and size of diffuser (Point Four), different sizes of bubble have been produced with different oscillatory frequency.

5.3.3 Bubble Density Analyses

This study is mainly about the effect of microbubbles generated with and without fluidic oscillator and assessing its improvement towards filtration membrane and biofilm detachment performance. Under oscillatory flow, different bubble sizes are generated. **Figure 5.4** shows bubbles generated under oscillation frequency ranging from 256 to 335Hz where the different size of the bubble is simply attributed to the

operating conditions of the fluidic oscillator. It can be observed that smaller size of microbubble could be achieved by increasing the oscillation frequency of the gas supply, with the exception that sufficiently high frequency reverses this trend (Desai et al., 2018).
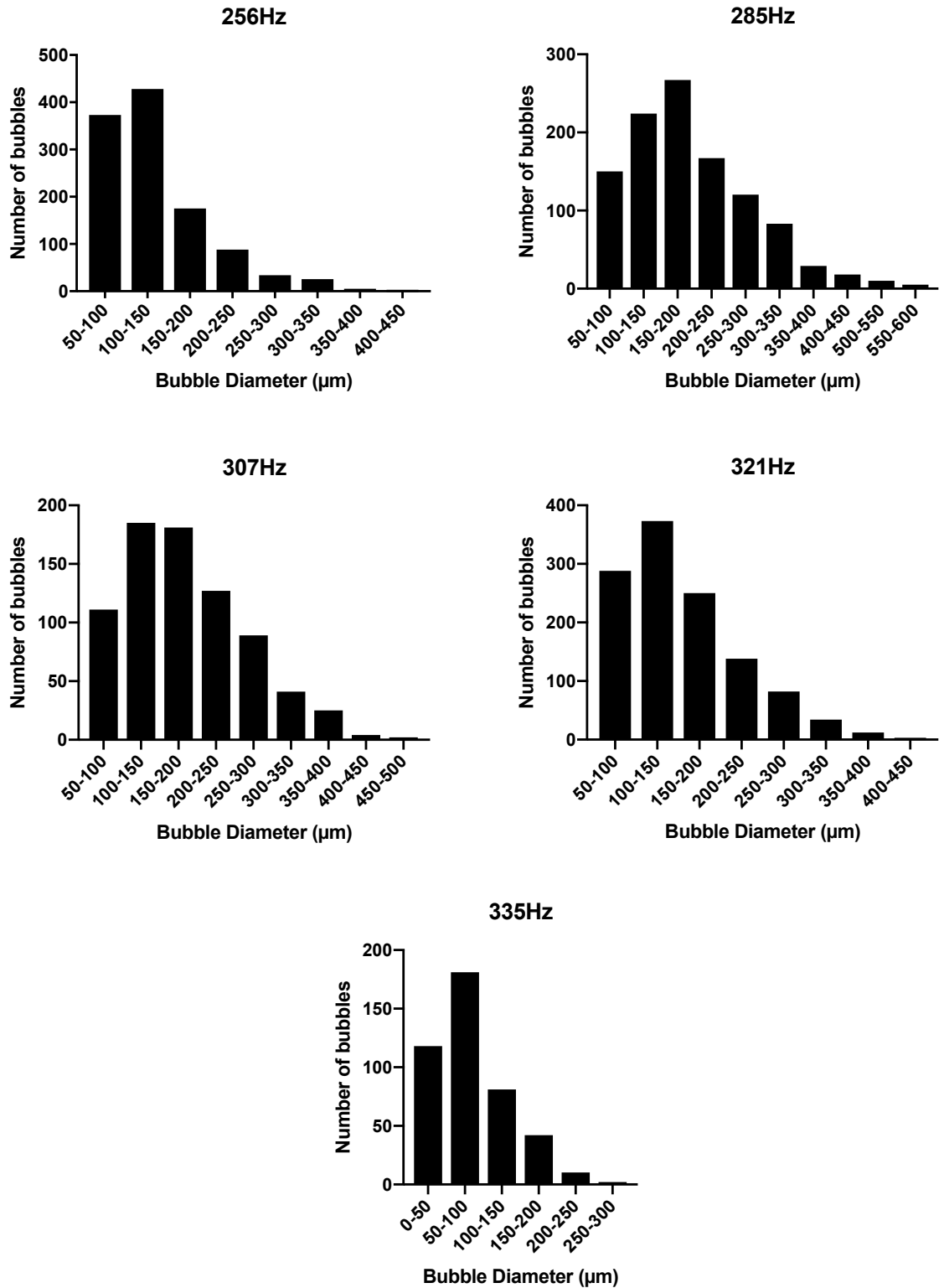
Figure 5.4 The bubble sizes have been measured using high speed camera phantom V210 and image *J*. The graph shows distribution of bubbles produced under oscillatory flow from point 4 membrane diffuser at operating pressure of under 2bar. A portion of the air supply downstream the oscillator was bled-off to match diffuser capacity. The average bubble size measured has minimum and maximum bubble sizes recorded to be ~35 and 300μm respectively

5.4 Summary

Microbubble sizes have successfully been measured using a high-speed camera and analysed using Image J. A fluidic oscillator is used to manipulate the oscillation frequency and microbubble size. It is observed that the compressed air flowrate channelled towards the diffuser and oscillation frequency are inversely related to the microbubble size in the regime of operation in this experimental set-up. In this chapter, conditions that create different microbubble sizes are produced for the intended to study their efficacy for biofilm detachment and membrane filtration defouling. By using flowrates of between 60 to 85 L/min, average microbubble sizes of ~35 and 300μm are produced. These regimes of bubbly flow are expected to have a different impact on the cleaning applications of membrane filtration, Chlamydomonas algae biofilm removal, and HeLa cell detachment to be explored in subsequent chapters. **Table 5.2** summarised the observation of oscillation frequency on the average microbubble size.

Table 5.2 Oscillation pulse and average bubble size generated at the respected flow of the bleed valve and pressure

Category	Condition	Vent valve flowrate (L/min)	Air flow pressure (bar)	Oscillation frequency (Hz)	Average bubble size (um)
A	I, II	Low	Low	High	Smallest
B	III, IV	Medium	Medium	Medium	Small
C	V, VI	High	High	Low	Largest

CHAPTER 6

FILTRATION MEMBRANE DEFOULING

6.1 Abstract

Impurities and colloidal substances are among the many fouling agents that have been used to reduce membrane filtration performance for wastewater treatment. This study investigates the potential of fluidic oscillation generated microbubbles (MBs) to defoul the filtration membrane. Cartridge filters of microfiltration (MF) of 1μm pore size have been fouled using surface seawater collected from the Hull coastal area. The seawater was circulated at 5.8L/min to actuate colloidal substance deposition on the membrane surface. The recorded feed channel pressure drop (ΔP) across the membrane filters shown rapid fouling occurred in the first 8 hrs of the circulation. Fluctuations of ΔP during the next 8hrs have been observed showing the colloids filling the pores of the membrane, then later remained steady for two hours indicating that the membrane was completely fouled. The filtration membrane was cleaned and defouled using fluidic oscillator generated MBs. The fouled membranes were sparged with 1L/min of air scouring for ~1 to ~2hrs to remove the deposited colloids and impurities on the surface of the membrane. The membrane, analysed under Scanning Electron Microscopy (SEM), UV_{254} and EC meter, shows the extent of MBs mediated removal of the deposited colloidal particle from the membrane surfaces. This study found that the highest defouling rate occurs with MBs generated by fluidic oscillator (closed vent), followed by MBs generated by fluidic oscillator (opened vent) and MBs generated without fluidic oscillator are 9.53, 6.22, and 3.41 mbar/min, respectively.

6.2 Introduction

Membrane filtration approaches such as microfiltration (MF), ultrafiltration (UF), nanofiltration (NF) and reverse osmosis (RO) are very important for wastewater treatment and waste recovery (Giacobbo et al., 2015; Bhattacharya et al., 2013; Galanakis et al., 2013). They provide many advantages such as high selectivity, capacity and feasibility. However, they are easily fouled by biofoulings, organic and colloidal substances which restrict the permeation rate and reduce the process efficiency. In general, fouling is usually caused by the deposition of small colloidal particles on the membrane surface and inner walls of membrane pores which results

95

in the formation of cake layer (Zhao & Yu, 2014; Chesters et al., 2013). Conventional defouling methods such as chemical cleaning and pre-treatment usually are destructive and cause waste problems. Recently, innovative studies were conducted to explore the potential of MBs to clean the filtration membrane. Mechanisms such as creating MB pulsating-like action (Wilson et al., 2013), the behaviour of MBs by adsorption (Hiroyuki et al., 2015), and swarm velocity (Lee & Lee, 2002) clearly described the role of MBs in cleaning applications. Agarwal et al. (2012) and Wibisono (2014) listed four steps of cleaning using MB: 1) generation of smaller MBs 2) MBs burst to generate high-pressure spot and shear force 3) continuous biofilm matrix disruption 4) biofilm detachment. Based on the cleaning mechanisms mentioned, it is important to generate smaller microbubble high-pressure spots, however, it is unlikely to generate small MBs by only depending on the various size of pores, shear and material of diffuser system. Zimmerman et al. (2009) generate smaller size of MBs from the diffuser pore using fluidic oscillation by oscillating the feed air stream by pinching off the bubbles knows as a hemispherical cap. Thus, fluidic oscillation microbubbles are generated to assist and compare with the conventional bubble cleaning method to restore membrane performance. MF membrane used as pre-treatment for desalination usually have shorter filter lifetimes due to fouling (Baker, 2004). This research mainly to exploit the advantage of using a cheaper way of producing smaller microbubbles in cleaning MF membrane (Zimmerman, Tesar, et al., 2011). Using MB cleaning, the performance of filtration membrane has been developed positively by prolong the membrane life and alleviating energy consumption (Wibisono et al., 2015; Fazel et al., 2013). Environmentally, this research will significantly bring the food and chemical industries towards green waste management by reducing the waste production and replacement of chemical cleaning agents (Chesters et al., 2013; Mercier-Bonin et al., 2004).

6.3 Membrane fouling and defouling

Fouling usually caused by the deposition of small colloidal particles on the inner walls of membrane pores. The blockages are a build-up of particles in the form of a cake layer on the membrane surface and membrane pore opening. The effect of permeation flux reduction due to fouling is twofold. First, pore blocking, and cake formation lead to the increase in flow resistance. After that, the presence of colloidal particles

deposited on the membrane surface hampers liquid mixing. Thus, a relatively high concentration of solutes persists near the membrane surface which causes the reduction of the solvent flux crossing the membrane (Henry et al., 2012).

The potential of microbubbles for removing the biofilm depends on the internal pressure of the bubble. As governed by the Young-Laplace equation for spherical microbubbles (**Equation 2.5**), the internal pressure of the bubble depends on the diameter of the bubble. The smaller the diameter of the bubble lead to the higher internal pressure and subsequently bubble collapse resulted in higher energy. High energy generated allows more detachment of the biofilm and the cleaning efficiency. **Figure 2.21** illustrates the pressure waves are distributed over the domain of the self-collapsing bubbles eventually dispel the fixed biomass from the membrane surface. The detachment of the biofilm is further simplified in **Figure 6.1** below. Microbubbles used in this experiment generated from the sources of compressed air which does not have wholly soluble properties in water. Furthermore, the microbubble interface is either electron-rich or electron-poor due to the composition of the gas/liquid, so acts as either a Lewis acid or Lewis base, when scouring the surface. Acid or caustic are well known cleaning approaches, but microbubbles leave no residue of acid or base.
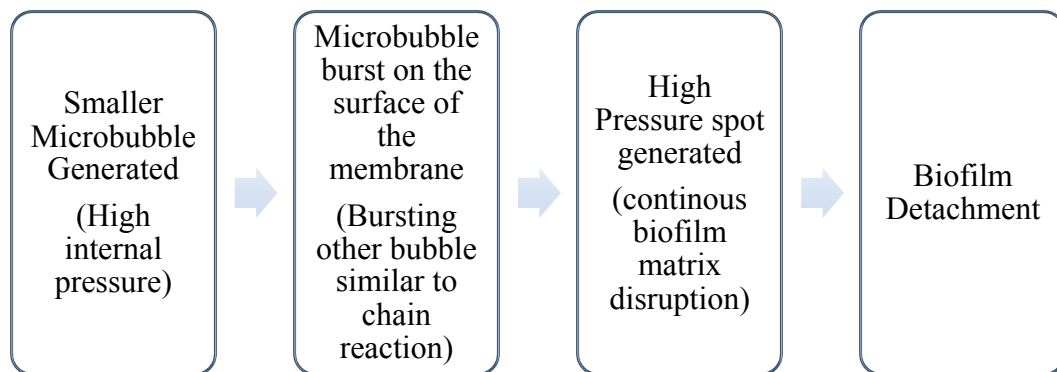
Figure 6.1 Simplified biofilm detachment using microbubble

6.4 Fluidic Oscillator Microbubble Defouling

The mechanisms of using MBs to defoul filtration membrane exemplified in **Figure 2.21** and **Figure 6.1** show great potential in utilizing MBs to control and prevent membrane fouling. Lu et al., (2008) concluded that higher gas flowrate and smaller bubble sparging restrict fouling more effectively on hollow fibre MF membranes. MBs

applied to MF membrane successfully enhance membrane performance by reducing TMP more effectively, enhance the critical flux, and induce lighter cake formation (Hwang & Wu, 2009; Lu et al., 2008; Yu et al., 2003). Lee et al., (2014) found that MBs are able to adhere to particulates and colloidal matters, thus causing them to float, disrupt the gel layer, and provide pyrolytic decomposition of protein.

Zimmerman & Tesar, (2010) patented a method of producing smaller microbubbles using a fluidic oscillator. This device acts as an amplifier by magnifying the control flow through the feedback loop to push the gas jet away from one outlet and toward the other. Symmetry results in these steps repeating, switching the jet back to the first outlet, thereby oscillating the gas passing through the device. Zimmerman, (2014), listed several applications of using smaller bubble generated by fluidic oscillator to strip components of liquid such as gas transfer in bioreactors, anaerobic digesters, and particle separation. Various applications of fluidic oscillator generated microbubble have been studied - better oil emulsion separation (Hanotu et al., 2013), higher separation efficiency via microbubble distillation (Al-yaqoobi et al., 2016), better algal growth (Kamaroddin et al., 2016), and efficient yeast recovery (Hanotu et al., 2014).

In this chapter, the study of defouling will be conducted using MBs generated by fluidic oscillation. A fluidic oscillator connected to the diffuser as shown in **Figure 6.2** is able to produce smaller bubble size (Hanotu et al., 2013). Instead of relying on the structure of porous material for the nozzles to generate smaller bubble, fluidic oscillations divert the jet overcoming the coanda effect to enable the pinch off of the hemispherical cap of bubble formation, resulting in nearly mono-dispersed, uniformly released microbubbles (Zimmerman et al., 2008). This device has no moving parts and is able to produce smaller microbubbles at higher energy efficiency (Tesař, 2014a).

6.5 Materials and Methods

6.5.1 Experiment Design and Setup

In this study, two main phases of experiment were conducted.

I. Membrane fouling by circulating the seawater – mainly increase in pressure drop

II. Microbubble sparging for membrane defouling – optimised membrane performance

6.5.2　Microfiltration membrane defouling
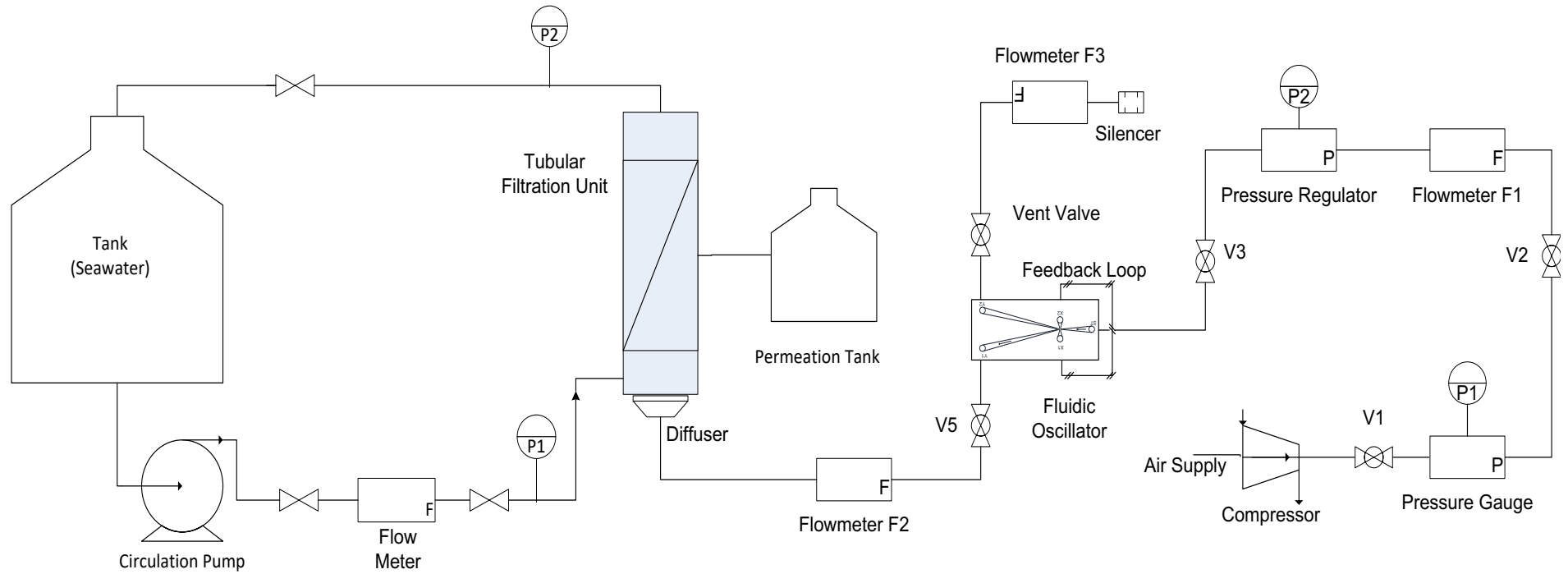
Figure 6.2 Schematic configuration of the membrane defouling system

The filtration system has been developed to remove colloidal substances from surface seawater and circulated at 5.4-5.8L/min. Filtration housing is fitted to a 10inch tubular MF membrane as shown in **Table 6.1**. Pressure drop of the filtration system recorded every one minutes. A flowmeter and pressure transducers (P1 and P2) are connected and recorded using an Arduino Data Logger. For the experimental start-up, the tubular unit was circulated with tap water for 24hr to allow soaking process and pressure to balance before being fed with seawater. 5ml of the effluent sample is collected at one minute intervals from the beginning and with every imposed pressure drop level. One tubular unit runs for 3 days. Once the pressure drop is constantly above 1.4bar, the system was sparged with microbubbles from air scouring unit. The air scouring unit consist of a control box (pressure regulator, valve, pressure gauge) were connected to the fluidic oscillator and diffuser. Air flow rate injected with the feed approximately 1L/min using alumina diffuser produces 100-1000μm size of microbubble to defoul the filtration membrane. The fluidic oscillator was operated with feedback loop length of 500mm. MBs sparged the membrane and membrane sample are analysed by SEM.

6.5.3 Main membrane characteristics, pore sizes, and composition

Table 6.1 presents the information of the main membrane characteristics. Microfiltration membrane (MF) of 1-micron pore size operated using crossflow configuration at room temperature during summer time. Seawater fed to the membrane are filtered specifically for the impurities and colloidal contained.

6.5.4 Seawater and membrane sources

Seawater was collected from the East Riding of Yorkshire, England at Spurn and stored at room temperature ($21\pm4°C$) prior to all test. UV_{254}, and pH of the seawater were at $0.034cm^{-1}$, an 8.0 respectively.

Table 6.1 Main membrane (Aqua Industrial Group) characteristics and operating conditions

	Properties
Type	Sediment cartridge (guard) filter
Material	propylene
Micron rating	1micron
Cartridge dimension	ID:30mm; OD:65mm; L: 255mm
Flow type	Inside-out

Membrane configuration	Tubular
Membrane System Setup	Cross-Flow
Temperature	Room ~22.7-25.1(°C)
Pressure initiation	2bar

6.5.5 MBs operating conditions

MBs were generated using the scouring unit which is connected through the alumina diffuser at the bottom of the filtration housing. The air was injected through the diffuser at flow rate and pressure of 1 l/min and 2.2bar respectively. The bubble size generated are in the range of 100-1000micron. The following MBs conditions were generated:

I.   1L/min of flow with slightly open vent valve

II.   1L/min of flow with fully closed vent valve

III.   Non-fluidic oscillator generated microbubbles/ steady flow sparging

6.6 Data Collection and Measurement

6.6.1 Arduino Pressure Transducer and flowmeter

Two pressure transducers were installed at the inlet, P1 and outlet, P2 to measure the pressure drop while the flowmeter connected after the circulation pump. The analogue reading for both of these instruments are connected to Arduino Uno data logger. The data were collected at 1minute intervals using the PLX-DAQ excel sheet.

6.6.2 Nutrition Controller

Continuous monitoring of the pH value, Total Dissolve Solids, TDS (EC) and temperature of the feed were inferred using the Continuous Monitor Hydroponics trimeter. The sensors were placed in the feed tank. The nutrition controller collected the pH value, TDS and temperature of the system. The sample was collected and analysed using UV/Vis spectrophotometer.

6.6.3 UV absorbance and SEM

The UV absorbance of the water was measured at 254nm using UV/Vis spectrophotometer (Jenway 6705). At the beginning of the experiment, during microbubble sparging, and if there were fluctuations of P2, UV absorbance were tested

at the intervals of 1 minute for twenty minutes. With steady pressure drop, the absorbance measured in the interval of 30mins to 1hr. The surface of the membranes after the experiment was dried at 50°C for one night and coated using gold. The gold coated membrane surface was examined for the colloidal deposition and removal under the Scanning Electron Microscope (SEM).

6.7 Results and Discussions

6.7.1 Effect of microbubbles on fluid properties

Figure 6.3 shows the Electrical Conductivity (EC) value collected from the trimeter nutrition controller. Both of the value decreases over time indicates that membrane was fouled. The rapid decrement of the absorbance and EC showing the dissolved solids were deposited on the surface of the membrane during the first 500minutes which is roughly after 8hrs of circulation. The values remain constant for about ~2hr showing the membrane filtration efficiency has dropped due to its ability to filter more particles is now limited. This finding is in agreement to the study conducted by (Gwenaelle et al., 2017) which stated that fouling could be initiated just after 15minutes of filtration. When the microbubbles were introduced to the system after the 700th minute, the absorbance value varies from 0.019cm^{-1} to 0.0225cm^{-1}. It could be assumed that some of the deposited particles on the membrane surface scrubbed by the microbubbles were recirculated through the filtration system. Antithetically, there are no changes in EC value after MB due to constant salt concentration as MF does not separate ions. The EC value however observed to have remarkable changes over 1000min filtration period due to some colloids breakdown and ion charged on the surface of the membrane which has been explored by Thomas & Cremers (1970). Both values, however, continue to decrease over time and after MB's treatment.
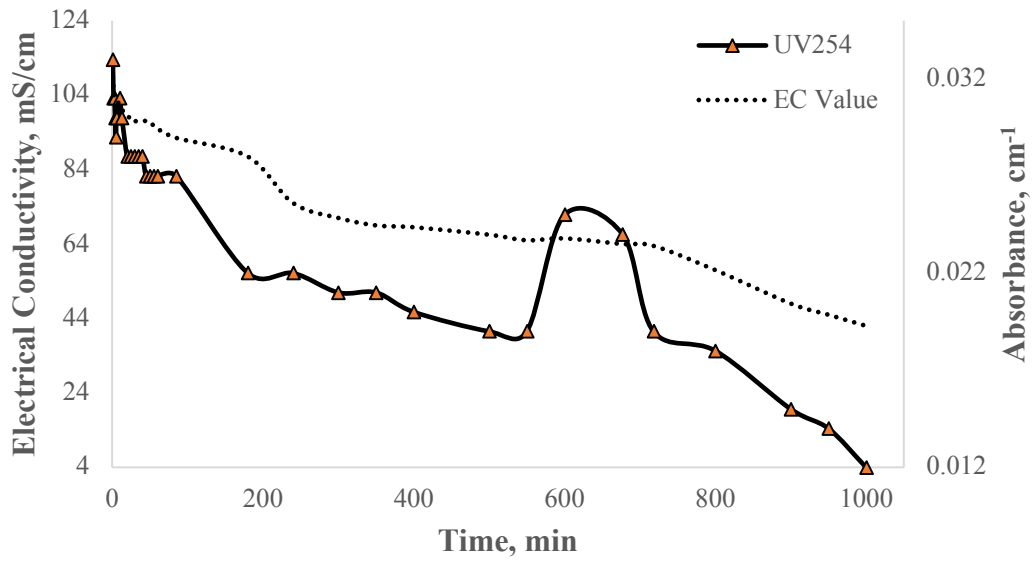
Figure 6.3 UV$_{254}$ and EC value

6.7.2 Overall fluidic oscillator generated microbubble cleaning

Pressure is the main probe for examining the properties and results of this study. Increasing in transmembrane pressure drop (TMP) means that the filter is continuing filtering the impurities from the seawater and particles were deposited on the surface of the membrane. In this study, the microbubbles were introduced at the 600th minute to remove the deposited particles from the surface of the membrane.

Fluctuations in **Figure 6.4** shows the following experimental configuration in order.

I.   Slightly open vent valve: Better TMP reduction

II.   Fully closed vent valve: Best TMP reduction

III. Non-fluidic oscillator generated MBs: Slowest TMP reduction
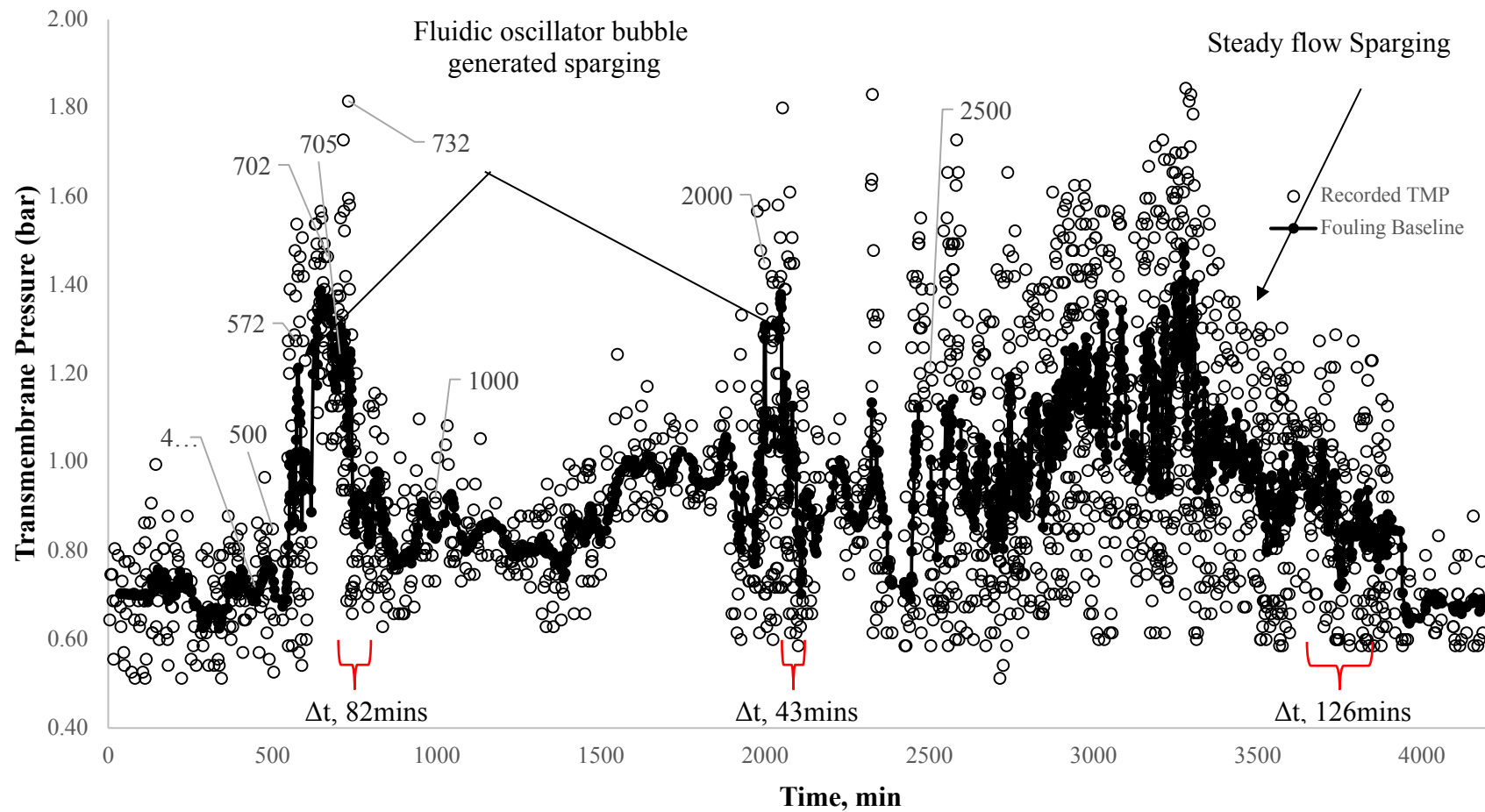
Figure 6.4 Membrane fouling and defouling with and without fluidic oscillator generated microbubble

Figure 6.4 shows the pressure drop recorded for each 1minute interval for the whole filtration cycle of 72hrs (3days). The difference between the inlet and outlet pressure gives the transmembrane pressure (TMP) across the membranes. At the 450th minute, the pressure transducer recorded small fluctuations of pressure which heralds that impurities started to deposit and filling the membrane surfaces and pores. Rapid fouling was observed from 500min to 572min and starts to record a constant pressure drop until minute 702. The TMP fluctuates at minute 732 showing the pressure fluctuations due to pressure release from diffuser once microbubbles were introduced at 705min. This preliminary data showing the positive relationship between the bubbles and cleaning due to shear forces, drag forces, and strong velocity fluctuations induced by the bubble flow (Nagaoka et al., 2006).

After the sparging processes were stopped, the TMP started to increase. At 2000 minutes, a similar trend of the fouling was observed for which the TMP remains constant showing the fouling reaching saturation. Fluidic oscillator generated MBs once again are introduced with zero vent flow to the system. This resulted in higher defouling rate; where the bubbles possess sufficient or higher shear and drag force to detach the deposited particles. Higher TMP is also recorded after 1000 and 2500 minutes showing the MBs defouling were not able to restore the performance of the membrane to its initial conditions. The slowest defouling rate was recorded as non-fluidic oscillator generated MBs were sparged to the system as shown in **Figure 6.4**. It requires approximately 125minutes to reduce the pressure drop before it was fouled. The data shows that MBs generated by fluidic oscillator without vent valve flow has the highest efficiency of the defouling followed by the MBs generated by fluidic oscillator with vent valve and MBs generated without fluidic oscillator. The defouling assumption was in line with the dissolve particles as shown in **Figure 6.3** where the fluid quality was improved over the time. This means that most of the particles were filling the pores and MBs sparging creates additional forces for better defouling.

6.7.3 Fluidic oscillator and defouling rate

The highest TMP for each defouling were recorded at the time elapsed. Details description of the process are tabulated in **Table 6.2**, the data obtained which similarly

presented by **Figure 6.4** are used to calculate the defouling rate using **Equation 6.1**. Three defouling methods were applied, where the highest recorded defouling rate achieved by using fluidic oscillator (condition: I) at 9.53mbar/min followed by fluidic oscillator (condition: II) at 6.22mbar/min and lowest defouling rate without fluidic oscillator (condition: III) at 3.41mbar/min. Attributable to greater flows with more shear and drag force, the MBs generated under condition I by using fluidic oscillator have the highest defouling rate of 9.53mbar/min. MBs generated under condition II by fluidic oscillation showing half of the defouling rate followed by the condition III generated MBs and it is agreed by Lee et al., (2014). This finding also have been studied by Wibisono et al. (2015), stated that higher velocity and more bubble flow (as condition II) reflect positive improvement in membrane process. Under condition III Zimmerman et al. (2008) stated that the bubble size are tenfold larger in size. Wu, et al., (2012) explained the limitation of larger size bubble on fouling control for the deposition of small particles.

Table 6.2 Process and pressure description of the highlighted procedure of Condition I, II, and III

Time (m)	Transmembrane Pressure (bar)	Description
450	0.78	Small fluctuation of pressure
500 - 572	0.8 to 1.4	Rapid fouling
572 - 702	1.20 – 1.40	Constant TMP
720-802	1.50 – 1.00	Microbubbles sparging (Condition: I)
1000 - 2000	0.88 - 1.1	Fouling
2000 - 2068	1.20 – 1.40	Constant TMP
2068 - 2011	1.46 – 0.90	Microbubbles sparging (Condition: II)
2111-2500	1.05	Fouling
2750-3300	1.20 – 1.40	Constant TMP
3303 - 3429	1.79 – 0.80	Microbubbles sparging (Condition: III), without FO
3429-4185	0.8 – 0.60	Fouling

$$Defouling\ rate = \frac{TMP_f - TMP_i}{T_f - T_i}$$

<div align="right">**Equation 6.1**</div>

<div align="right">
TMP_f is Final Transmembrane Pressure
TMP_i is Initial Transmembrane Pressure
T_f is Time when stop MB sparging
T_i is Time start of MB sparging
</div>

Example calculation for defouling rate for condition I.

$$Defouling\ rate = \frac{1.52 - 1.01}{802 - 720} = 6.22\ \mathbf{mbar/min}$$

Generally, the most efficient MF defouling is achieved by scouring the MF under fluidic oscillator generated MBs. This finding shows that fluidic oscillator generates smaller MBs. This results in higher efficiency of cleaning effect to scrub the colloids and impurities deposited on the surface of the MF (Lee et al., 2014; Wibisono, 2014). Zimmerman, (2014) explains the MBs generated by fluidic oscillations would inhibit repulsion between bubbles and particles for better particle separations which is also in agreement with the study conducted by Hiroyuki et al., (2015) and Agarwal, Ng, & Liu, (2011). This, however, leads to a different finding of using the fluidic oscillator towards the cleaning effect. The highest defouling observed while using oscillator without flow of air in vent valve (condition: II). The basic inference from this is because more flow of air to the diffuser results in more bubbles generated compared to the oscillator with open vent valve. Manipulation of oscillator frequency by changing feedback loop length and bleeding flowrate is crucial to ensure smaller bubble generation (Brittle et al., 2015; Zimmerman et al., 2008). **Figure 2.19** and **Figure 3.1** illustrate the characteristics and function of the fluidic oscillator which need to be further investigated.

6.7.4 Colloids deposition and its removal - Scanning Electron Microscopy (SEM)

Colloids deposited on the surface of the fouled membrane

Colloids removal resulted from microbubble cleaning

Remaining colloids after microbubble defouling/sparging
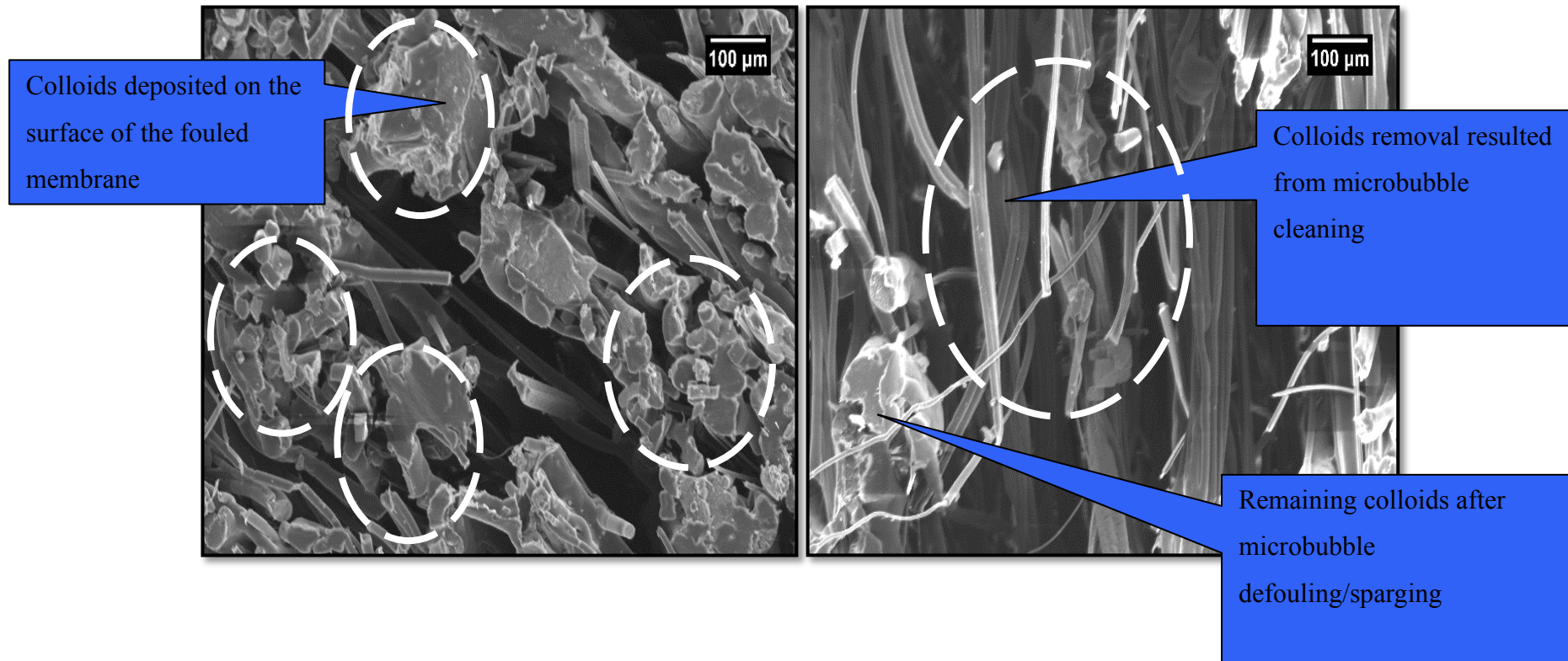
Figure 6.5 (a) SEM images for the fouled and 4.7(b) defouled membrane

Figure 6.5(a) shows SEM images of the colloids deposited on the surface of the MF membrane. Because of MF has large pores, the filtration process will basically remove large size molecules such as colloids. However, some salt particles might be also present due to the process of drying prior to SEM analysis. **Figure 6.5**(b) shows the defouled membrane filter after MB scouring. It can be clearly seen that MBs generated by fluid oscillation scrubbed all of the impurities from the surface of the membrane. Nevertheless, not all of the impurities are removed. The result obtained is similar to the ones conducted by Gwenaelle et al., (2017) where less than 100% impurities are removed by MBs. It has also been suggested that combining MBs with chemical agents such as coagulants may help to improve the rate of impurity removal. The image however only showing the removal of the impurities by the end of the final sparging interval (after 72hrs).

6.8 Conclusions

Microbubbles generated by fluidic oscillation are able to increase the effectiveness of membrane cleaning and defouling. These microbubbles resulted in higher defouling efficiency of filtration membrane. The TMPs recorded able to distinguish the relationship of fluidic oscillator and defouling rate. The results show that microbubbles generated without fluidic oscillation have the lowest defouling rate of 3.41 mbar/min. This value shows that by using fluidic oscillator at higher frequency generated microbubbles, defouling rate increased by 64.2%. It is observed that microbubble under the influence of low oscillation frequency of fluidic oscillator has the defouling rate of 6.22 mbar/min which is 45% higher. The defouling rate also increased by having microbubbles generated at higher frequency fluidic oscillation. Generally, the microbubbles generated at higher venting flow have higher frequency as described in Chapter 5.

CHAPTER 7

USING MICROBUBBLE ON CHLAMYDOMONAS AS BIOFILM DETACHMENT

7.1 Introduction

Microbubbles have been widely used for various application of cleaning such as membrane filtration, pipe cleaning, and column flotation (Watabe et al., 2016; Hiroyuki et al., 2015; Agarwal et al., 2011; Miyamoto et al., 2007; Lee & Lee, 2002). In many cleaning applications, the main objective is to remove the biofilm formed during operation. Biofilms usually consist of various adherent cells embedded by extracellular polymeric substances (Jang et al., 2017; Lee et al., 2014; Agarwal et al., 2012). In this study, Chlamydomonas is chosen as a source of biofilm. The effects of the microbubbles on the detachment of Chlamydomonas from the surface of microscope slides are studied.

The fluidic Oscillation (FO) driven microbubbles have different characteristics from other classes of generation methods due to their production in and maintenance of laminar flow (Zimmerman et al., 2008). The low kinetic energy environment allows high relative shear rates on surfaces, as well as more effective attachment to particles upon collision due to absence of floc breakup mechanisms. The details and mechanisms of the fluidic oscillator have been discussed and reviewed throughout this thesis especially in section 2.8 and 3.2. Compressed air sparged through a microporous diffuser generates different sizes of microbubbles as explained in 0. The microbubbles generated have different cleaning efficacy for the detachment of Chlamydomonas from a microscope slide. To assess the effectiveness of cleaning by microbubbles, the algae have been exposed under same conditions such as time exposure, pH value, and temperature. In this chapter, the effectiveness of microbubbles as cleaning agents for the detachment of Chlamydomonas algae is inferred by measuring luminous transmission with a lux meter. The fully cultured algae have a thick green colour due to chlorophyll which occludes the light transmission through the microscope slide. After the cleaning process, greater light transmission indicates a greater level microalgae removal – effective cleaning.

7.2 Methodology

A representative experiment involves four simple steps to investigate the effectiveness of the microbubbles for biofilm detachment from a surface. It starts with culturing the biofilm in media deposited on the surface, followed by microbubble actuated detachment with detachment analysis using lux meter capture data. In this chapter, Chlamydomonas algae have been cultured using Bold's Basal Medium (BBM) onto the microscope slide. The steps shown in **Figure 7.1(a)** and **(b)** are the most crucial steps to control the experiment, where the evolution of the biofilm layer formed on the surface of the microscope slide is monitored regularly using step (d). The consistencies of the lux meter reading are set to 60 lx to initiate the experiment. The microscope slides are placed on the microscope slide holder and submerged into 1L microbubble tank contained 0.5L of Phosphate Buffer Solution (PBS).

As shown in **Figure 7.1(c)**, the microscope slide holder is positioned at three angles, 90º, 45º and 0º. For comparability of results, each microscope slide holder has been submerged in the quiescent liquid for two hours prior sparging. The biofilms are detached from the surface of the microscope slide using six conditions as described and explained in 0 at time intervals of 2 minutes for 1hour. The remaining biofilm on the microscope surface is measured as shown in **Figure 7.1(d).** The lux meter is interpreted that the higher the reading, the more light transmits through so better cleaning is achieved. The experimental design used of this chapter is similar to the experimental set up used in CHAPTER 8 for HeLa cell detachment aimed for dental and tissue culture applications.

The recorded lux values have been used to calculate the detachment rate using **Equation 7.1** where Lx_f and Lx_i represents final lux and initial lux value.

$$\boldsymbol{Detachment\ rate = \frac{Lx_f - Lx_i}{Time\ (min)}}$$

Equation 7.1

(a) Chlamydomonas culture

(b) Cultured and transferred onto microscope slide

(c) Microbubble cleaning

(d) Lux meter reading
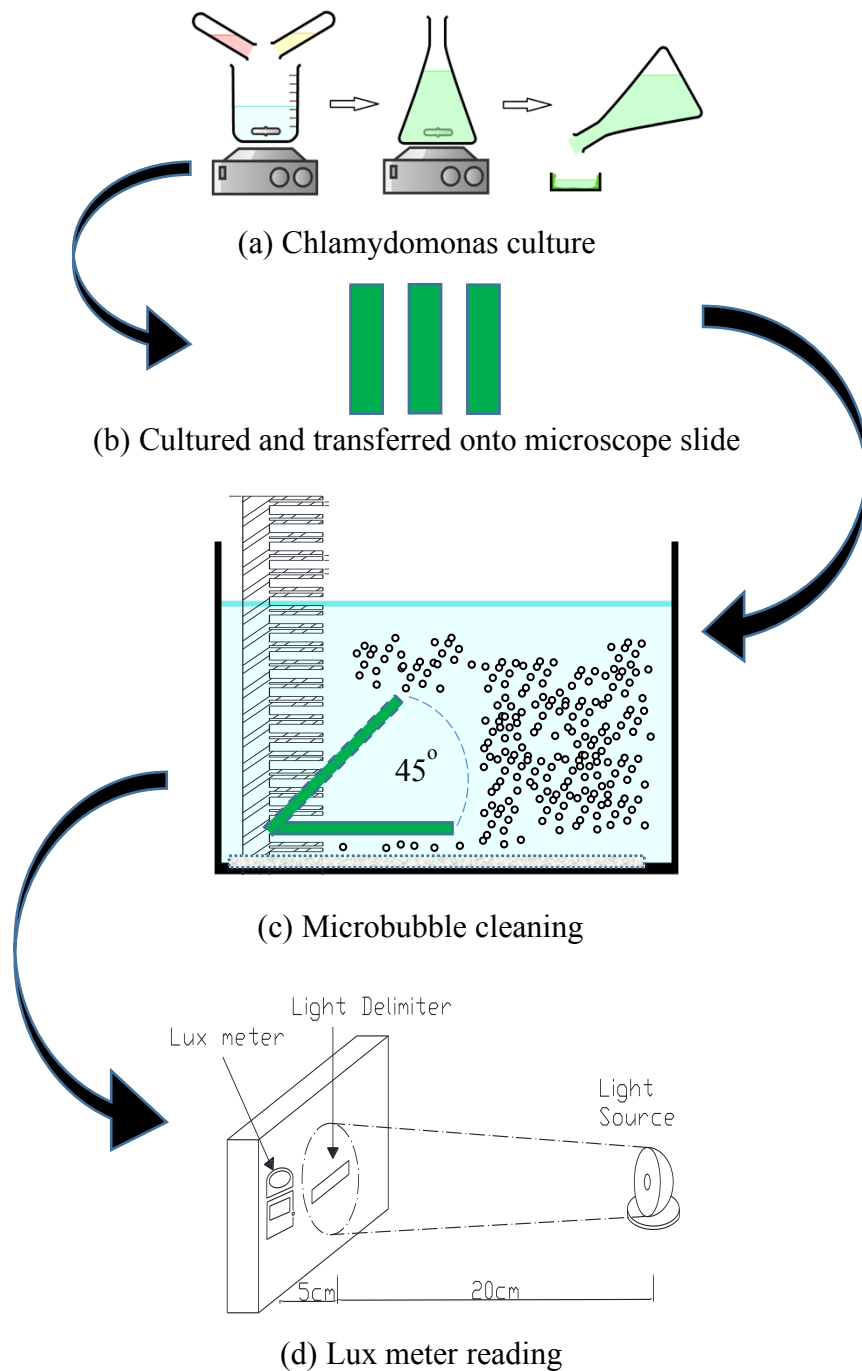
Figure 7.1 Simplified illustration of biofilm detachment using microbubble.

7.2.1 Chlamydomonas (biofilm) culture and preparation

Figure 7.2 shows a Chlamydomonas algae cultured in the flask and microscope slide. The algae are cultured using growth media stock 1 (micronutrients) and 2 (trace elements. Every 1 litre of distilled water, 10mil and 1mil of stock 1 and 2 are mixed carefully and cultured for at least 14 days prior the cleaning process is initiated.

Figure 7.2 Chlamydomonas algae culture

The standard media recipe to culture Chlamydomonas is provided by the Scottish Associations of Marine Sciences, located on the west coast of Scotland. Chlamydomonas is a fresh water algae, they only needs small proportions of micronutrients and trace elements for their growth. **Table 7.1** shows the detail properties of the media recipe of stock 1 and 2 used to culture Chlamydomonas Algae. For every one litre of distilled water, the 10ml and 1ml of the prepared stock 1 (micronutrients) and 2 (trace elements) are added.

Table 7.1 Bold's Basal Medium (BBM) for freshwater algae by *Culture and Collection of Algae and Protozoa (CCAP) Scotland*

Stock	Properties	Per 400ml
1	$NaNO_3$	10 g
	Properties	**Per litre**
2	Trace elements solution (autoclave to dissolve):	
	$ZnSO_4.7H_2O$	8.82 g
	$MnCl_2.4H_2O$	1.44 g
	MoO_3	0.71 g
	$CuSO4.5H2O$	1.57 g
	$Co(NO_3)_2.6H_2O$	0.49 g

The confluent algae on the surface of the microscope slide as shown in **Figure 7.2** are positioned and held on the microscope holder as shown in **Figure 4.9** and **Figure 7.1(c)**. Microscope slides are positioned in three different angles, 90º, 45º and 0º and sparged using the conditions for bubbly flow described in 0. **Figure 7.1(c)** explains and illustrated the experimental set up of microbubble cleaning scenario, which is also

shown by the actual set up in **Figure 7.3**. Confluent Chlamydomonas algae is mounted on microscope slide holder and submerged into the microbubble cleaning tank.
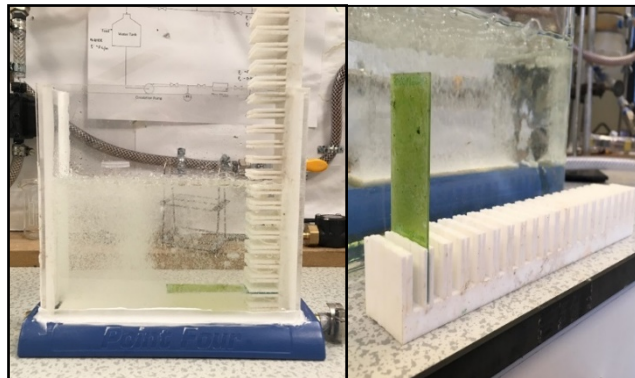
Figure 7.3 Microscope slide holder submerged in microbubble cleaning tank holding confluent Chlamydomonas algae

7.2.2 Biofilm Imaging

Chalmydomonas algae images are captured using an optical microscope as shown in **Figure 7.4**. This step is necessary to check the morphology, thickness, and colour of the algae. It is difficult to get a perfect picture; however, the magnification of the microscope is adjusted for the morphology of the algae shown in **Figure 7.5**.
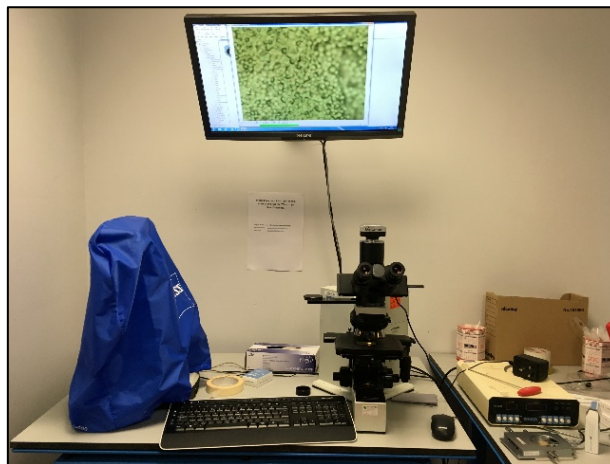
Figure 7.4 Chlamydomonas algae examined under optical microscope

The morphology and characteristics of the Chlamydomonas algae are examined before and after the cleaning process with microbubbles. The cleaning effects by microbubbles generated by using low and high oscillation frequency for the detachment of this algae from the surface of microscope slide are compared. Microbubbles generated by fluidic oscillations (low oscillation: condition I, II) induce destructive morphological change of the algae such as the detachment of flagella.

114
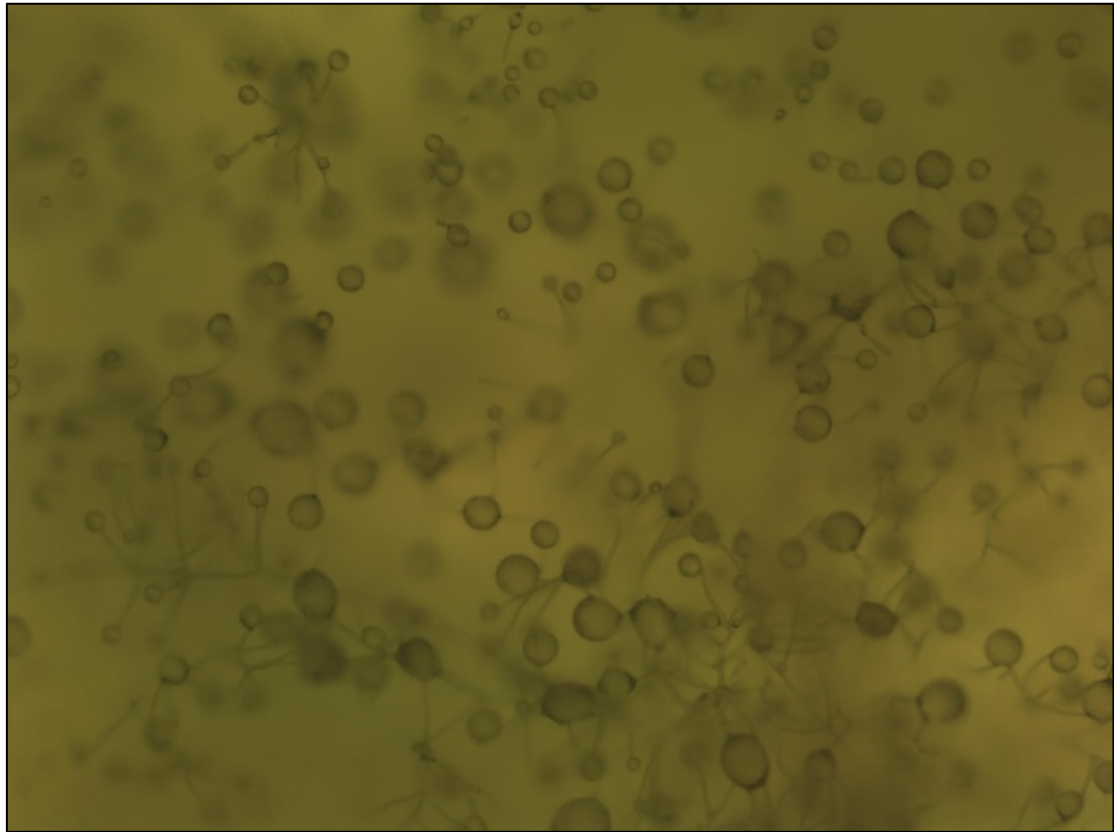
Figure 7.5 Chlamydomonas algae imaging

7.3   Biofilm detachment

7.3.1   Microbubble exposure

Figure 7.6 shows the evolution of the profile of the Chlamydomonas algae biofilm resulting from exposure to the flow of microbubbles over time. The confluent algae is sparged with microbubbles for 1hr. The images of the algae in **Figure 7.6** are captured every 10 minutes showing the biofilm is removed until the microscope slide is completely transparent. At the beginning, a thick green biofilm layer is observed, which begins to fade in colour and diminish in thickness. This supports of the hypothesis of effectiveness for microbubbles flows to detach biofilms. Chlamydomonas algae removal have been observed. Since the algae were obviously cleaned and removed from the surface of the microscope slide, the removals have been measured using lux meter as shown in **Figure 4.10**. This method would allow the biofilm layer reduction is quantified.
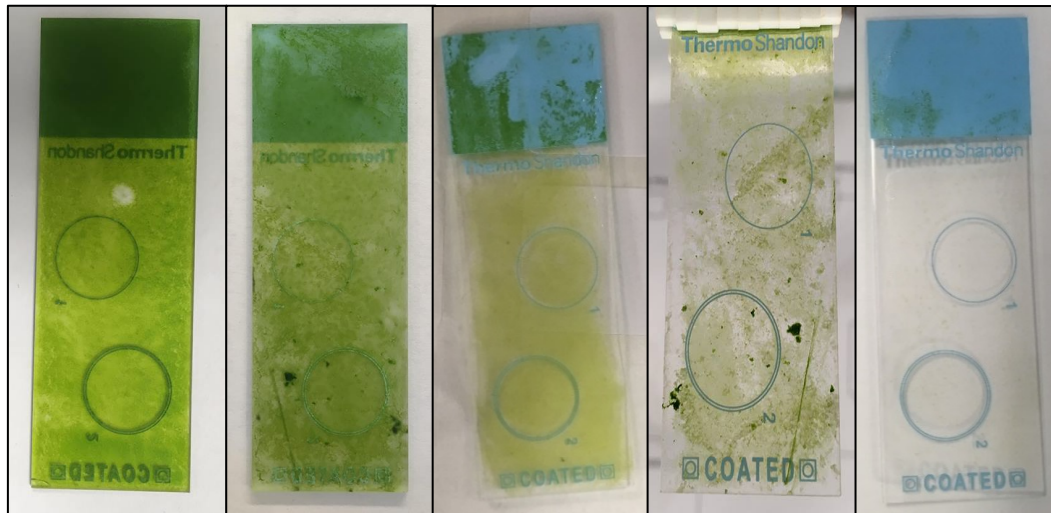
Figure 7.6 Biofilm detachment resulted from the microbubbles cleaning

The algae have been examined by microscopy as shown in **Figure 7.7**. Depending on the camera filters and growth media, the colour of the confluent Chlamydomonas algae observed is usually to be green. Before and after images of Chlamydomonas algae show the contrast between the confluent algae grown on microscope slide versus the remaining algae attached on the surface of the microscope slide. It is observed that microbubbles detached a high proportion of the Chlamydomonas algae from the surface of the microscope slide under the exposure to microbubbles sparging. This is due to the continuous disruption of the biofilm matrix caused by the bursting of microbubbles on its surface which generates high pressure spot as illustrated in **Figure 6.1** and Agarwal et al., (2012).
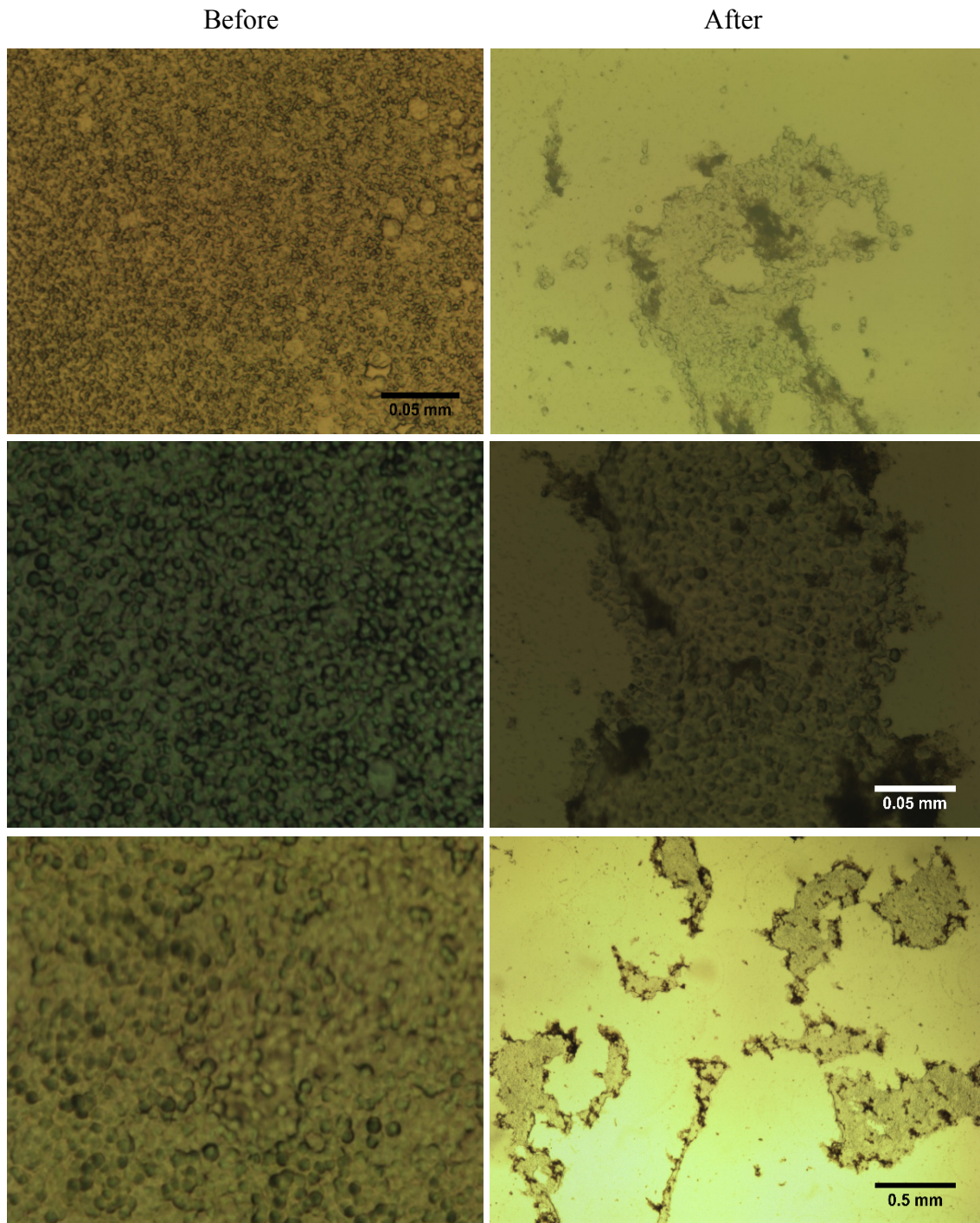
Figure 7.7 Chlamydomonas algae under microscope before and after microbubbles exposure

7.3.2 Detachment rate

The results present in **Figure 7.8** shows incident light passed through microscope slide measured by lux meter. High lux value represents less Chlamydomonas algae present on the surface of the microscope slide which allow more light to pass through the slide (Bowsher, 1987). **Figure 7.8(a)** shows a lux value measured by mounting the microscope slide at 0° as the microbubbles are sparged and clean the Chlamydomonas algae biofilm. A positive correlation between biofilm removal and exposure time is established. Microbubble-biofilm surface contact area are higher using a higher number density of microbubbles (Hiroyuki et al., 2015; Matsuura et al., 2015; Agarwal et al., 2012). Similar trends have been observed through three different angle of microscope slide mounted at 0°, 45°, and 90°.

The main objective of this research to explore the potential of microbubbles for biofilm detachment is achieved. This however would be further intensified by using microbubbles generated by fluidic oscillator designed and pioneered by Zimmerman & Tesar, (2010) and Zimmerman et al., (2008), to have more uniform and smaller size distribution of microbubbles. This important factor, in agreement with Jang et al., (2017) and Agarwal et al., (2012) shows higher biofilm detachment rates are achieved by using smaller microbubbles at an oscillation frequency of 335Hz. In this regime, the higher the frequency of the fluidic oscillator, the smaller the microbubbles that emerge, consistent with the higher lux value measured as shown in **Figure 7.8(a), (b)**, and **(c)**. Microbubbles generated without fluidic oscillation have the lowest Chlamydomonas algae biofilm detachment rate (with lowest recorded lux value).

The lux values observed increase with microbubbles generated by using higher oscillation frequency. Similar trends are observed throughout the experiment using three different angles for microscope slide holder mounted to its holder. The lowest lux value recorded using microbubbles generated without fluidic oscillation monotically increasing oscillation frequency of 256Hz, 285Hz and 335Hz. The results obtained show the microscope slide under configuration of 45° inclination had the best biofilm detachment. The maximum of lux value recorded was 128lx which represents a total transparent and clean microscope slide. Under highest oscillation of (335Hz), corresponding to the smallest size of microbubbles in the experimental campaign, the

maximum lux value is achieved within 40 minutes exposure time. Contrariwise, under same flow conditions, it took at least 60 minutes for the microscope slide to be free from Chlamydomonas biofilm algae.

Under vertical configuration or 90°, the lux value recorded shows the lowest level of biofilm detachment. **Figure 7.8(c)** shows the biofilm achieves full detachment after 90 minutes of microbubbles sparging exposure which is 40 minutes longer than the other two microscope slide configurations. With frequency 335Hz, the detachment rates calculated are 0.722, 1.775 and 1.183 lux/min for microscope configuration of 90°, 45°, and 0° respectively. This study identifies that the highest detachment rate is observed by using microbubbles under oscillation 335Hz and microscope slide inclination of 45° angle. For the vertical microscope slide configuration of 90° shows a very steady detachment rates during the first 50 minutes of exposure. The smallest detachment rate is recorded under this condition. This configuration reflects the smallest microbubbles-biofilm surface contact, hence the smallest contact area for disruptive detachment of the Chlamydomonas biofilm algae (Agarwal et al., 2012).

Five different oscillations frequencies correspond to five different average size of microbubbles ranging from 30 to 300μm that are used to study the efficacy of the microbubble sparging on the biofilm detachment rate. The influence of microbubbles generated by fluidic oscillation is compared to those without the fluidic oscillation. From the observations the recorded by the lux meter, it shows that microbubbles generated without fluidic oscillator induced the smallest detachment rate for every microscope slide configuration. Naturally, the microbubbles generated without fluidic oscillator are far from uniform microbubble size distributions, as observed by Hanotu, (2013) and **Figure 2.19**. Agarwal et al., (2012) and Sharma et al., (2005) mentioned the smaller microbubbles provide higher contact surface area which disrupt the biofilm, while the 45° provide higher shear stress force and contact time.
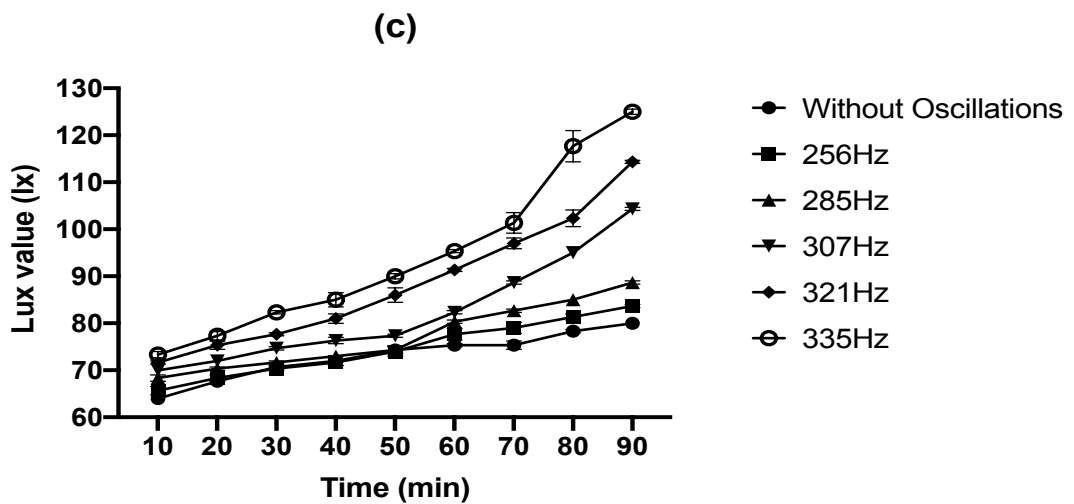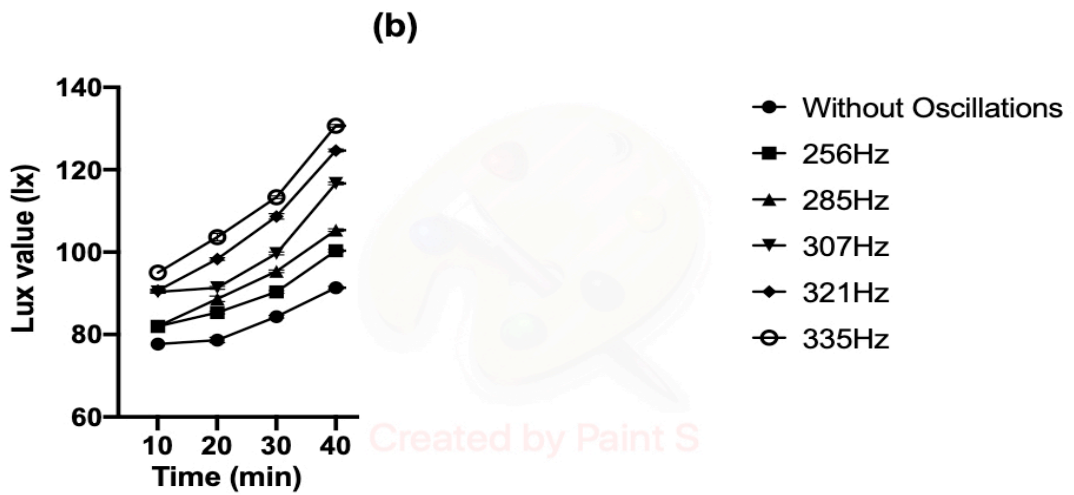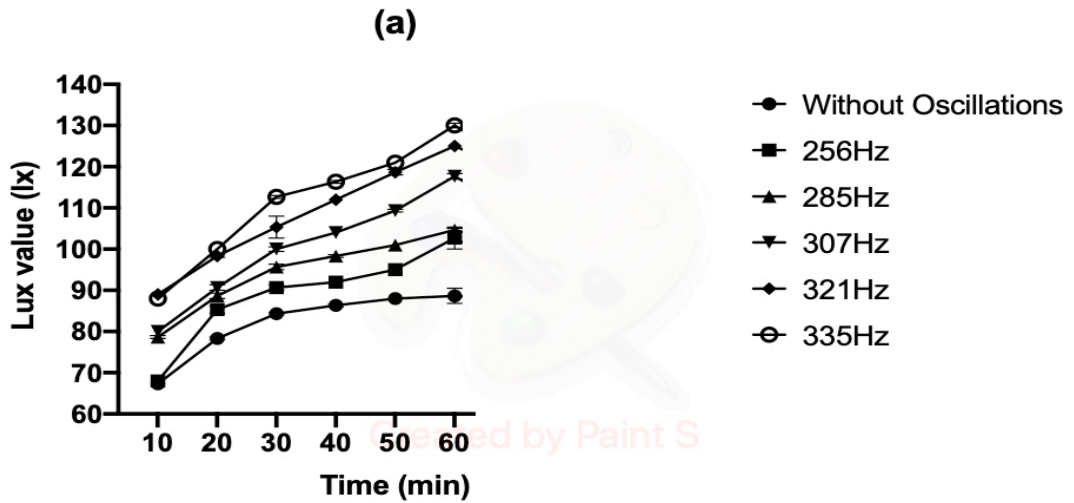
Figure 7.8 Chlamydomonas algae detachment measured by Lux meter using three different microscope slide configuration (a) 0º (b) 45º (c) 90º

7.4 Effect of angular configuration

Figure 7.9 illustrates the amount of microbubble contact area with the biofilm on a surface. Both figures represent the microbubble detachment from the surface of the microscope slide. Smaller microbubbles shown in **Figure 7.9(b)** have higher microbubble-biofilm contact area compared to **Figure 7.9(a)**. In theory, with smaller size of microbubbles, there is higher surface area. According to Tesař, (2017) and Burns et al., (1997), smaller microbubbles not only provide higher surface area, they also allow higher contact area with more complex particle shapes. Moreover, the higher the bubble-biofilm contact area, the higher shear force is exerted between them. Sharma et al., (2005) distinguished that microbubble flow increased the bacteria detachment from 40 to 98% compared to the flow in the absence of microbubbles. In most cases, extremely high strength fluid flows would be effective in stimulating detachment of microorganisms, however the addition of the microbubbles to the flow also allows mature, stable and overgrown layers of biofilms to be detached. Smaller size of microbubbles in this research have been generated by using higher oscillation frequency of fluidic oscillator. **Figure 7.9** illustrates perfectly how the smaller size of microbubbles have higher bubble-biofilm contact area, shear force, and detachment rate.
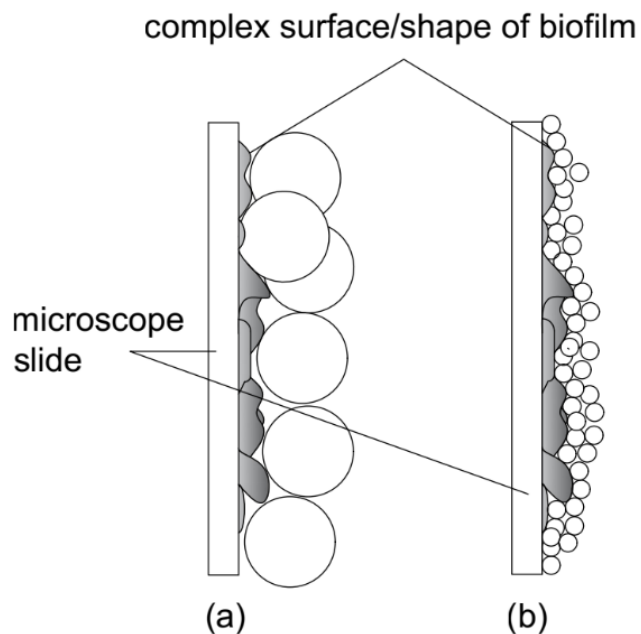
Figure 7.9 bubble-biofilm contact area (a) large bubbles size make minimum contact with the biofilm (b) smaller microbubbles cover and touch entire surface of biofilm

Figure 7.10 shows a microbubble journey pattern on three different microscope slides configuration of 0º 45º and 90º. These trajectories have been studied and observed using the high-speed camera Phantom V210. The microbubbles trajectories on microscope slide of 0º configurations shows non-uniform flow. In contrast, the microbubbles trajectories using the other two configurations are consistent with very uniform flow. The study found that the microscope slides that is mounted at 45º has the highest microbubble-biofilm surface contact. The number of microbubbles generated are very well exposed towards biofilm and detach them from its surface. Using this configuration, the surface of microbubbles also is very well exploited. **Figure 7.11** illustrates the microbubble is actually rolling with a 'snowball effect' where its surface accumulates more and more materials. This effect combined with uniform bubble path line, explained how the highest biofilm detachment rate is obtained and calculated.
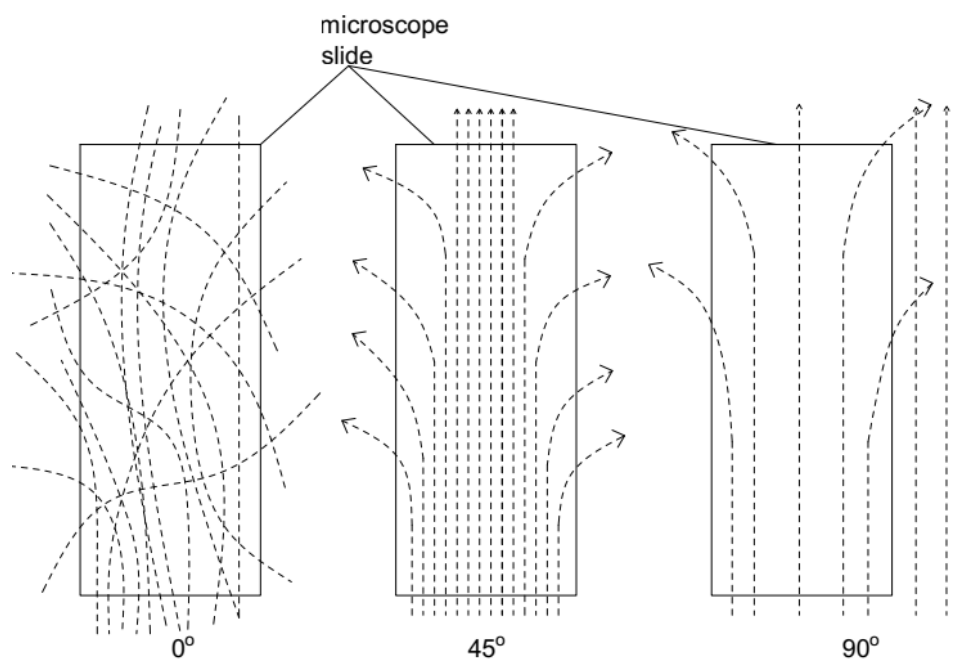
Figure 7.10 bubble path line on three microscope slide configurations of 0º 45º and 90º
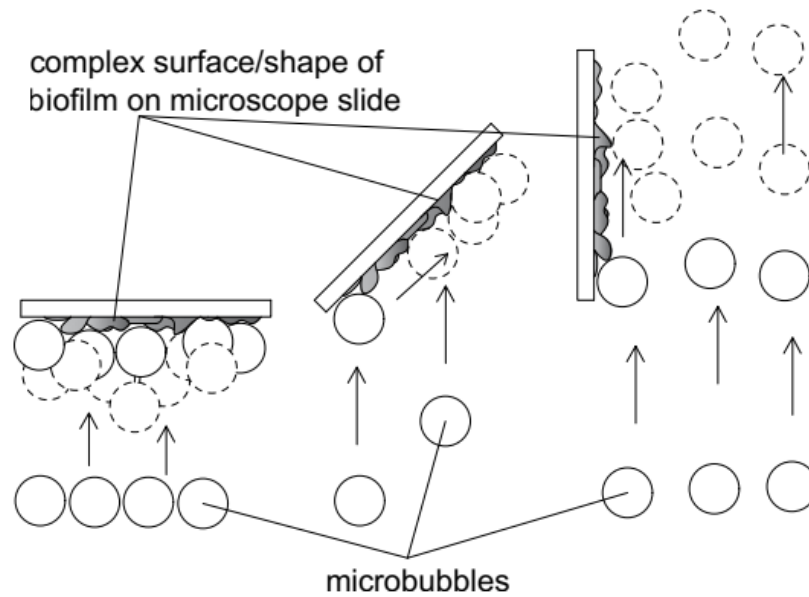
Figure 7.11 microbubbles sparging towards the biofilm cultivated on microscope holder mounted at 0º, 45º and 90º

7.5 Summary

This chapter mainly achieves greater evidence to support the hypothesis of the inducement by microbubbles generated by fluidic oscillator for intensified biofilm detachment. It is observed that microbubbles generated by fluidic oscillation show the higher detachment rates. It is also observed that microbubbles generated with higher oscillation frequency in this regime show higher detachment rates. These conclusions echo those of CHAPTER 6 extended to testing further the idea of shear force mechanisms to detach biofilm from a surface. These conclusions about shear forces follow from using three sparging configurations by mounting microscope slide under three different angles namely 0º, 45º, and 90º. The confluent Chlamydomonas algae biofilm are sparged by using microbubble flows. The incident light passing through is measured using a lux meter. Microbubbles with the highest oscillation frequency of 335Hz and with 45º slide inclination angle, have the highest detachment rate, 1.775 lux/min. Detachment rate is non-monotonic with inclination angle, as the lower values are 1.183 lux/min and 0.722 lux/min under configuration of 0º and 90º respectively. This non-monotonic behaviour is consistent with different detachment mechanisms being dominant above and below the 45º inclination, and those mechanisms constructively reinforcing at 45º inclination.

123
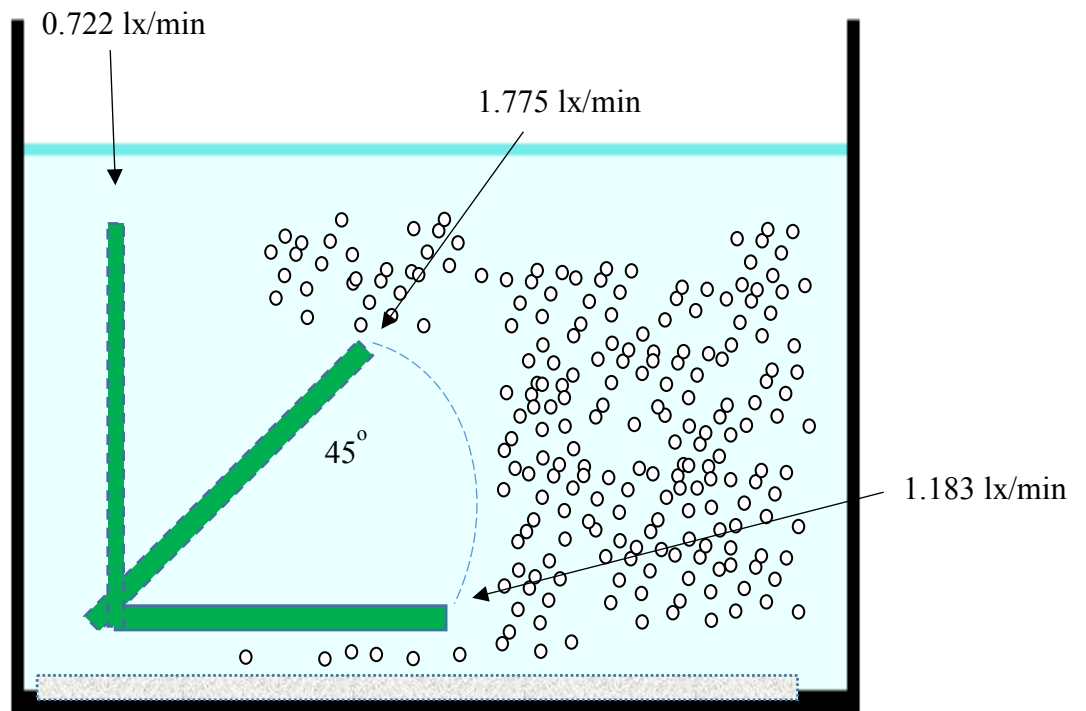
Figure 7.12 Three configurations of microscope slide holder sparged with microbubbles to investigate the detachment rate

CHAPTER 8

CANCER CELL (HELA) DETACHMENT

8.1 Introduction

This chapter follows on from work of 0 and CHAPTER 7 to develop further support for the central hypothesis and a deeper understanding of microbubble flow for biofilm detachment. The main part of this chapter covers the HeLa cells detachment sparging by using microbubbles, where it is hypothesised that the microbubbles generated by using fluidic oscillation at higher oscillation frequency have the highest biofilm detachment rate and cell viability reduction performance. To investigate the hypothesis the experiments have been carried out under similar conditions as CHAPTER 7 which are:

- HeLa cells detachment using microbubbles generated without fluidic oscillator.
- HeLa cells detachment using microbubbles generated by using fluidic oscillation at five different oscillation frequency ranging from 256 to 335Hz.

Each experimental condition has been run five times in series for an exposure duration of 15 minutes. The hypothesis is investigated by morphological examination by microscopy and viable cell counting using hemocytometry.

8.2 Methodology

8.2.1 Media Preparation

Media Preparation (DMEM-high glucose + 1% Pen Strep +1% Glutamine + 10% Fetal Calf Serum) has been prepared using the following compounds and amounts.

- 440ml of Dulbecco's Modified Eagle's Medium (DMEM) – high glucose is prepared.
- 5ml of Penicillin Streptomycin (Pen Strep) is added.
- 5ml of glutamine is added.
- 50ml of Fetal Calf Serum (FCS) is added.

Figure 8.1 shows the preparation of 500ml of growth media has been prepared in the tissue culture laboratory for HeLa cell cultivation on microscope slides. 5ml of Pen Strep are added into the culture media to prevent bacterial contamination. HeLa cells are a type of mammalian cell. 5ml of glutamine is also added as the main source energy for cells growth. This solution represents 1% to the total composition of the mixture. 50ml of FCS also is added into the mixture which constitutes 10% of the mixture. These four main ingredients are shaken well before use and stored at 8°C.
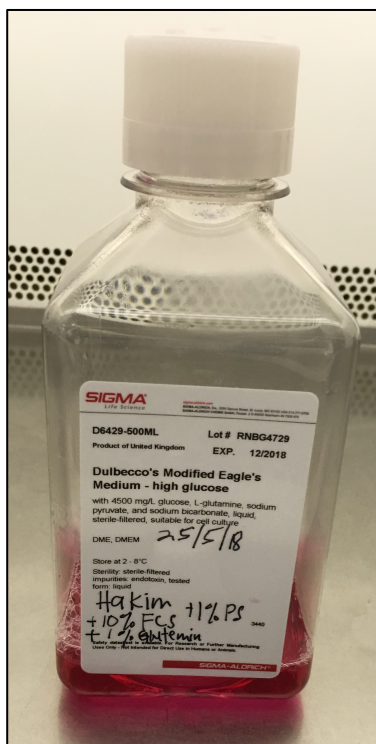
Figure 8.1: Prepared culture media with 10% FCS and 1% Pen Strep and glutamine

8.2.2 Cell Culture

HeLa cells are cultured in T75 flask as shown in **Figure 8.2** and are then transferred into a clear petri dish housing a microscope slide. The cells undergo a segregation process to ensure that only viable cells are transferred and grown on the surface of the microscope slide. This cell segregation procedure comprises of rinsing with a phosphate buffer solution prior cell transfer, using serum to deactivate the Trypsin, and adding the necessary new growth media. Depending on the flask type used, culturing HeLa cells culture could take up to 10 days to reach confluent and desired cell concentration. According to Percell Biolytica and Thermo Fisher Sceintific, HeLa

concentration varies considerably, however could range up to 3.5 to 8.4 million cells/ml.

Figure 8.2: HeLa Cell cultured in 550mL culture flask (T75) and split into microscope slide embedded petri dish (on the left)

HeLa cells cultured on the surface of the microscope slide have been examined under microscope to ensure its confluency and viability. HeLa cells at full confluency grown on the surface of microscope slide record a cell density of 5×10^5 cells/ml. The cells are submerged in 500ml phosphate buffer solution without microbubble sparging as experimental control for 1 and 2 minutes. The control sample is sparged but without fluidic oscillation. This step has been repeated on each case of microbubble sparging. The microscope slides confluent with HeLa cells are then sparged under five different microbubble conditions to test the hypothesis of this chapter. **Figure 8.3(b)** shows the confluent HeLa cells exposed to microbubble sparging for one minute. By this stage, microbubbles have detached the HeLa cells from the surface of the microscope slide. The residual of the viable cells are then transferred into clean petri dish filled with Trypsin to remove the residual cells attached to the slide as shown in **Figure 8.3(c)**. While subject to the action of Trypsin, the cell counting is conducted as quickly as possible or within 1 minutes to oppose cell aggregation. **Figure 8.3 (d)** and **(e)** shows that the Trypan Blue solutions are mixed with the cell to assess the cell viability using hemocytometry as shown in **Figure 8.3 (f)**.
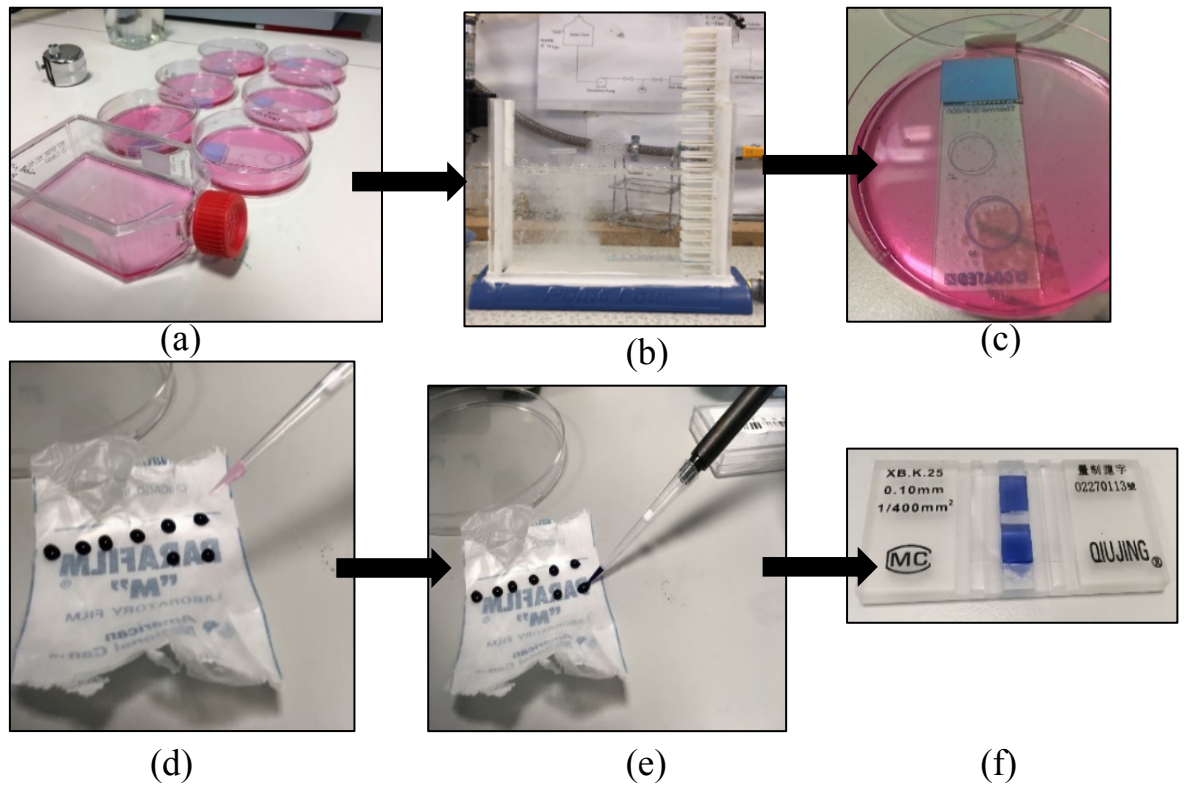
Figure 8.3 (a) and (b) depict cell culture and sparging by microbubbles, (c) represents remaining cell trypsinised, (d) and (e) represents HeLa cells mixed with Trypan Blue, (f) counting and viability using haemocytometer after detachment by microbubble sparging

The haemocytometer is prepared and cleaned with alcohol before use. The cover slip is moistened with water and affixed to the haemocytometer. For cell counting, appropriate sterile handling techniques are applied with hygienic care for the cell suspension preparation. The flask is gently swirled to have an even cell distribution and 10μl of cells are quickly pipetted and mixed with 10μl of Trypan Blue (see section 3.5.3). The microscope magnification objective is set to 10x as shown in **Figure 8.4(a)** and cells appearing on the image segments are counted. One of the four large segments is shown with a bold light blue border in blue as shown in **Figure 8.4(b)**. The cell densities hence can be calculated using **Equation 8.1** where average cell number is the total number of cells counted divided by four. The experiments have been replicated at least three times to improve the accuracy of mean estimation.

$$\textit{Cell densities} = \textit{Average cells} \times \mathbf{10^4}$$

Equation 8.1
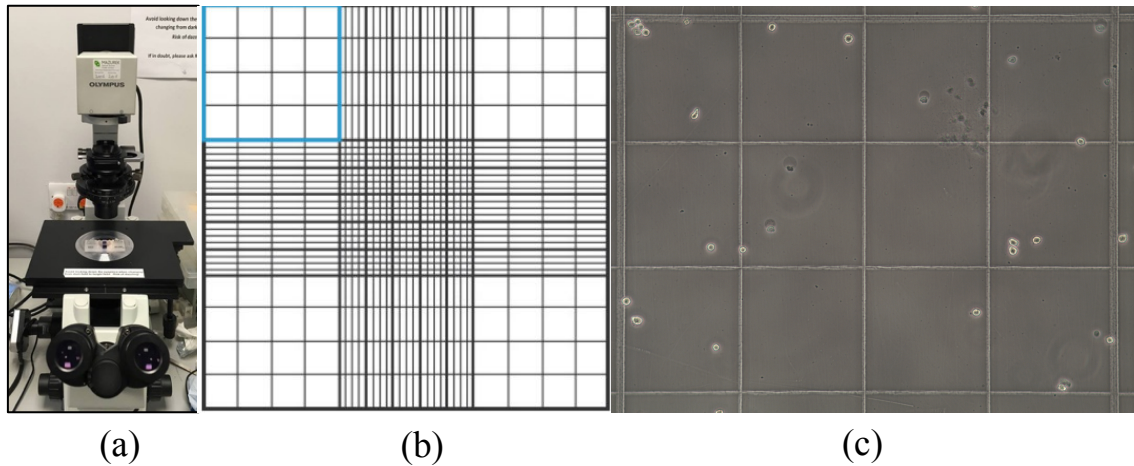
Figure 8.4 (a) Cell counting under 10x magnification using light microscope (b) highlighted four large squares (each containing 16 smaller squares) of the haemocytometer (c) HeLa cells image (20x)

8.2.3 Growth Abnormalities

In tissue culture experiments, growing cells in a controlled environment flask such as T75 without any additional features is considered an effective method. These experiments, however, are more challenging due to submerged microscope slide within the petri dish. Some HeLa cell growth abnormalities are observed. **Figure 8.5** shows a multiple layer of overgrown cell upon a red spot, with an undergrown cell in the yellow spot. Microscope slide exhibiting these growth abnormalities are rejected from the experimental study.
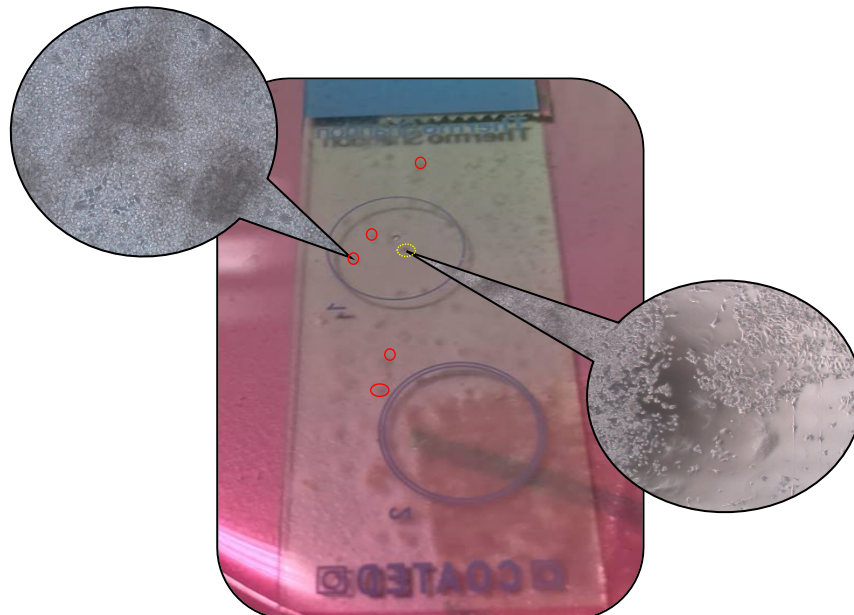
Figure 8.5 HeLa cells non-uniform growth on a surface of microscope slide

The morphology of HeLa cells has been described and shown in **Figure 2.6** (see section 2.4.2.2). **Figure 8.6** shows a top view of the HeLa cell growth abnormalities under 4x magnification exhibiting overgrown and undergrown cell spots. Since each experiment requires at least six uniformly confluent HeLa cells cultured on the surface of microscope slide and repeated five times. Hence, confluent T75 HeLa cells have been split and cultured on at least forty microscope slide including control.
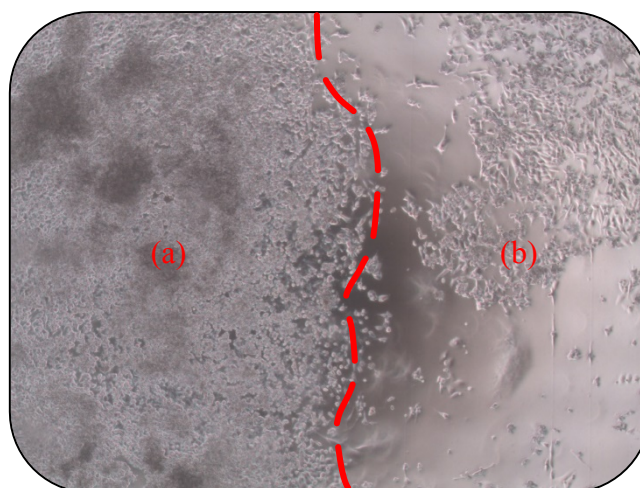
Figure 8.6 Close up HeLa cells growth abnormalities under 4x microscope magnification (a) multi-layer and overgrown cell spot (b) undergrown cell spot

8.3 Detaching HeLa cell from a surface for quantification

Tissue engineered oral mucosal equivalents (OME) are being increasingly used to measure toxicity, drug delivery, and to model oral diseases. The preparation of the OME requires an incubator to culture the cell. The cultured cells attached on the surface of the petri dish need to be detached for quantification purposes. Typically, a chemical, e.g. Trypsin, is used to detach the cell from the surface. The main objective of this research is to explore the potential of microbubbles to detach the cell from the surface of microscope slide. Microbubbles should be able to detach such substances without harming or altering the physical properties of the cell. Bubble flow provides non-invasive detachment for cell quantification, in the sense that nothing enters the cell. The effect to the environment is minimal compared to the trypsin. Longer exposure of the cell to trypsin is likely toxic.

The following schematics show how conventional and microbubble mediated tissue culture quantification proceeds. It involves two simple steps: cell suspension and cell

counting. In this research as shown by the illustration below, Trypsin-EDTA are replaced by microbubbles to suspend the cell from the surface of the flask. By using microbubbles, the cell segregation process could be done without the disadvantages of Trypsin dosing, such as cell agglomeration and harmful chemical loading released to environment (Thermo Fisher, Cat No: T360-500). In this research, HeLa cells are submerged in a solution containing Phosphate Buffer Solutions (PBS) and the microbubbles.

Conventional quantification

| Cultured Cell | Trypsin added | Quantification |
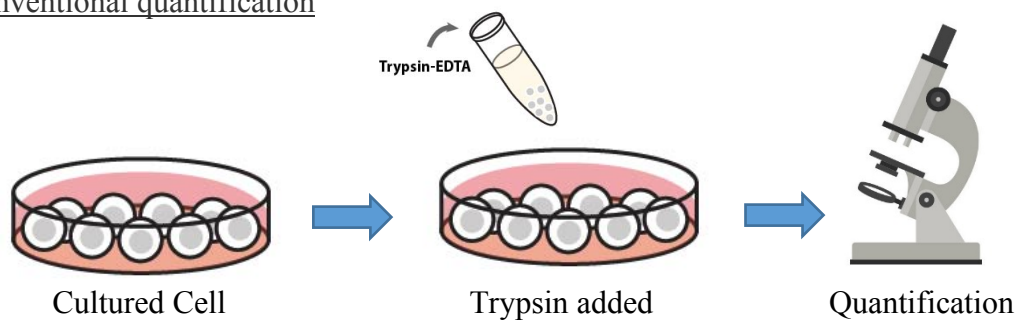
Microbubble quantification
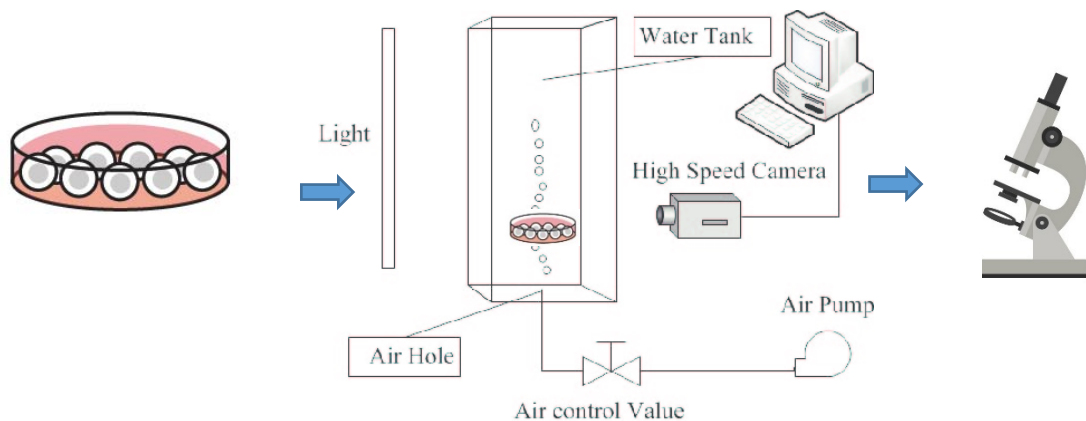
| Cultured Cell | Microbubbles flow detachment | Quantification |

Testing the hypothesis and assessing the outcome follows a similar conceptual approach to the microalgal biofilm experiments in CHAPTER 7. **Figure 8.7** demonstrates how densities of HeLa cells decrease over 10s exposure of sparging by microbubbles. From the left, HeLa cells have been exposed under 10s, followed by 20s, 30s and 40s of microbubbles exposure. The decrement in cell densities shows the capacity of microbubbles to detach the HeLa cells from the surface of the microscope

slide. The colour of the image depends on the microscope lens filter. The main idea of this research inspired by Agarwal et al., (2012) states that microbubbles should detach biofilms from a surface by continuous disruption with a high pressure fluctuation occurring within the biofilm matrix (in this case HeLa cells). This research however also in agreement with Zimmerman et al., (2008) states that a microbubble must be able to completely dissolve in the liquid in order to cause such a "cavitation-like bubble collapse pressure wave". Air microbubbles have a practically insoluble nitrogen gas core -- the oxygen could complete dissolve. The previous experiments, however, removed biofilms with long exposure times to microbubble sparging, the liquid have become saturated with both O_2 and N_2.

In addition, positive results presented by Sharma et al., (2005) shows that microbubbles not only disrupt the biofilm matrix, but also shearing that effectively detaches any resolute bacteria from surface. These authors reported that microbubbles are almost ineffective for larger bacteria entities. This, however contradicts the results presented in this research, where it is found that HeLa cells and Chlamydomonas algae are both detached successfully regardless its size. The microbubble generation approach of Sharma et al. (2005) inevitable creates high energy dissipation that is incompatible with laminar flow. The contradiction in their findings and those in this thesis must hinge on the properties of laminar flow with dispersed microbubbles, indicating that the high gradients / shear forces achievable in laminar flow are central to mechanical /physicochemical mechanism for removing cells from biofilms
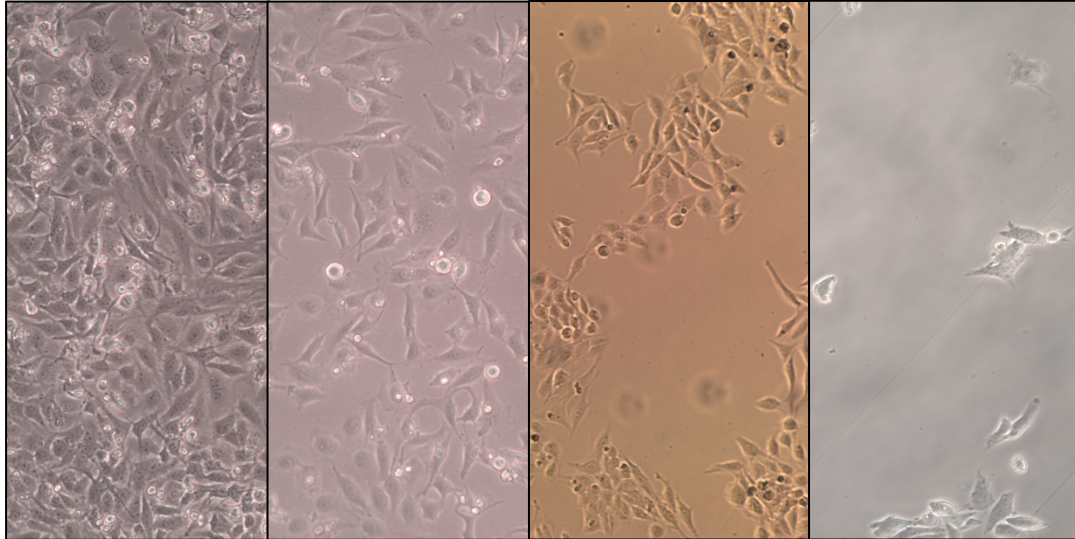
Figure 8.7 HeLa cell on the surface of the microscope slide after microbubble sparging. Image from left to right represent microbubbles sparging of 10s interval difference

8.3.1 Detachment using Fluidic Oscillation: Low Oscillation

Initially, the HeLa cells are cultured using the procedure described in 3.5.2. Subsequently, they are detached using microbubbles as shown in **Figure 8.3(b)** of 0° configurations. Similar trends however are observed as with microalgae biofilms. HeLa cells have been detached effectively using the configuration of 45° inclination angle. The fully confluent HeLa cells have been sparged using microbubbles at 10s interval each. Some of the adhesive HeLa cells have been detached from the microscope slide surface and the leftover of the HeLa cells are then trypsinised. These cells, which have been detached from the slide due to Trypsin reaction, are then counted via hemocytometry. In this range of frequencies, the size of microbubbles size are inversely related to the frequency of the fluidic oscillation. In this chapter, the frequencies of 226 and 256Hz are used as low FO frequency to investigate the detachment efficiency of HeLa cells. This frequency induces the upper range of microbubble sizes, which would have suffice effects on cell detachment.

Figure 8.8 shows the viable cell count profile from hemocytometry over time. Using the lower frequency of 226hz, a single 10s duration of microbubble sparging shows the undetached viable cell density is 3.4×10^4 cell/ml. for the fully confluent HeLa cells cultured on the microscope slide, it is are 5×10^5 cells/ml. This value, the lowest measured, yields a removal by microbubbles of 93.2% of the initial cells washed away

within 10s. The upstream pressure of 2.0bar produced the highest flowrate of sparging microbubbles with the greatest bubble flux. The graph shows steady decrement of cell density with time, reaching the value of calculated and reach 0.1×10^4 cell/ml by one minute of sparging. Higher cell density is registered using lower oscillation frequency. After 10s of sparging with frequency of 256 and 226Hz, the calculated cell density is 21.9×10^4 and 3.4×10^4 cell/ml respectively. Similar trends in both data sets are found where the cell density decrement is explained by the longer cell exposure to the microbubbles.

Similar results are obtained in   CHAPTER 6 showing that higher bubble flowrates have higher biofilm detachment rates. According to Lee et al., (2014) and Nagaoka et al., (2006), stated that higher number density of the same size bubbles provide higher shear force to shear off the biofilm from a surface. However, higher bubbles density is opposed by larger bubble size creating less momentum transfer due to the resulting large shear force from bubbles surface colliding or in contact. Therefore, it is important to keep the size of bubbles as small as possible which eventually leads to higher contact area to detach HeLa cells from a surface (Hiroyuki et al., 2015; Agarwal et al., 2012). **Figure 8.8** implies that microbubbles generated at 256hz have higher removal densities of cells due to exposure to a higher bubble flux.
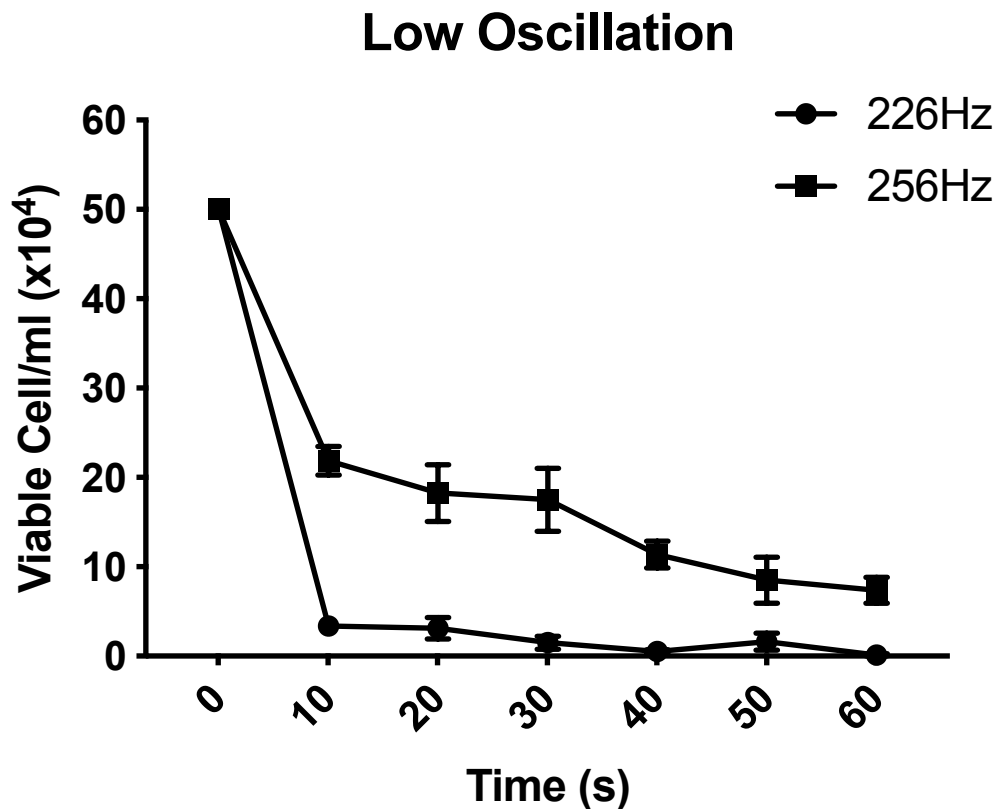
Figure 8.8 Viable cell detachment counted using low oscillation microbubbles, error bar represents standard error of the mean (SEM)

8.3.2 Cell Detachment using Fluidic Oscillation: High

Figure 8.9 shows the cell density calculated once the cells are sparged with high frequency. At oscillation frequency of 321 and 335Hz, the flowrates of compressed air into the point four diffuser are about 25% lower. The data shows at 10s of sparging using 321 and 335Hz, the cell density calculated are 20.3 and 46×10^4 cell/ml respectively. The highest cell density in both low and high frequency ranges is recorded with the high frequency of 335Hz at 1.2bar of upstream pressure. Microbubbles sparging at 335Hz has been theoretically reduced HeLa cells attached on microscope slide by 8% after 10s of microbubbles exposure. Cell density reduces steadily throughout the sparging process, reaching zero cell density after 1minute of sparging. A similar trend is observed where more HeLa cells are detached during beginning with applied frequency, however the decrement of cell densities is more rapid after the first 10s of exposure.

High Oscillation
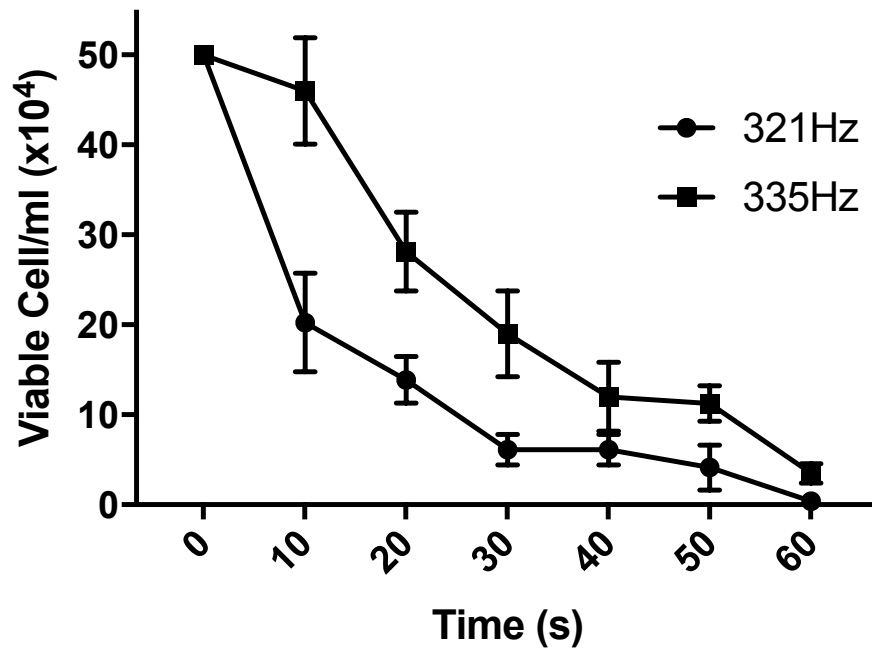
Figure 8.9: Viable cell detachment counted using high frequency fluidic oscillation, error bar represents standard error of the mean (SEM)

Generally, the results presented in **Figure 8.11** shows microbubble generated by fluidic oscillation are very effective at detaching HeLa cells from surface. The data obtain shows 226Hz is the best frequency with 0.804 detachment rate, followed by 256Hz, 321Hz and 335Hz. As expected from the presentation of the profiles, the end point detachment rates follow the same trends as the end point removal efficiencies. This result shows that the microbubbles generated using higher oscillation frequency has the smallest size of microbubbles. The smaller size of microbubbles provides higher surface area to detach HeLa cells from the surface of microscope slide. The higher surface area of microbubbles allows higher contact area between the bubble and the biofilm matrix in this case HeLa cells (Tesař, 2014b; Agarwal et al., 2012; Zimmerman & Tesar, 2010).

Figure 8.10 shows HeLa cells detachment for four selected frequencies; 226Hz, 256Hz, 321Hz, and 335Hz. As mention earlier in, 226 and 256Hz were categorized as low frequency microbubble generations. The detachment or cleaning of HeLa cells were started at 5×10^5 cells/ml explains the initial value at time=0s for every set of

experiments. Within 10s of microbubbles exposure, the number of HeLa cells detached from the microscope slide recorded the highest detachment using 226Hz. This agrees with the concept that the higher the flowrate, the higher number of bubbles generated which generate higher energy. Meanwhile, the data shows frequency of 335Hz which supposed to have the lowest microbubbles size has smaller detachment number of HeLa cells recorded.
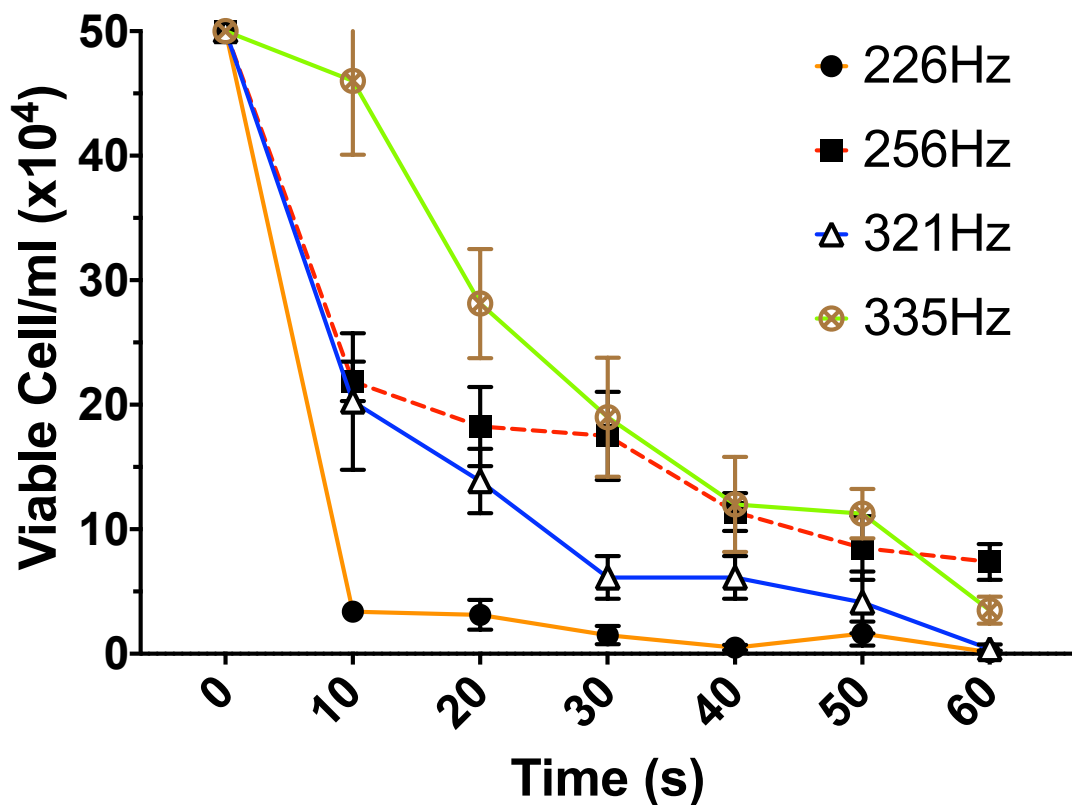
Figure 8.10 Overall (both low and high frequency) Viable cell detachment counted using high frequency fluidic oscillation, error bar represents standard error of the mean (SEM)

Equation 8.2 is used to determine the detachment rate of the HeLa cells detachment. The value is easily obtained using linear trendline function in Microsoft excel shown in Appendices.

137

$$Cells\ detachment\ rate = linear\ gradient\ of\ data\ set$$

Cell Detachment Rate
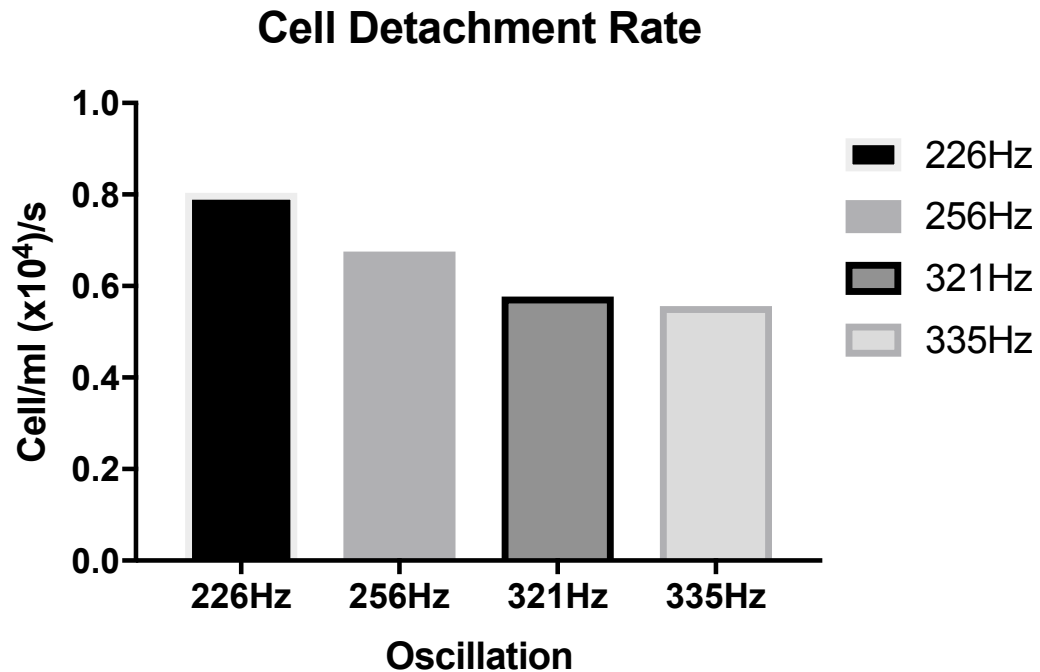
Figure 8.11 Comparison of HeLa cells densities detachment rate at both high and low oscillation frequency

Both **Figure 8.8** and **Figure 8.9** illustrate the viable cell attached on the microscope slide after a certain amount of time microbubbles exposure. **Figure 8.12** however shows the measurement of viability of HeLa cells that have been detached from the microscope slide. Confluent cultivated HeLa cells on microscope slide are submerged in Phosphate Buffer Solution (PBS) and have been exposed to microbubbles. Due to shear force and bubble-biofilm contact, HeLa cells have been detached from the surface into PBS solutions. It is very difficult to sample HeLa cells in 500ml PBS solution. Instead, the entire PBS solution in the sparging tank is centrifuged to obtain as many detached HeLa cells as possible. From **Figure 8.12** it is observed that microbubbles generated under oscillation frequency of 335Hz are less destructive compared to 226Hz. According to Rehman et al., (2015) and Hanotu, (2013), microbubbles generated by fluidic oscillator pioneered by Zimmerman et al., (2008)

are nearly uniform under a constant upstream gas injection into a steady liquid flow regime. Maintaining laminar flow, periodic microbubble formation and uniform size provide a gentler detachment rather than creating a high-pressure which breaks the biofilm matrix. Conventional microbubbles have high turbulence intensity, inducing rough contact and high-pressure collision force resulting the death of HeLa cells. Microbubbles generated using oscillation frequency of 226Hz (lowest in the study) achieve the lowest detached cell viability: 26.5%.
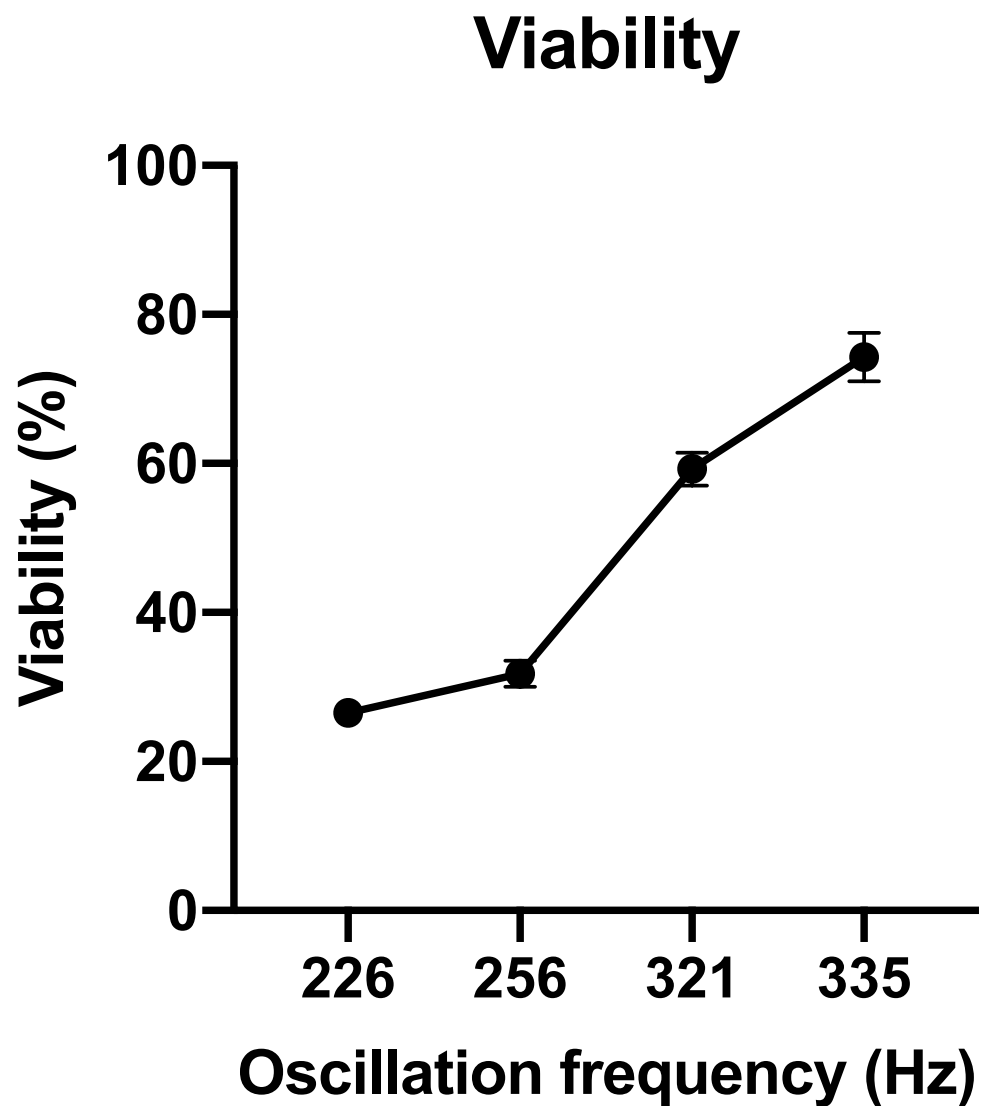
Figure 8.12 The detached HeLa cells viability in 500ml of PBS solutions

8.4 Summary

The main finding of the cell detachment rate study is the ability of smaller microbubbles to detach HeLa cells from the surface non-destructively. The smaller microbubbles with higher oscillation frequency exhibit more uniform bubble size distribution. This is the key factor which increases the probability of bubble-HeLa cell contact to detach the cells from the microscope slide surface. Uniform size and regularly spaced flow of bubbles provides higher shear force through the surface area of smaller bubbles. Higher venting flow means lower air flowrate fed into the diffuser, not only causing the death of HeLa cells but also achieving lower detachment rates. This condition is not preferable for tissue culturing, especially the cell segregation process. Cell segregation, conventionally done by adding Trypsin EDTA with the downside of cell agglomeration if exposed for more than 5minutes, could be replaced by microbubble sparging. Microbubbles generated by fluidic oscillation are expected detach tissue cells without producing extra waste. The detachment is through non-invasive means (nothing crosses the cell membrane) procedure has been successful to achieve almost all of cell removal from biofilms as using trypsin EDTA, at a faster rate with low energy consumption.

CHAPTER 9

9.1 General Discussions

Microbubbles generated by fluidic oscillation are characterised based on the frequency and their resultant size distribution. Generally, all hypothesises of this research have been addressed and supported. The central hypothesis is that fluidic oscillation driven microbubbles should effectively defoul/detach biofilms from surfaces has been successfully achieved in three different, practically important exemplars. Microbubble flow is able to defoul filtration membranes by reducing the Transmembrane Pressure (TMP) of the systems. Although a higher flowrate of microbubbles detaches more components of a biofilm from a surface, that does not mean it has higher detachment rate. Results obtained have been published in International Water Association (IWA) – Water Supply Journal is part of this thesis and presented by Chapter 6. Defouling recorded are lowest without fluidic oscillator followed by low oscillation and high oscillation frequencies: 9.53, 6.22 and 3.41 mbar/min respectively. To provide a better understanding on how microbubbles detach biofilms from surface, two different biofilms (Chlamydomonas algae and HeLa cells) have been investigated. Both are treated by exposure for defined durations while sparging with microbubbles generated by fluidic oscillations. Similar trends of the results for Chlamydomonas algae biofilm is obtained where microbubble sparging at higher oscillation frequency achieves higher detachment rates. Contradictory finding however found in HeLa cells. Highest frequency of 335Hz recorded lowest cells detachment rate of 0.556 viable cells/ml/s. The shear force induced by bubble-biofilm contacting, dislodges the cells from the biofilm by attachment to the surface of the microbubble. High oscillation frequency microbubble exposure is observed to be non-destructive of HeLa cells during detachment and the results shows a good potential for cell splitting applications.

Generally, smaller microbubbles have higher surface area and are able to contact with a more complex particle shape. The higher shear force is a consequence of from the higher bubble-biofilm contacting efficiency. The detachment of Chlamydomonas algae cultivated on microscope slide surface occurs due to sparging has been explored using three different configurations. The highest detachment rate has been observed

using configuration of 45°. The detachment rate for this configuration are explored using five different oscillation frequencies. The detachment rate calculated using oscillation frequency of 335Hz and 256Hz are 1.774lx/min and 1.025lx/min respectively. The analysis of this data shows that the detachment rate of Chlamydomonas algae is 41% lower using the lowest oscillation frequency generated microbubbles 256Hz compared to 335Hz.

Contradictory trends are observed by using HeLa cells cultured on the surface of microscope slide. The same experimental apparats are used to study this detachment rate as with microalgae. The nature / constituency of the biofilms used in this research are different (colloids in filtration system, microalgae, and mammalian cell). Microbubbles generated by fluidic oscillation require at least 43 minutes to restore the Transmembrane Pressure (TMP) of microfiltration. Chlamydomonas cells however require only 40minutes to be completely cleaned from the surface of the microscope slide. The shortest time recorded shows that HeLa cells has the lowest time of exposure to achieve complete detachment: under 1 minute. The results obtained for each experimental programme are not comparable directly that they are recorded using different measurements to infer performance: transmembrane pressure, luminous light transmission, and viable cell density. These measures can, however, be used to infer detachment rate for relative comparison of performance for microbubble sparging generated by using or without fluidic oscillation.

9.1.1   Contribution factor

There are few contribution factors that lead to this research and this helps to obtain such result.

- Microbubbles do not generate any by product, thus it's a very clean and environmentally friendly option in cleaning industry.
- Fluidic oscillator is a device with no moving part and requires no electricity. Thus it is the most efficient way to reduce the size of microbubbles.

9.2 General Conclusions

Sparging with microbubbles generated with fluidic oscillator has a more promising performance on biofilm detachment than conventional approaches with many advantages, but no disadvantages identified. Without fluidic oscillation, the biofilm detachment rate is lower due to smaller shear force and bubble-biofilm contact area. However, in my opinion, the fluidic oscillator can be time consuming and requires expertise to understand how the oscillatory flow works. Device should be carefully set up with precision to avoid the generation of microbubbles similar to conventional bubbles. This study concluded that microbubbles generated at higher oscillation frequency is the best for biofilm detachment and filtration membrane defouling compared to low frequency oscillation and without fluidic oscillation.

In my opinion, microbubbles can act as disruption in the flow. This provide extra energy to the flow in the sense of foreign/impurities presence in the fluid flow. Scientifically, microbubbles for cleaning in this thesis are aimed to improved wastewater pre-treatment process, to clean microfiltration membrane. In practice, this FO generated microbubbles would benefit any agriculture sector such as turtle and marine life sanctuary. It is convinced that the designed systems for this PhD project would provide better alternatives as well as improving the future technology of filtration cleaning industry. For me, Arduino is very reliable of data logger and most importantly, the cheapest option available. The instruments manual is usually available at zero cost. The sensors are the best alternative to record the date, however, requires some expertise to learn about the electrical circuit which could be tricky when come to simultaneous data logging.

9.3 Future Works

General assumptions and preliminary relationship between fluidic oscillation and defouling are made as the membranes are defouled more rapidly with fluidic oscillations. This, however, requires further data measurement and analysis to distinguish a figurative relationship below.

I. More testing needed on different size of filtration membrane to distinguish the relationship of set microbubbles size on defouling rate.

II.   Measurement of the adhesion force of the biofilm on microscope slide and shear force provided by microbubbles generated by fluidic oscillation.

III.   Analysis of the mechanical vibrations generated by the fluidic oscillator. It has an effect on the detachment rate where the energy is directly transferred or through microbubbles on the detachment rate system.

IV.   Microbubbles sparging and various cells viability to replace the Trypsin in tissue culture lab for cell splitting.

I believe, should the above relationship to be elucidated, it should improve the microbubble-biofilm contact (the fluid-particle interaction is controlling) and achieve higher efficiencies or detachment rate than demonstrated in this thesis. The understanding of influence of such factors would allow robust process design methodologies for a wide range of cleaning application.

BIBLIOGRAPHY

Abdulrazzaq, N., Al-Sabbagh, B., Rees, J. M. & Zimmerman, W. B. (2015). Separation of Azeotropic Mixtures Using Air Microbubbles Generated by Fluidic Oscillation. *AIChE*, 62(504), 1192–1199.

Adair, W. S. & Appel, H. (1989). Identification of a Highly Conserved Hydroxyproline-Rich Glycoprotein in the Cell Walls of Chlamydomonas Reinhardtii and Two Other Volvocales. *Planta*, 179(3), 381–386. Retrieved November 7, 2018, from http://www.ncbi.nlm.nih.gov/pubmed/24201668

Agarwal, A., Ng, W. J. & Liu, Y. (2011). Principle and Applications of Microbubble and Nanobubble Technology for Water Treatment. *Chemosphere*, 84(9), 1175–1180. Retrieved from http://dx.doi.org/10.1016/j.chemosphere.2011.05.054

Agarwal, A., Xu, H., Ng, W. J. & Liu, Y. (2012). Biofilm Detachment by Self-Collapsing Air Microbubbles: A Potential Chemical-Free Cleaning Technology for Membrane Biofouling. *Journal of Materials Chemistry*, 22(5), 2203–2207. Retrieved from http://apps.webofknowledge.com/full_record.do?product=UA&search_mode=GeneralSearch&qid=1&SID=3Ea3L18I4b73DKAn9GO&page=2&doc=16

Akagi, Y., Okada, K., Kosaka, K. & Takahashi, T. (1987). Liquid Weeping Accompanied by Bubble Formation at Submerged Orifices. *Industrial and Engineering Chemistry Research*, 26(8), 1546–1550.

Al-Malack, M. H. & Anderson, G. K. (1997). Crossflow Microfiltration with Dynamic Membranes. *Water Research*, 31(8), 1969–1979.

AL-Mashhadani, M. K. H., Wilkinson, S. J. & Zimmerman, W. B. (2015). Airlift Bioreactor for Biological Applications with Microbubble Mediated Transport Processes. *Chemical Engineering Science*, 137, 243–253. Retrieved from http://linkinghub.elsevier.com/retrieve/pii/S0009250915004406

Al-yaqoobi, A., Hogg, D. & Zimmerman, W. B. (2016). Microbubble Distillation for Ethanol-Water Separation. *International Journal of Chemical Engineering*, 2016, 10.

Amini, N., Majid, F. A. A., Marvibaigi, M., Supriyanto, E., Jaganathan, S. K., Tet Soon, W., Nasiri, R. & Hamzehalipour, J. (2016). Cervicare[TM] Induces Apoptosis in HeLa and CaSki Cells through ROS Production and Loss of Mitochondrial Membrane Potential. *RSC Advances*, 6(29), 24391–24417.

Anderson, D. M., Glibert, P. M. & Burkholder, J. M. (2002). Harmful Algal Blooms and Eutrophication: Nutrient Sources, Composition, and Consequences. *Estuaries*.

Antoniadis, D., Mantzavinos, D. & Stamatoudis, M. (1992). Effect of Chamber Volume an Diameter on Bubble Formation at Plate Orifices. *Chemical Engineering Research and Design*.

Aslan, M. M., Crofcheck, C., Tao, D. & Pinar Mengüç, M. (2006). Evaluation of Micro-Bubble Size and Gas Hold-up in Two-Phase Gas-Liquid Columns via Scattered Light Measurements. *Journal of Quantitative Spectroscopy and Radiative Transfer*, 101(3), 527–539.

Auger, P., Bourgouin, J. & Bagot, C. (1988). The Microalga Chlamydomonas Reinhardtii as a Platform for the Production of Human Protein Therapeutics. *Current Therapeutic Research - Clinical and Experimental*, 43(3), 494–502.

Bae, K., Go, G. S., Noh, N. S., Lim, Y.-I., Bae, J. & Lee, D. H. (2019). Bubble Characteristics in Pressurized Bubble Column Associated with Micro-Bubble Dispersion. *Chemical Engineering Journal*, (xxxx), 1–13. Retrieved from https://linkinghub.elsevier.com/retrieve/pii/S1385894719306862

Baker, R. (2004). *Membrane Technology and Applications*. Chichester: J. Wiley.

Balmann, de H. & Nobrega, R. (1989). The Deformation of Dextran Molecules. Causes and Consequences in UF. *Journal of Membrane Science*, 40, 311–327.

Barber, R., Horra, M. & Crespo, J. (2013). Control Practices Using Simulink with Arduino as Low Cost Hardware. *IFAC Proceedings Volumes*, 46(17), 250–255. Retrieved December 25, 2018, from https://www.sciencedirect.com/science/article/pii/S1474667015341094

Basu, I., Mitra, R., Saha, P. K., Ghosh, A. N., Bhattacharya, J., Chakrabarti, M. K., Takeda, Y. & Nair, G. B. (1999). Morphological and Cytoskeletal Changes Caused by Non-Membrane Damaging Cytotoxin of Vibrio Cholerae on Int 407 and HeLa Cells. *FEMS Microbiology Letters*, 179(2), 255–263.

Bhattacharya, P., Roy, A., Sarkar, S., Ghosh, S., Majumdar, S., Chakraborty, S., Mandal, S., Mukhopadhyay, A. & Bandyopadhyay, S. (2013). Combination Technology of Ceramic Microfiltration and Reverse Osmosis for Tannery Wastewater Recovery. *Water Resources and Industry*, 3, 48–62.

Borin, D., Puzzi, L., Martinelli, V., Cibinel, M., Lapasin, R. & Sbaizero, O. (2017). An Engineering Insight into the Relationship of Selective Cytoskeletal Impairment and Biomechanics of HeLa Cells. *Micron*, 102(August), 88–96. Retrieved from http://dx.doi.org/10.1016/j.micron.2017.09.002

Bowsher, J. M. (1987). Automatic Hand-Held Photographic Light Meters. , (19). Retrieved from https://patents.google.com/patent/US4636052A/en

Brittle, S., Desai, P., Choon, W., Dunbar, A., Howell, R., Tesar, V. & Zimmerman, W. B. (2015). Chemical Engineering Research and Design Minimising Microbubble Size through Oscillation Frequency Control. *Chemical Engineering Research and Design*, 4, 357–366.

Bugg, J. D. & Rowe, R. D. (1993). Modelling Large-bubble Formation at Submerged Orifices. *International Journal for Numerical Methods in Fluids*.

Burns, S. E., Yiacoumi, S. & Tsouris, C. (1997). Microbubble Generation for Environmental and Industrial Separations. *Separation and Purification Technology*, 11(3), 221–232.

Cantwell, A. (2018). HEPG2 CELLS. *Celeromics*, 1. Retrieved November 1, 2018, from http://www.celeromics.com/en/Support/cell-lines/HeLa.php

Cao, Y. jun, Gui, X. hui, Ma, Z. long, Yu, X. xia, Chen, X. dong & ZHANG, X. pin. (2009). Process Mineralogy of Copper-Nickel Sulphide Flotation by a Cyclonic-Static Micro-Bubble Flotation Column. *Mining Science and Technology*, 19(6),

784–787. Retrieved from http://dx.doi.org/10.1016/S1674-5264(09)60143-5

Chahine, G. L., Hsiao, C. T., Lin, P., Chuang, M., Chang, S., Rodríguez-Rodríguez, J., Sevilla, A., Martínez-Bazán, C., Gordillo, J. M., Dastgheyb, S. S., Eisenbrey, J. R., Kanchan Maske, S., Shalini Rai, D., Swati Kale, V., Deepika Raut, B., Ashwini Chintale, G. & Klopfer, M. J. (2015). Generation of Microbubbles with Applications to Industry and Medicine. *Journal of Hydrodynamics*, 00(Ahfe), 169–183. Retrieved from http://dx.doi.org/10.1016/B978-0-323-22805-3.00011-6

Chesters, S. P. (2009). Innovations in the Inhibition and Cleaning of Reverse Osmosis Membrane Scaling and Fouling. *Desalination*, 238(1–3), 22–29.

Chesters, Stephen P, Armstrong, M. W. & Fazel, M. (2013). Cleaning Biofouled Membranes Early Improves Plant Operation. Comparison of Autopsy and Cleaning Results on a Small BWRO and Large SWRO. *AMTA/AWWA Membrane Technology Conference and Exposition 2013*, 717–727. Retrieved from http://www.scopus.com/inward/record.url?eid=2-s2.0-84890377388&partnerID=tZOtx3y1

Chesters, Stephen P, Armstrong, M. W., Fazel, M., Wilson, R. & Golding, D. A. (2013). RO Membrane Cleaning, Past, Present, Future – Innovations for Improving Ro Plant Operating Efficiency. *The International Desalination Association World Congress on Desalination and Water Reuse*.

Chesters, S P, Pena, N., Gallego, S., Fazel, M., Armstrong, M. W. & del Vigo, F. (2013). Results from 99 Seawater RO Membrane Autopsies. *IDA Journal of Desalination and Water Reuse*, 5(1), 40–47. Retrieved from http://openurl.ingenta.com/content/xref?genre=article&issn=1947-7953&volume=5&issue=1&spage=40

Choung, J. W., Luttrell, G. H. & Yoon, R. H. (1993). Characterization of Operating Parameters in the Cleaning Zone of Microbubble Column Flotation. , 39, 31–40.

Chu, L. B., Xing, X. H., Yu, A. F., Sun, X. L. & Jurcik, B. (2008). Enhanced Treatment of Practical Textile Wastewater by Microbubble Ozonation. *Process Safety and*

Environmental Protection, 86(5), 389–393.

Costerton, J. W., Stewart, P. S. & Greenberg, E. P. (1999). Bacterial Biofilms: A Common Cause of Persistent Infections. *Science*, 284(5418), 1318–1322.

Cui, L., Chen, P., Zhang, B., Zhang, D., Li, J., Martin, F. L. & Zhang, K. (2015). Interrogating Chemical Variation via Layer-by-Layer SERS during Biofouling and Cleaning of Nanofiltration Membranes with Further Investigations into Cleaning Efficiency. *Water Research*, 87, 282–291. Retrieved from http://dx.doi.org/10.1016/j.watres.2015.09.037

Cummings, P. J. & Obom, K. M. (2007). HeLa Cell Morphology. Retrieved September 13, 2018, from http://www.asmscience.org/content/education/imagegallery/image.3132

Dastgheyb, S. S. & Eisenbrey, J. R. (2013). *Microbubble Applications in Biomedicine*. Elsevier Inc. Retrieved from http://dx.doi.org/10.1016/B978-0-323-22805-3.00011-6

Desai, P. D., Hines, M. J., Riaz, Y. & Zimmerman, W. B. (2018). Resonant Pulsing Frequency Effect for Much Smaller Bubble Formation with Fluidic Oscillation. *Energies*, 11(10).

Ducom, G., Matamoros, H. & Cabassud, C. (2002). Air Sparging for Flux Enhancement in Nanofiltration Membranes: Application to O/W Stabilised and Non-Stabilised Emulsions. *Journal of Membrane Science*, 204(1–2), 221–236.

Ducom, G., Puech, F. & Cabassud, C. (2003). Gas/Liquid Two-Phase Flow in a Flat Sheet Filtration Module: Measurement of Local Wall Shear Stresses. *The Canadian Journal of Chemical Engineering*, 81(3–4), 771–775. Retrieved from http://www3.interscience.wiley.com/journal/119193741/abstract

Ducom, G., Puech, F. P. & Cabassud, C. (2002). Air Sparging with Flat Sheet Nanofiltration: A Link between Wall Shear Stresses and Flux Enhancement. *Desalination*, 145(1–3), 97–102.

Eagle, H. (1959). Amino Acid Metabolism in Mammalian Cell Cultures. *Science*,

130(3373), 432–437.

Fazel, M. & Chesters, S. P. (2015). RO Membrane Cleaning Using Microbubbles at 6,800 M3d Wastewater RO Plant in UAE. *Desalination and Water Treatment*, 55, 3358–3366.

Fazel, M., Wilson, R., Darton, T., Eckersley, J. & Chesters, S. (2013). Safe Use of Microbubbles for Removal of Ro Membrane, in: *The International Desalination Association World Congress on Desalination and Water Reuse 2013*, (p. 18). Tianjin: The International Desalination Association.

Feng, D., van Deventer, J. S. J. & Aldrich, C. (2006). Ultrasonic Defouling of Reverse Osmosis Membranes Used to Treat Wastewater Effluents. *Separation and Purification Technology*.

Figurski, S. & Shockley, R. (2009). Division of Water - DNREC. *State of Delaware*, 2. Retrieved December 23, 2018, from https://dnrec.alpha.delaware.gov/water/

Flemming, H.-C. (1997). Reverse Osmosis Membrane Biofouling. *Experimental Thermal and Fluid Science*, 14(4), 382–391.

Gac, J. M. & Gradoń, L. (2014). Hollow Fibre Membrane Oscillations against Fouling Process - A Numerical Study. *Chemical and Process Engineering - Inzynieria Chemiczna i Procesowa*, 35(1), 149–158.

Galanakis, C. M., Markouli, E. & Gekas, V. (2013). Recovery and Fractionation of Different Phenolic Classes from Winery Sludge Using Ultrafiltration. *Separation and Purification Technology*, 107, 245–251.

Giacobbo, A., Do Prado, J. M., Meneguzzi, A., Bernardes, A. M. & De Pinho, M. N. (2015). Microfiltration for the Recovery of Polyphenols from Winery Effluents. *Separation and Purification Technology*, 143, 12–18.

Gong, B., Liang, X., Li, Y., Xiao, Q., Yang, P. & Wu, Y. (2018). Expression and Purification of Cytochrome P450 55B1 from Chlamydomonas Reinhardtii and Its Application in Nitric Oxide Biosensing. *Applied Biochemistry and Biotechnology*, 184(1), 102–112.

Griffith, H., Smith, A., Jonikas, M., Fee, D. & Shi, N. (2013). Algae | CAPP. *Worpress*, 3. Retrieved November 6, 2018, from https://cambridgecapp.wordpress.com/improving-photosynthesis/algae/

Gwenaelle, M. P. O., Jung, J., Choi, Y. & Lee, S. (2017). Effect of Microbubbles on Micro Fi Ltration Pretreatment for Seawater Reverse Osmosis Membrane. *Desalination*, 403, 153–160. Retrieved from http://dx.doi.org/10.1016/j.desal.2016.06.012

Hanotu, J., Bandulasena, H. C. H., Chiu, T. Y. & Zimmerman, W. B. (2013). Oil Emulsion Separation with Fluidic Oscillator Generated Microbubbles. *International Journal of Multiphase Flow*, 56, 119–125. Retrieved from http://dx.doi.org/10.1016/j.ijmultiphaseflow.2013.05.012

Hanotu, J., Bandulasena, H. C. H. & Zimmerman, W. B. (2012). Microflotation Performance for Algal Separation. *Biotechnology and Bioengineering*, 109(7), 1663–1673.

Hanotu, J., Karunakaran, E., Bandulasena, H., Biggs, C. & Zimmerman, W. B. (2014). Harvesting and Dewatering Yeast by Microflotation. *Biochemical Engineering Journal*, 82, 174–182. Retrieved from http://dx.doi.org/10.1016/j.bej.2013.10.019

Hanotu, J., Kong, D. & Zimmerman, W. B. (2016). Intensification of Yeast Production with Microbubbles. *Food and Bioproducts Processing*, 100, 424–431. Retrieved from http://dx.doi.org/10.1016/j.fbp.2016.07.013

Hanotu, J. O. (2013). Development of a Fluidic Oscillator-Driven Flotation System. , (January).

Heisler, J., Glibert, P. M., Burkholder, J. M., Anderson, D. M., Cochlan, W., Dennison, W. C., Dortch, Q., Gobler, C. J., Heil, C. A., Humphries, E., Lewitus, A., Magnien, R., Marshall, H. G., Sellner, K., Stockwell, D. A., Stoecker, D. K. & Suddleson, M. (2008). Eutrophication and Harmful Algal Blooms: A Scientific Consensus. *Harmful Algae*, 8(1), 3–13. Retrieved December 23, 2018, from https://www.sciencedirect.com/science/article/pii/S1568988308001066

Henry, C., Minier, J. P. & Lefevre, G. (2012). Towards a Description of Particulate Fouling: From Single Particle Deposition to Clogging. *Advances in Colloid and Interface Science*, 185–186, 34–76. Retrieved from http://dx.doi.org/10.1016/j.cis.2012.10.001

Hiroyuki, A., Kenji, A., Masato, F., Takakusagi, F., Tabei, K. & Noda, Y. (2010). Study on Cleaning of Pipe Inner Wall by Micro-Bubble Flow. *Japanese Journal of Multiphase Flow*, 24(4), 545–461.

Hiroyuki, A., Kenji, A., Masato, F., Takakusagi, F., Tabei, K., Noda, Y., Matsuura, K., Ogawa, S., Kasaki, S., Koyama, K., Kodama, M. & Yanase, S. (2015). Study on Cleaning of Pipe Inner Wall by Micro-Bubble Flow. *Separation and Purification Technology*, 142(4), 242–250. Retrieved from http://dx.doi.org/10.1016/j.seppur.2015.01.009

Hjort, A. & Holmberg, M. M. (2015). *Measuring Mechanical Vibrations Using Arduino as a Slave I/O to an EPICS Control System*.

Hwang, K.-J. & Chen, L. (2010). Effect of Air-Sparging on the Cross-Flow Microfiltration of Microbe/Protein Bio-Suspension. *Journal of the Taiwan Institute of Chemical Engineers*, 41(5), 564–569.

Hwang, K.-J. & Hsu, C.-E. (2009). Effect of Gas–Liquid Flow Pattern on Air-Sparged Cross-Flow Microfiltration of Yeast Suspension. *Chemical Engineering Journal*, 151(1), 160–167.

Hwang, K.-J. & Wu, S.-F. (2009). Effects of Air-Sparging on the Filtration Flux and Cake Properties in Cross-Flow Microfiltration of Size-Distributed Fine Particles. *Separation Science and Technology*, 44(15), 3485–3505. Retrieved from http://www.tandfonline.com/doi/abs/10.1080/01496390903183345

Hwang, K. J., Chen, H. C. & Tsai, M. H. (2010). Analysis of Particle Fouling in Constant-Pressure Submerged Membrane Filtration. *Chemical Engineering & Technology*, 33(8), 1327–1333. Retrieved from http://doi.wiley.com/10.1002/ceat.201000103

Institutions, W. & Ships, U. (1952). *Marine Fouling and Its Prevention ; Prepared for Bureau of Ships, Navy Dept.* Woods Hole, MA: United States Naval Institute. Retrieved from https://hdl.handle.net/1912/191

Jang, H., Rusconi, R. & Stocker, R. (2017). Biofilm Disruption by an Air Bubble Reveals Heterogeneous Age-Dependent Detachment Patterns Dictated by Initial Extracellular Matrix Distribution. *npj Biofilms and Microbiomes*, 3(1), 0–1. Retrieved from http://dx.doi.org/10.1038/s41522-017-0014-5

Janssen, L. J. J. & Hoogland, J. G. (1973). The Effect of Electrolytically Evolved Gas Bubbles on the Thickness of the Diffusion Layer-II. *Electrochimica Acta*, 18(8), 543–550.

Jongseon, J., Haksoo, K., Lee, S., Byoungsub, H., Kim, W. & Wilsoo, K. (2016). Development of Nuclear Facilities Piping Cleaning System Using Microbubble, in: *ASME 2011 14th International Conference on Environmental Remediation and Radioactive Waste Managemen*, (pp. 1–5). Reims, France: ASME.

Kamaroddin, M. F., Hanotu, J., Gilmour, D. J. & Zimmerman, W. B. (2016). In-Situ Disinfection and a New Downstream Processing Scheme from Algal Harvesting to Lipid Extraction Using Ozone-Rich Microbubbles for Biofuel Production. *Algal Research*, 17, 217–226. Retrieved from http://linkinghub.elsevier.com/retrieve/pii/S221192641630162X

Kanchan Maske, S., Shalini Rai, D., Swati Kale, V., Deepika Raut, B. & Ashwini Chintale, G. (2012). Microbubble and Its Applications. *Int. J. of Pharm. & Life Sci. (IJPLS)*, 3(12), 2228–2235.

Karami, M., McMorrow, G. V. & Wang, L. (2018). Continuous Monitoring of Indoor Environmental Quality Using an Arduino-Based Data Acquisition System. *Journal of Building Engineering*, 19, 412–419. Retrieved December 25, 2018, from https://www.sciencedirect.com/science/article/pii/S2352710218301025

Khataee, A. R., Zarei, M. & Pourhassan, M. (2009). Application of Microalga Chlamydomonas Sp. for Biosorptive Removal of a Textile Dye from Contaminated Water: Modelling by a Neural Network. *Environmental*

Technology, 30(14), 1615–1623.

Khuntia, S., Majumder, S. K. & Ghosh, P. (2012). Microbubble-Aided Water and Wastewater Purification: A Review. *Reviews in Chemical Engineering*, 28(4–6), 191–221.

Klassen, V., Blifernez-Klassen, O., Wibberg, D., Winkler, A., Kalinowski, J., Posten, C. & Kruse, O. (2017). Highly Efficient Methane Generation from Untreated Microalgae Biomass. *Biotechnology for Biofuels*, 10(1), 1–12.

Kroner, K. H., Schutte, H., Hustedt, H. & Kula, M. R. (1984). Cross-Flow Filtration in the Downstream Processing of Enzymes. *Process biochemistry*, v. 19.

Kukizaki, M. & Goto, M. (2006). Size Control of Nanobubbles Generated from Shirasu-Porous-Glass (SPG) Membranes. *Journal of Membrane Science*, 281(1–2), 386–396.

Kushner, D. (2011). The Making of Arduino - IEEE Spectrum. *Institute of Electrical and Electronics Engineers*. Retrieved December 25, 2015, from https://spectrum.ieee.org/geek-life/hands-on/the-making-of-arduino

Lee, E.-J., Kim, Y.-H., Kim, H.-S. & Jang, A. (2014). Influence of Microbubble in Physical Cleaning of MF Membrane Process for Wastewater Reuse. *Environmental Science and Pollution Research*, 22(11), 8451–8459. Retrieved from http://link.springer.com/10.1007/s11356-014-3928-y

Lee, J.-E. & Lee, J.-K. (2002). Effect of Microbubbles and Particle Size on the Particle Collection in the Column Flotation. *Korean Journal of Chemical Engineering*, 19(4), 703–710. Retrieved from http://link.springer.com/10.1007/BF02699321

Li, L., Liu, J., Wang, L. & Yu, H. (2010). Numerical Simulation of a Self-Absorbing Microbubble Generator for a Cyclonic-Static Microbubble Flotation Column. *Mining Sceince and Technology*, 20(11), 350–356. Retrieved from http://linkinghub.elsevier.com/retrieve/pii/S0009250915004406

Li, Q. . Y., Cui, Z. . F. & Pepper, D. . S. (1997). Effect of Bubble Size and Frequency on the Permeate Flux of Gas Sparged Ultrafiltration with Tubular Membranes.

Chemical Engineering Journal, 67(1), 71–75.

Lin, P., Chuang, M. & Chang, S. (2015). ScienceDirect Research on the Cleaning Efficacy of Micro-Bubbles on Dental Plaque. *Procedia Manufacturing*, 00(Ahfe), 1293–1300. Retrieved from http://dx.doi.org/10.1016/j.promfg.2015.07.102

Liu, Y., Yan, G., Gao, M. & Zhang, X. (2018). Magnetic Capture of Polydopamine-Encapsulated Hela Cells for the Analysis of Cell Surface Proteins. *Journal of Proteomics*, 172(October 2017), 76–81. Retrieved from https://doi.org/10.1016/j.jprot.2017.10.009

Lu, Y., Ding, Z., Liu, L., Wang, Z. & Ma, R. (2008). The Influence of Bubble Characteristics on the Performance of Submerged Hollow Fiber Membrane Module Used in Microfiltration. *Separation and Purification Technology*, 61(1), 89–95.

Lucey, B. P., Nelson-Rees, W. A. & Hutchins, G. M. (2009). Henrietta Lacks, HeLa Cells, and Cell Culture Contamination. *Archives of Pathology & Laboratory Medicine*, 133(9), 1463–1467. Retrieved from http://www.archivesofpathology.org/doi/abs/10.1043/1543-2165-133.9.1463

Matsumoto, Y. (2011). Surfactant Effects on Bubbly Flows. *Annual Review of Fluid Mechanics*, 43(1), 615–36.

Matsuura, K., Ogawa, S., Kasaki, S., Koyama, K., Kodama, M. & Yanase, S. (2015). Cleaning Polymer Ink from a Glass Substrate Using Microbubbles Generated by a Hydrogen Bubble Method. *Separation and Purification Technology*, 142, 242–250. Retrieved from http://dx.doi.org/10.1016/j.seppur.2015.01.009

Mavredaki, E., Stathoulopoulou, A., Neofotistou, E. & Demadis, K. D. (2007). Environmentally Benign Chemical Additives in the Treatment and Chemical Cleaning of Process Water Systems: Implications for Green Chemical Technology. *Desalination*, 210(1–3), 257–265.

McLachlan, D. (2010). The Defouling of Membranes Using Polymer Beads

Containing Magnetic Micro Particles. *Water SA*, 36(5), 641–650.

Mehta, A. (2012). Ultraviolet-Visible (UV-Vis) Spectroscopy-Limitation and Deviations of Beer-Lambert Law. *Analytical Chemistry*, 1–4.

Mercier-Bonin, M., Fonade, C. & Gésan-Guiziou, G. (2004). Application of Gas/Liquid Two-Phase Flows during Crossflow Microfiltration of Skimmed Milk under Constant Flux Conditions. *Chemical Engineering Science*, 59(11), 2333–2341.

Miyamoto, M., Ueyama, S., Hinomoto, N., Saitoh, T., Maekawa, S. & Hirotsuji, J. (2007). Degreasing of Solid Surfaces by Microbubble Cleaning. *Japanese Journal of Applied Physics, Part 1: Regular Papers and Short Notes and Review Papers*, 46(3 A), 1236–1243.

Modjarrad, K. & Ebnesajjad, S. (2014). *Handbook of Polymer Applications in Medicine and Medical Devices*.

Mussgnug, J. H., Klassen, V., Schlüter, A. & Kruse, O. (2010). Microalgae as Substrates for Fermentative Biogas Production in a Combined Biorefinery Concept. *Journal of Biotechnology*, 150(1), 51–56. Retrieved November 7, 2018, from http://www.ncbi.nlm.nih.gov/pubmed/20691224

Nagaoka, H., Kurosaka, M., Shibata, N. & Kobayashi, M. (2006). Effect of Bubble Flow Velocity on Drag-Force and Shear Stress Working on Submerged Hollow Fibre Membrane. *Water Science and Technology*, 54(10), 185–192.

Oncel, S. & Vardar-Sukan, F. (2011a). Application of Proton Exchange Membrane Fuel Cells for the Monitoring and Direct Usage of Biohydrogen Produced by Chlamydomonas Reinhardtii. *Journal of Power Sources*, 196(1), 46–53. Retrieved from http://dx.doi.org/10.1016/j.jpowsour.2010.07.042

Oncel, S. & Vardar-Sukan, F. (2011b). Application of Proton Exchange Membrane Fuel Cells for the Monitoring and Direct Usage of Biohydrogen Produced by Chlamydomonas Reinhardtii. *Journal of Power Sources*, 196(1), 46–53.

Parmar, R. & Majumder, S. K. (2013). Microbubble Generation and Microbubble-

Aided Transport Process Intensification—A State-of-the-Art Report. *Chemical Engineering & Processing: Process Intensification*, 64, 79–97.

Peña, N., Gallego, S., del Vigo, F. & Chesters, S. P. (2012). Evaluating Impact of Fouling on Reverse Osmosis Membranes Performance. *Desalination and Water Treatment*, 3994(April 2015), 1–11.

Penman, S. (1966). RNA Metabolism in the HeLa Cell Nucleus. *Journal of Molecular Biology*, 17(1), IN4-130. Retrieved from http://dx.doi.org/10.1016/S0022-2836(66)80098-0

Pimentel-Domínguez, R., Hernández-Cordero, J. & Zenit, R. (2012). Microbubble Generation Using Fiber Optic Tips Coated with Nanoparticles. *Optics Express*, 20(8), 8732.

Pospíšil, P., Wakeman, R. J., Hodgson, I. O. A. & Mikulášek, P. (2004). Shear Stress-Based Modelling of Steady State Permeate Flux in Microfiltration Enhanced by Two-Phase Flows. *Chemical Engineering Journal*, 97(2–3), 257–263.

Raghu, S. (2013). Fluidic Oscillators for Flow Control. *Experiments in Fluids*, 54(2).

Rao, M. D. & Pennathur, G. (2017). Green Synthesis and Characterization of Cadmium Sulphide Nanoparticles from Chlamydomonas Reinhardtii and Their Application as Photocatalysts. *Materials Research Bulletin*, 85, 64–73. Retrieved from http://dx.doi.org/10.1016/j.materresbull.2016.08.049

Rehman, F., Medley, G. J. D., Bandulasena, H. & Zimmerman, W. B. J. (2015). Fluidic Oscillator-Mediated Microbubble Generation to Provide Cost Effective Mass Transfer and Mixing Efficiency to the Wastewater Treatment Plants. *Environmental Research*, 137, 32–39. Retrieved from http://dx.doi.org/10.1016/j.envres.2014.11.017

Shamriz, S. & Ofoghi, H. (2017). Outlook in the Application of Chlamydomonas Reinhardtii Chloroplast as a Platform for Recombinant Protein Production. *Biotechnology and Genetic Engineering Reviews*, 32(1–2), 92–106. Retrieved from http://dx.doi.org/10.1080/02648725.2017.1307673

Sharma, P. K., Gibcus, M. J., Mei, H. C. Van Der & Busscher, H. J. (2005). Influence of Fluid Shear and Microbubbles on Bacterial Detachment from a Surface. *ASM :American Society for Microbiology; APPLIED AND ENVIRONMENTAL MICROBIOLOGY*, 71(7), 3668–3673.

Shin, W. T., Mirmiran, A., Yiacoumi, S. & Tsouris, C. (1999). Ozonation Using Microbubbles Formed by Electric Fields. *Separation and Purification Technology*, 15(3), 271–282.

Simmons, J. A., Sprittles, J. E. & Shikhmurzaev, Y. D. (2015). The Formation of a Bubble from a Submerged Orifice. *European Journal of Mechanics, B/Fluids*, 53, 24–36. Retrieved from http://dx.doi.org/10.1016/j.euromechflu.2015.01.003

Sinnott, R. . (2005). *Coulson and Richardson's Chemical Engineering Design* (Intergovernmental Panel on Climate Change, Ed.). Cambridge: Cambridge University Press. Retrieved from http://ebooks.cambridge.org/ref/id/CBO9781107415324A009

Sobota, J., PiŜl, R., Balda, P. & Schlegel, M. (2013). Raspberry Pi and Arduino Boards in Control Education. *IFAC Proceedings Volumes*, 46(17), 7–12. Retrieved December 25, 2018, from https://www.sciencedirect.com/science/article/pii/S1474667015340684

Sorentrue, J. (2016). Martin County Businesses Hurt by Algae Outbreak Can Apply for Disaster Loans | Malled! , 1. Retrieved December 23, 2018, from http://malled.blog.palmbeachpost.com/2016/07/25/martin-county-businesses-hurt-by-algae-outbreak-can-apply-for-disaster-loans/

Sutherland, K. (2004). *Profile of the International Filtration & Separation Industry*. Retrieved from http://www.sciencedirect.com/science/article/pii/B9781856174480500099

Taft, H. L. (2015). Water Scarcity: Global Challenges for Agriculture. *Food, Energy, and Water*, 395–429. Retrieved December 23, 2018, from https://www.sciencedirect.com/science/article/pii/B9780128002117000168

Taghavi, N. & Robinson, G. (2016). Improving the Optimum Yield and Growth of Chlamydomonas Reinhardtii CC125 and CW15 Using Various Carbon Sources and Growth Regimes. *African Journal of Biotechnology*, 15(23), 1083–1100.

Tasaki, T., Wada, T., Fujimoto, K., Kai, S., Ohe, K., Oshima, T., Baba, Y. & Kukizaki, M. (2009). Degradation of Methyl Orange Using Short-Wavelength UV Irradiation with Oxygen Microbubbles. *Journal of Hazardous Materials*, 162(2–3), 1103–1110.

Tatalick, L. M., Gerard, C. J., Takeya, R., Price, D. N., Thorne, B. A., Wyatt, L. M. & Anklesaria, P. (2005). Safety Characterization of HeLa-Based Cell Substrates Used in the Manufacture of a Recombinant Adeno-Associated Virus-HIV Vaccine. *Vaccine*, 23(20), 2628–2638.

Terasaka, K., Aoki, S. & Kobayashi, D. (2008). Removal of Iron Oxide Fine Particles from Waste Water Using Microbubble Flotation. *Progress in Multiphase Flow Research*, 3, 43–50. Retrieved from http://joi.jlc.jst.go.jp/JST.JSTAGE/pmfr/3.43?from=CrossRef

Terasaka, K. & Yasuyuki, S. (2007). Separation of Fine Particles Suspended in Water Using Micro Bubble Function. *Journal of Multiphase Flow*, 21, 77–83.

Tesař, V. (2014a). Mechanisms of Fluidic Microbubble Generation Part II: Suppressing the Conjunctions. *Chemical Engineering Science*, 116, 849–856.

Tesař, V. (2014b). Mechanisms of Fluidic Microbubble Generation Part 1: Growth by Multiple Conjunctions. *Chemical Engineering Science*, 116, 849–856.

Tesař, V. (2014c). Microbubble Generator Excited by Fluidic Oscillator's Third Harmonic Frequency. *Chemical Engineering Research and Design*, 92(9), 1603–1615.

Tesař, V. (2015). Fluidic Generator of Microbubbles - Oscillator with Gas Flow Reversal for a Part of Period. *Acta Mechanica et Automatica*, 9(4), 195–203.

Tesař, V. (2017). What Can Be Done with Microbubbles Generated by a Fluidic Oscillator? (Survey). *EPJ Web of Conferences*, 143, 02129.

Thomas, H. C. & Cremers, A. E. (1970). Electrical Conductivity of Suspensions of Colloidal Particles. *The Journal of Physical Chemistry*, 74(5), 1072–1075. Retrieved from http://pubs.acs.org/doi/abs/10.1021/j100700a018

Tian, J., Xu, Y., Chen, Z., Nan, J. & Li, G. (2010). Air Bubbling for Alleviating Membrane Fouling of Immersed Hollow-Fiber Membrane for Ultrafiltration of River Water. *Desalination*, 260(1), 225–230. Retrieved January 2, 2017, from http://www.sciencedirect.com/science/article/pii/S0011916410002389

Tsuge, H. (2014). *Micro- and Nanobubbles: Fundamentals and Applications* (H. Tsuge, Ed.). Taylor & Francis.

United States Environmental Protection. (2017). The Effects: Environment. Retrieved December 23, 2018, from https://www.epa.gov/nutrientpollution/effects-environment

Vera, L., Delgado, S. & Elmaleh, S. (2000). Dimensionless Numbers for the Steady-State Flux of Cross-Flow Microfiltration and Ultrafiltration with Gas Sparging. *Chemical Engineering Science*, 55(17), 3419–3428.

Vera, L., Villarroel, R., Delgado, S. & Elmaleh, S. (2000). Enhancing Microfiltration through an Inorganic Tubular Membrane by Gas Sparging. *Journal of Membrane Science*, 165(1), 47–57.

Wang, J., Wang, L., Hanotu, J. & Zimmerman, W. B. (2017). Improving the Performance of Coal Flotation Using Oscillatory Air Supply. *Fuel Processing Technology*, 165, 131–137. Retrieved from http://dx.doi.org/10.1016/j.fuproc.2017.05.022

Watabe, T., Matsuyama, K., Takahashi, T. & Matsuyama, H. (2016). Use of Microbubbles to Reduce Membrane Fouling during Water Filtration. *Desalination and Water Treatment*, 57(9), 3820–3826.

Wibisono, Y. (2014). Two-Phase Flow for Fouling Control in Membranes. *Igarss 2014*, (1).

Wibisono, Y., El Obied, K. E., Cornelissen, E. R., Kemperman, A. J. B. & Nijmeijer,

K. (2015). Biofouling Removal in Spiral-Wound Nanofiltration Elements Using Two-Phase Flow Cleaning. *Journal of Membrane Science*, 475, 131–146.

Wicaksana, F., Fane, A. G. & Chen, V. (2006). Fibre Movement Induced by Bubbling Using Submerged Hollow Fibre Membranes. *Journal of Membrane Science*, 271(1), 186–195.

Wilson, R, Fazel, M., Jarrige, S., Chesters, S. & Wilson, Rachel. (2013). Air Bubbles Enhance Membrane Cleaning: A Future Perspective. *The International Desalination Association World Congress on Desalination and Water Reuse 2013*, 13, 18.

Wirth, R., Lakatos, G., Maróti, G., Bagi, Z., Minárovics, J., Nagy, K., Kondorosi, É., Rákhely, G. & Kovács, K. L. (2015). Exploitation of Algal-Bacterial Associations in a Two-Stage Biohydrogen and Biogas Generation Process Philippe Soucaille. *Biotechnology for Biofuels*, 8(1), 1–14.

Wu, J., He, C. & Zhang, Y. (2012). Modeling Membrane Fouling in a Submerged Membrane Bioreactor by Considering the Role of Solid, Colloidal and Soluble Components. *Journal of Membrane Science*, 397–398, 102–111. Retrieved from http://dx.doi.org/10.1016/j.memsci.2012.01.026

Wu, Z. H., Chen, H. B., Dong, Y. M., Mao, H. L., Sun, J. L., Chen, S. F., Craig, V. S. J. & Hu, J. (2008). Cleaning Using Nanobubbles: Defouling by Electrochemical Generation of Bubbles. *Journal of Colloid and Interface Science*, 328(1), 10–14. Retrieved from www.elsevier.com/locate/jcis

Xia, W., Yang, J. & Wang, Y. (2011). Reliability of Gas Holdup Measurements Using the Differential Pressure Method in a Cyclone-Static Micro-Bubble Flotation Column. *Mining Science and Technology*, 21(6), 797–801. Retrieved from http://dx.doi.org/10.1016/j.mstc.2011.06.026

Xu, Q., Nakajima, M., Ichikawa, S., Nakamura, N. & Shiina, T. (2008). A Comparative Study of Microbubble Generation by Mechanical Agitation and Sonication. *Innovative Food Science and Emerging Technologies*, 9(4), 489–494.

Yamanoi, I. & Kageyama, K. (2010). Evaluation of Bubble Flow Properties between Flat Sheet Membranes in Membrane Bioreactor. *Journal of Membrane Science*, 360(1), 102–108.

Yan, X., Liu, J., Cao, Y. & Wang, L. (2012). A Single-Phase Turbulent Flow Numerical Simulation of a Cyclonic-Static Micro Bubble Flotation Column. *International Journal of Mining Science and Technology*, 22(1), 95–100. Retrieved from http://dx.doi.org/10.1016/j.ijmst.2011.07.009

Yoon, J. K. & Lee, S. H. (2015). Fabrication of Ozone Bubble Cleaning System and Its Application to Clean Silicon Wafers of a Solar Cell. *Electrical Engineering Technology*, 10, 742–745. Retrieved from http://dx.doi.org/10.5370/JEET.2015.10.?.742

Yu, K., Wen, X., Bu, Q. & Xia, H. (2003). Critical Flux Enhancements with Air Sparging in Axial Hollow Fibers Cross-Flow Microfiltration of Biologically Treated Wastewater. *Journal of Membrane Science*, 224(1–2), 69–79.

Zhao, D. & Yu, S. (2014). A Review of Recent Advance in Fouling Mitigation of NF/RO Membranes in Water Treatment: Pretreatment, Membrane Modification, and Chemical Cleaning. *Desalination and Water Treatment*, 55(July), 1–22. Retrieved from http://www.tandfonline.com/doi/abs/10.1080/19443994.2014.928804

Zimmerman, W. B. (2011a). Electrochemical Microfluidics. *Chemical Engineering Science*, 66(7), 1412–1425. Retrieved from http://dx.doi.org/10.1016/j.ces.2010.03.057

Zimmerman, W. B. (2011b). Microbubbles Keep Green Energy Blooming. *ANSYS Advantage*, 1, 44–45.

Zimmerman, W. B., Hewakandamby, B. N., Tesar, V., Bandulasena, H. C. H. & Omotowa, O. A. (2009). On the Design and Simulation of an Airlift Loop Bioreactor with Microbubble Generation by Fluidic Oscillation. *Food and Bioproducts Processing*, 87(3), 215–227.

Zimmerman, W. B. J. (2014). Bubble Generation to Strip Components of a Liquid.

Zimmerman, W. B. J. & Tesar, V. (2010). Bubble Generation for Aeration and Other Purposes. , 1(19), US 2010/0002534 A1.

Zimmerman, W. B., Tesar, V. & Bandulasena, H. C. H. (2011). Towards Energy Efficient Nanobubble Generation with Fluidic Oscillation. *Current Opinion in Colloid and Interface Science*, 16(4), 350–356.

Zimmerman, W. B., Tesar, V., Butler, S. & Bandulasena, H. H. (2008). Microbubble Generation. *Recent Patents on Engineering*, 2(1), 1–8. Retrieved from http://www.eurekaselect.com/openurl/content.php?genre=article&issn=1872-2121&volume=2&issue=1&spage=1

Zimmerman, W. B., Zandi, M., Hemaka Bandulasena, H. C., Tesař, V., James Gilmour, D. & Ying, K. (2011). Design of an Airlift Loop Bioreactor and Pilot Scales Studies with Fluidic Oscillator Induced Microbubbles for Growth of a Microalgae Dunaliella Salina. *Applied Energy*, 88(10), 3357–3369.

Expressing HeLa Cell Line. Retrieved September 13, 2018, from https://www.sigmaaldrich.com/catalog/product/mm/scc112?lang=en&region=GB

APPENDICES

A. Arduino Code

Flowmeter

```
float falowrate; //Variable to store the value in L/min
float average=0; //variable to take the average every 1 minute
int contaPulse; //variable for the number of pulses
int i=0; //variable for counting


void setup()
{
  Serial.begin(9600); //Initiate a serial baud rate at 9600

  pinMode(2, INPUT);
  attachInterrupt(0, incpulse, RISING);
  Serial.println("\n\nInitiate\n\n"); //Print start on serial
}


void loop ()
{
  contaPulse = 0;    //Zero the variable counts turn per second
  sei();       //Enables interrupt
  delay (1000); // data collected every 1s
  cli();       //Disable interupt

  flowrate = contaPulse / 5.5; //Converts to L/min
  average=average+flowrate; //total of the flow calculation for the mean
  i++;

  Serial.print(flowrate); //Print serial value of flowrate
  Serial.print(" L/min - "); //print L/min
  Serial.print(i); //print the count every 1s
  Serial.println("s"); //unit for second

  if(i==60)
  {
    averag = average/60; //average taken divided by 60
    Serial.print("\nflowrate per minute = "); //
    Serial.print(flowrate); //
    Serial.println(" L/min - "); //
    media = 0; //zero the average for the new count
    i=0; //zero the variable I for new count
    Serial.println("\n\nInicio\n\n"); //print starts
  }

}

void incpulse ()
{
  contaPulse++; //increment of the pulse
}
```

164

Pressure Transducer

```
int sensorVal=analogRead(A0);
void setup() {
  Serial.begin(9600);
}

void loop(){
  int sensorVal=analogRead(A0);
{
float voltage = (sensorVal*5.0)/1024.0;
float pressure_pascal = (3.0*((float)voltage-0.47))*1000000.0;
float pressure_bar = pressure_pascal/10e5;

Serial.print("DATA,TIME");
Serial.print(",");
Serial.print("Volts");
Serial.print(",");
Serial.print(sensorVal);
Serial.print(",");
Serial.print("Pressure");
Serial.print(",");
Serial.print(pressure_bar);
Serial.print(",");
Serial.println("bars ");

}
delay(1000);
}
```

Pressure Transducer and flowmeter (collection data at the same time and PLX-DAQ data)

```
int contaPulso; //
int sensorVal=analogRead(A1);
int sensorVals=analogRead(A0);
float vazao; //
float media=0; //
float voltage=(sensorVal*5.0)/1024.0;
float voltages=(sensorVal*5.0)/1024.0;
float pressure_pascal=(3.0*((float)voltage-0.47))*100000;
float pressure_bar=pressure_pascal/1e5;
float pressure_pascals=(3.0*((float)voltages-0.47))*100000;
float pressure_bars=pressure_pascals/1e5;

void setup()
{
  Serial.begin(9600); //
  pinMode(2, INPUT);
  attachInterrupt(0, incpulso, RISING); //
Serial.println("\n\nInitiate\n\n"); //
}
```

```
void loop ()
{
  int sensorVal=analogRead(A1);
  int sensorVals=analogRead(A0);
  float voltage = (sensorVal*5.0)/1024.0;
  float voltages = (sensorVals*5.0)/1024.0;
  float pressure_pascal = (3.0*((float)voltage-0.47))*1000000.0;
  float pressure_bar = pressure_pascal/10e5;
  float pressure_pascals = (3.0*((float)voltages-0.47))*1000000.0;
  float pressure_bars = pressure_pascals/10e5;
  contaPulso = 0;   //Zera a variável para contar os giros por segundos
  sei();      //Habilita interrupção
  delay (1000); //1000 represents 1 seconds
  cli();

  vazao = contaPulso/(5.5*1); //Converts to L/min //divide with delay
  media=media+vazao; //Soma a vazão para o calculo da media

  Serial.print("DATA,TIME");
  Serial.print(",");
  Serial.print(vazao);
  Serial.print(",");
  Serial.print(sensorVal);
  Serial.print(",");
  Serial.print(pressure_bar*10);
  Serial.print(",");
  Serial.print((sensorVals/2)-10);
  Serial.print(",");
  Serial.println(pressure_bars/2);

  {
    media = media/60;
    Serial.print("\nAverage per Minute = ");
    Serial.print(media); //
    Serial.println(" L/min - ");
    media = 0;
    Serial.println("\n\nInitiate\n\n");
  }

}


void incpulso ()
{
  contaPulso++;
});
}
```

Accelorometer

```
const int groundpin = 18;              // analog input pin 4 -- ground
const int powerpin = 19;               // analog input pin 5 -- voltage
const int xpin = A3;                   // x-axis of the accelerometer
```

166

```
const int ypin = A2;                    // y-axis
const int zpin = A1;                    // z-axis (only on 3-axis models)

void setup() {
  // initialize the serial communications:
  Serial.begin(9600);


  pinMode(groundpin, OUTPUT);
  pinMode(powerpin, OUTPUT);
  digitalWrite(groundpin, LOW);
  digitalWrite(powerpin, HIGH);
}

void loop() {
  // print the sensor values:
  Serial.print(analogRead(xpin));
  // print a tab between values:
  Serial.print("\t");
  Serial.print(analogRead(ypin));
  // print a tab between values:
  Serial.print("\t");
  Serial.print(analogRead(zpin));
  Serial.println();
  // delay before next reading:
  delay(100);
}
```
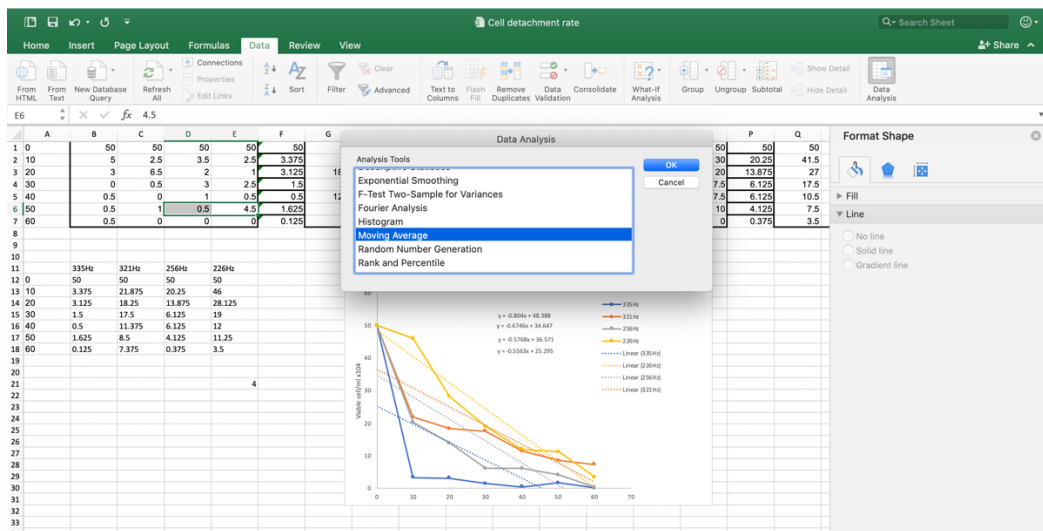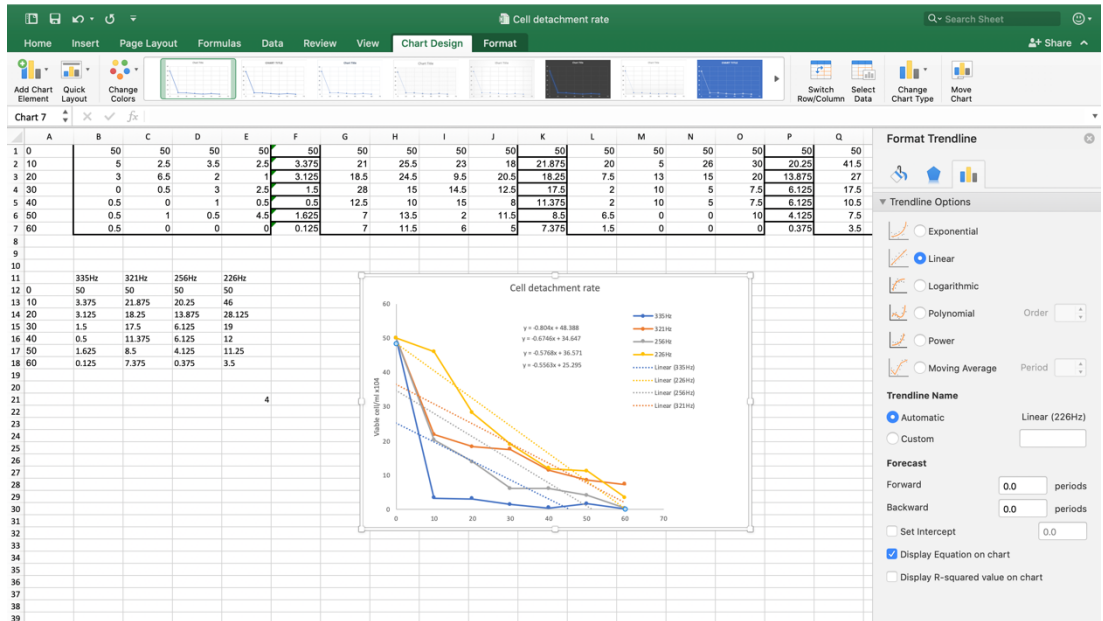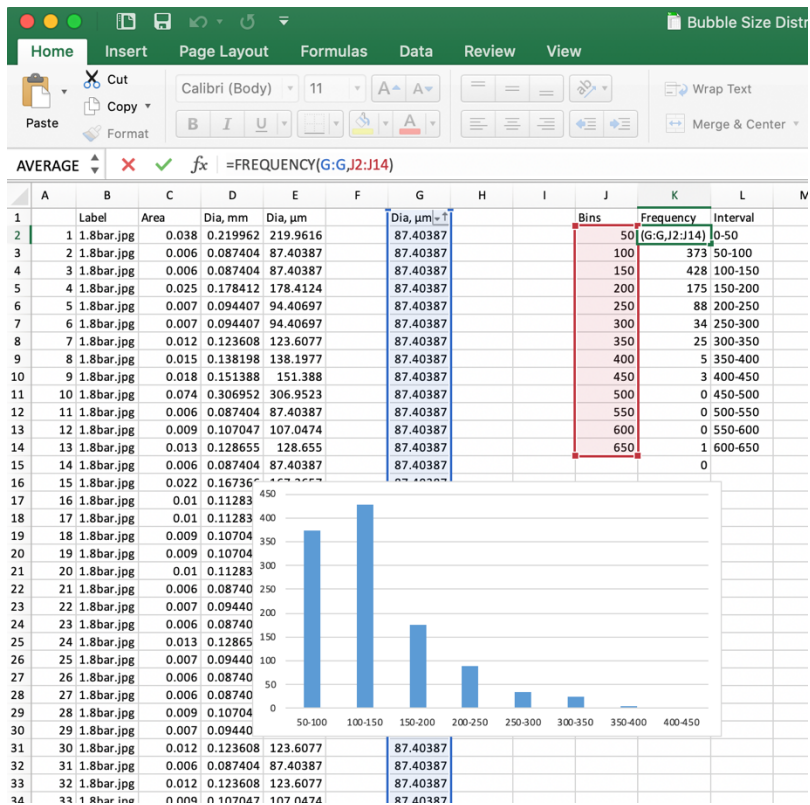
B. Microsoft Excel

Moving Average

Trend line

Frequency Distribution
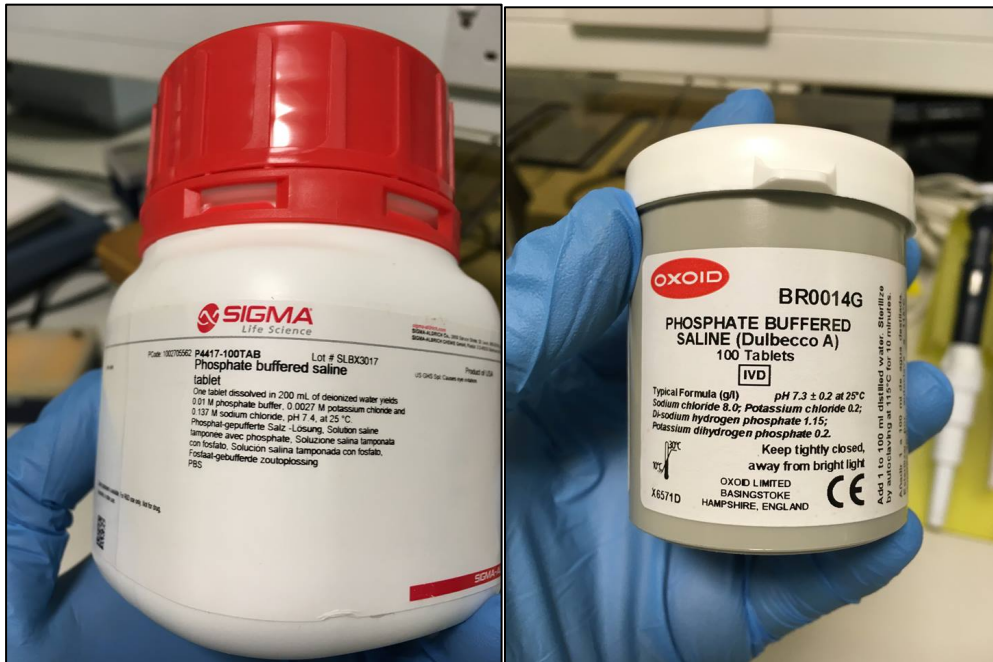
C. List of materials

Figure 9.1 PBS tablet diluted in distilled water for PBS solution for HeLa cells detachment
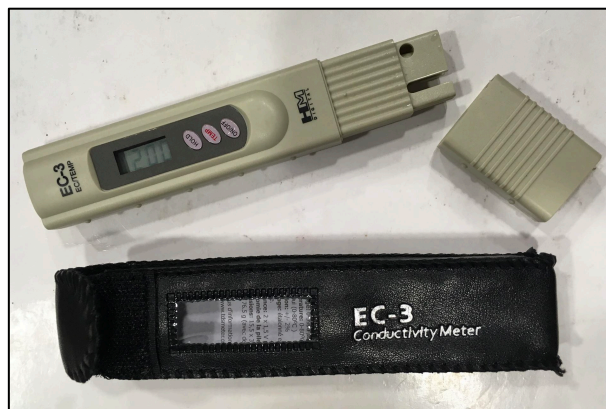

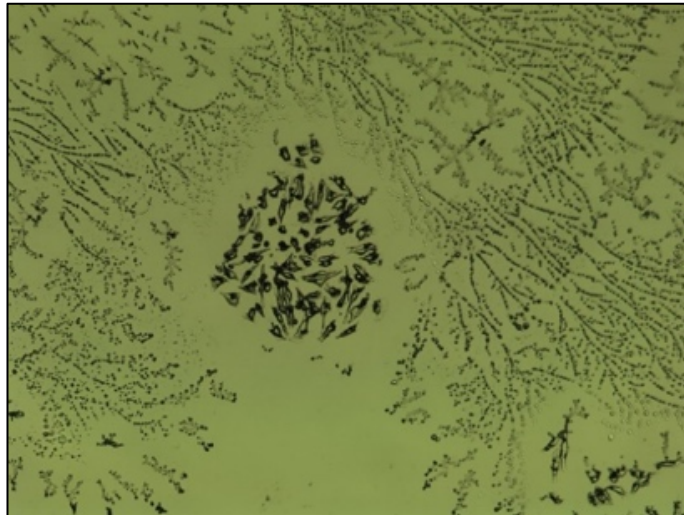**Figure 9.2 Electroconductivity meter used to measure low EC**

Figure 9.3 HeLa cells after sparged with microbubbles. A colonial of the cells are tenaciously attached to the microscope slide holder due to microbubbles used is large and low time exposre

Table 9.1 Specifications of light meter - Maplin Order Code N76CC

Specifications	Properties
Display	Maximum 1,999 counts
Polarity	Automatic
Measurement Rate	1.5 times/s, nominal
Power	12V
Dimensions	188 (H) x 64.5 (W) x 24.5 (D) mm/160g
Photo Detector Dimensions/weight	115 x 60 x 27mm/80g
Measurement Range	200/2000/20000/50000 Lux/FC (1Fc=10.76 Lux)
Accuracy	±5% rdg ±10dgts (<10000Lux/fc) ±10% rdg ±10dgts (>10000Lux/fc) (20000lux range reading x10/50000 lux range reading x 100)
Repeatability	±2%
Temperature Characteristics	±0.1%/ºC
Photo Detector	One silicon photo diode with filter

D. Publication

Harun, M. H. & Zimmerman, W. B. (2018). Membrane Defouling Using Microbubble Generated by Fluidic Oscillation. Water Science and Technology: Water Supply, 1–10. Retrieved from http://ws.iwaponline.com/lookup/doi/10.2166/ws.2018.056

Membrane defouling using microbubbles generated by fluidic oscillation

M. H. C. Harun and William B. Zimmerman

ABSTRACT

Impurities and colloidal substances are two of many fouling conditions that reduce the membrane filtration performance used in wastewater treatment. This study investigates the potential of fluidic-oscillation-generated microbubbles (MBs) to defoul the filtration membrane. Cartridge filters for microfiltration (MF) of 1 μm pore size were fouled using surface seawater collected from the Hull coastal area. The seawater was circulated at 5.8 L/min to actuate colloidal substance deposition on the membrane surface. The recorded feed channel pressure drop (ΔP) across the membrane filters showed rapid fouling occurred in the first 8 hrs of the circulation. Fluctuations of ΔP during the next 8 hrs were observed showing the colloids filling the pores of the membrane, and remaining steady for 2 hrs showing the membrane was completely fouled. The filtration membrane was cleaned and defouled using fluidic-oscillator-generated MBs. The fouled membranes were sparged with 1 L/min of air scouring for ~1 to ~2 hrs to remove the deposited colloids and impurities on the surface of the membrane. The membrane, analysed by Scanning Electron Microscopy (SEM), UV_{254} and Electrical Conductivity (EC) meter, showed the extent of MBs-mediated removal of the deposited colloidal particle from the membrane surfaces. This study found that the highest defouling rate occurs with MBs generated by fluidic oscillator (closed vent), followed by MBs generated by fluidic oscillator (opened vent) and MBs generated without fluidic oscillator at 9.53, 6.22, and 3.41 mbar/min, respectively.

Key words | defouling, membrane, microbubble

M. H. C. Harun
William B. Zimmerman (corresponding author)
Department of Chemical and Biological
  Engineering,
University of Sheffield,
Sheffield, S1 3JD,
United Kingdom
E-mail: w.zimmerman@sheffield.ac.uk

M. H. C. Harun
School of Ocean Engineering,
Universiti Malaysia Terengganu,
Kuala Terengganu, Terengganu 21030,
Malaysia

INTRODUCTION

Membrane filtration approaches such as microfiltration (MF), ultrafiltration (UF), nanofiltration (NF) and reverse osmosis (RO) are very important for wastewater treatment and waste recovery (Bhattacharya et al. 2013; Galanakis et al. 2013; Giacobbo et al. 2015). They provide many advantages such as high selectivity, capacity and feasibility. However, they are easily fouled by biofoulings, and organic and colloidal substances which restrict the permeation rate and reduce the process efficiency. In general, fouling is usually caused by the deposition of small colloidal particles

defouling methods such as chemical cleaning and pre-treatment usually are destructive and cause waste problems. Recently, innovative studies were conducted to explore the potential of MBs to clean the filtration membrane. Mechanisms such as creating MB pulsating-like action (Wilson et al. 2013), the behaviour of MBs by adsorption (Akuzawa et al. 2010), and swarm velocity (Lee & Lee 2002) clearly described the role of MBs in cleaning applications. Agarwal et al. (2012) and Wibisono (2014) listed four steps of cleaning using MB: (1) generation of smaller MBs; (2) MBs burst to